Pressurised Solid Oxide Fuel Cells: From Electrode Electrochemistry to Hybrid Power Plant System Integration

Von der Fakultät Energie-, Verfahrens- und Biotechnik der Universität Stuttgart zur Erlangung der Würde eines Doktors der Ingenieurwissenschaften (Dr.-Ing.) genehmigte Abhandlung

vorgelegt von

Moritz Henke

aus Hamburg

Hauptberichter: Prof. Dr. K. Andreas Friedrich
Mitberichter: Prof. Massimo Santarelli

Tag der mündlichen Prüfung: 06.11.2015

Institut für Thermodynamik und Wärmetechnik der Universität Stuttgart

2015

Acknowledgements

I thank Prof. Andreas Friedrich and Prof. Josef Kallo for giving me the opportunity to carry out my research on this interesting topic. I furthermore thank them for the support and advise they gave me whenever needed. I also thank Prof. Massimo Santarelli for co-supervising my work. Furthermore, I thank Prof. Wolfgang Bessler for his extensive support during my first years at DLR and for showing me how to write scientific publications.

Special thanks go to my colleagues Stephanie Seidler, Florian Leucht, Caroline Willich, Christina Westner, Mike Steilen, Christian Schnegelberger, Amrei Tomaszewski, Marc Riedel, Marc Heddrich, Christopher Fischer, Robert Leibinger, Tobias Gabriel, Silvan Hillius and Wadim Siebert who like me have been working on the hybrid power plant project. Thank you for the many interesting discussions, your help in finding the right path through ups and downs in science (and beyond), the many hours in the lab, the dry (and sometimes dryer) humour and good company in and outside the office. I also thank my colleagues Axel Widenhorn, Martina Hohloch, Tobias Panne, Andreas Huber, Melanie Herbst and Sandro Bücheler from the DLR Institute of Combustion Technology for their good cooperation, their advice on gas turbines and for providing the gas turbine model.

I further thank my colleagues Max Eschenbach, Peter Leschinski and Jörg Weiss-Ungethüm for fruitful and interesting discussions and for advice on programming. I also thank Marcel Vogler, Christian Hellwig, Vitaliy Yurkiv and Jonathan Neidhardt from the DENIS helpdesk for the modelling and simulation support. Furthermore, I thank Robert Ruckdäschel, Ina Plock and Gudrun Steinhilber for their support in microsopy imaging and Michael Lang for many SOFC discussions.

Finally, I thank all colleagues of the Institute of Engineering Thermodynamics for their help, support, encouragement and cooperation and Sascha Schade without whom I would not have started this work.

Nobody believes the data of a model except for the guy who wrote it, whereas everyone believes the data of an experiment except for the guy who took it.

Abstract

Hybrid power plants consisting of a gas turbine and solid oxide fuel cells (SOFC) promise high electrical efficiencies if both components are directly coupled and the SOFC is operated at elevated pressure. This thesis covers the different aspects of this topic ranging from pressure influences on electrochemistry at the electrodes to operating strategies of a hybrid power plant.

The influence of pressure on SOFC performance is investigated theoretically and experimentally. Experiments are carried out using a test rig that allows for characterisation of SOFC stacks at pressures up to 0.8 MPa. Polarisation curves and electrochemical impedance spectra are used for evaluations. In addition to experimental investigations an SOFC stack model is developed based on an existing electrochemistry modeling framework. The stack model is experimentally validated and used for a theoretical analysis of pressure effects. Results show that Nernst potential increases with increasing pressure causing a higher open circuit voltage. Furthermore, gas diffusion is enhanced with increasing pressure and the charge transfer reaction is facilitated due to higher adsorption rates of reactants at the electrode surfaces. These effects significantly improve SOFC performance. At constant operating conditions and efficiency an increase in SOFC power density of up to 83 % is measured. If power density is kept constant, electrochemical efficiency is improved by up to 14 %. Results generally show that pressure influence is stronger at low pressures up to 0.5-1 MPa and weakens towards higher pressures.

The influence of pressure on formation of nickel oxide and solid carbon is investigated. An analytical evaluation of the nickel oxidation propensity shows that nickel oxidation is more likely to occur at higher pressures because the equilibrium partial pressure of oxygen in the anode gas increases. However, further investigations are necessary as electrochemical oxidation of nickel is not considered in this study. Carbon deposition is another degradation mechanism that can decrease the performance of an SOFC system. It was investigated via thermodynamic simulations using the software package Cantera. Thermodynamic equilibrium of gas mixtures with different oxygen to carbon ratios is calculated showing that the tendency to carbon deposition is highly pressure dependent. Carbon deposition should be avoidable if oxygen to carbon ratio is kept above two within conditions that are relevant for hybrid power plants.

The developed stack model is integrated into an existing validated gas turbine model that is extended to include further SOFC system components. A system operating

strategy is presented that is based on a gas turbine control. Operating conditions of the SOFC are not directly controlled. A sensitivity analysis is carried out showing that the power ratio between gas turbine and SOFC is the most important parameter in order to achieve a high electrical efficiency. Other parameters like the number of SOFC stacks as well as gas and heat recirculation rates are of less importance. Thermal losses can significantly reduce electrical efficiency if they occur downstream of the recuperator.

Finally, the operating range of a hybrid power plant based on the proposed system control is investigated. It is found that high electrical efficiencies above 60 % (based on the HHV) are achievable within an electrical power range from 310 to 670 kW if gas turbine speed and SOFC electrical power are adjusted. A further reduction in electrical power output of the power plant is possible but will result in a significant drop in electrical efficiency.

Zusammenfassung

Hybridkraftwerke bestehend aus Festoxidbrennstoffzelle (SOFC) und Gasturbine versprechen hohe elektrische Wirkungsgrade, wenn beide Komponenten direkt gekoppelt werden. Dabei wird die SOFC bei erhöhtem Druck betrieben. In dieser Doktorarbeit werden verschiedene Aspekte dieses Themengebiets detailliert untersucht. Die Inhalte dieser Arbeit reichen thematisch von der Elektrochemie an den Elektroden bis hin zu Betriebsstrategien für das Hybridkraftwerk.

Der Einfluss von Druck auf das Leistungsverhalten der SOFC wird theoretisch und experimentell untersucht. Die Experimente werden mit Hilfe eines Teststands durchgeführt, der die Charakterisierung von SOFC bei Drücken bis zu 0,8 MPa erlaubt. Polarisationskurven und Impedanzspektren werden für die Bewertung verwendet. Neben den experimentellen Untersuchungen wird ein SOFC-Stackmodell entwickelt, welches auf ein bestehendes elektrochemisches SOFC-Modell aufbaut. Das Modell wird parametriert, experimentell validiert und für eine theoretische Analyse von Druckeffekten verwendet. Die Ergebnisse zeigen einen Anstieg der Nernstspannung mit steigendem Druck, was eine höhere Leerlaufspannung zur Folge hat. Außerdem werden mit steigendem Druck die Diffusion von Gasen verstärkt sowie die Ladungstransferreaktion durch höhere Adsorptionsraten der Reaktanten auf den Elektrodenoberflächen gefördert. Durch diese Effekte kann die Leistungsfähigkeit der SOFC signifikant gesteigert werden. Bei gleichbleibenden Betriebsbedingungen und kostantem elektrochemischen Wirkungsgrad wird ein Anstieg der Leistungsdichte von bis zu 83 % gemessen. Bei konstanter Leistungsdichte kann der elektrochemische Wirkungsgrad um bis zu 14 % gesteigert werden. Generell zeigt sich, dass der Druckeinfluss bei niedrigen Drücken bis zu 0,5 bis 1 MPa am stärksten ist und mit steigendem Druck stark abnimmt.

Der Druckeinfluss auf die Bildung von Nickeloxid und abgeschiedenem Kohlenstoff wird untersucht. Eine analytische Betrachtung zeigt, dass die Neigung zur Bildung von Nickeloxid mit steigendem Druck zunimmt, da der Gleichgewichtspartialdruck von Sauerstoff im Anodengas ansteigt. Allerdings sind weitere Untersuchungen notwendig, da die elektrochemische Oxidation von Nickel bei dieser Untersuchung nicht berücksichtigt ist. Die Ablagerung von Kohlenstoff ist ein weiterer Degradationsmechanismus, der die Leistungsfähigkeit eines SOFC-Systems verringern kann. Die thermodynamische Neigung zu Kohlenstoffablagerungen wird mit Hilfe der Software Cantera untersucht. Die Berechnung des thermodynamischen Gleichgewichts von Gasgemischen mit verschiedenen

Verhältnissen von Sauerstoff zu Kohlenstoff zeigt, dass die Neigung zu Kohlenstoffablagerungen stark druckabhängig ist. Unter Bedingungen, wie sie im Hybridkraftwerk auftreten, sollten Ablagerungen jedoch vermeidbar sein, indem das Verhältnis von Sauerstoff zu Kohlenstoff über einem Wert von zwei gehalten wird.

Das entwickelte Stackmodell wird in ein bestehendes und validiertes Gasturbinenmodell integriert und dabei um zahlreiche weitere Kraftwerkskomponenten ergänzt. Eine Betriebsstrategie für ein Hybridkraftwerk wird vorgestellt, welches auf der Regelung einer Gasturbine beruht. Die Betriebsbedingungen der SOFC werden dabei nicht direkt beeinflusst. Eine Sensitivitätsanalyse zeigt, dass das Verhältnis der elektrischen Leistung zwischen SOFC und Gasturbine einen erheblichen Einfluss auf den Wirkungsgrad des Kraftwerks hat. Andere Parameter wie die Anzahl der Zellen oder Wärme- und Gasrezirkulationsraten spielen nur eine untergeordnete Rolle. Wärmeverluste können den Wirkungsgrad erheblich vermindern, sofern sie (in Gasflussrichtung) hinter dem Rekuperator auftreten.

Abschließend wird der Betriebsbereich des Hybridkraftwerks mit dem zuvor vorgestellten Betriebskonzept näher untersucht. Es zeigt sich, dass elektrische Wirkungsgrade über 60 % (basierend auf dem oberen Heizwert) innerhalb eines Leistungsbereichs zwischen 310 und 670 kW möglich sind, sofern die Drehzahl der Gasturbine und die elektrische Leistung der SOFC aufeinander abgestimmt werden. Eine weitere Reduzierung der elektrischen Leistung ist möglich, führt jedoch zu einer deutlichen Verringerung des elektrischen Wirkungsgrads.

Contents

List of Figures

List of Tables

Abbreviations

AC	alternating current
ASC	anode supported cell
AU	air utilisation
BMU	Bundesministerium für Umwelt, Naturschutz und Reaktorsicherheit / Federal Ministry for the Environment, Nature Conservation and Nuclear Safety
BMWi	Bundesministerium für Wirtschaft und Energie / Federal Ministry for Economic Affairs and Energy
BRD	Bundesrepublik Deutschland / Federal Republic of Germany
CHP	combined heat and power
CSC	cathode supported cell
DC	direct current
DLR	Deutsches Zentrum für Luft- und Raumfahrt / German Aerospace Center
ESC	electrolyte supported cell
FU	fuel utilisation
GT	gas turbine
HHV	higher heating value
IEA	International Energy Agency
KIER	Korean Institute of Energy Research
LHV	lower heating value
LSCF	lanthanum strontium cobalt ferrite
LSM	lanthanum strontium manganite
MEA	membrane electrode assembly
MHI	Mitsubishi Heavy Industries
MSC	metal supported cell
NETL	National Energy Technology Laboratory
nlpm	norm liter per minute (at 293.15 K and 101325 Pa)
O/C	oxygen to carbon ratio
OCV	open circuit voltage
PSOFC	pressurised solid oxide fuel cell(s)
ScSZ	scandia stabilised zirconia

SEM	scanning electron microscopy
SOFC	solid oxide fuel cell(s)
STP	standard temperature and pressure (298.15 K and 101325 Pa)
TT	Institut für Technische Thermodynamik / DLR Institute of Engineering Thermodynamics
UCI	University of California, Irvine
VT	Institut für Verbrennungstechnik / DLR Institute of Combustion Technology
YSZ	yttria-stabilised zirconia

Nomenclature

A	area (m^2)
a	activity
a_K	measure for Knudsen diffusion resistance ($N\,A^{-1}$)
a_{ord}	measure for ordinary diffusion resistance ($m^2\,A^{-1}$)
b	oxygen exponent
c_{cell}	heat capacity of single cell ($J\,kg^{-1}\,K^{-1}$)
c_0	concentration gradient ($mol\,m^{-3}$)
d	thickness (m)
D^{ij}_{eff}	effective bosanquet diffusion coefficient of species i and j ($cm^2\,s^{-1}$)
D^{i}_{K}	Knudsen diffusion coefficient of species i ($cm^2\,s^{-1}$)
D^{ij}_{ord}	ordinary diffusion coefficient of species i and j ($cm^2\,s^{-1}$)
E	cell voltage / potential (V)
E_{th}	thermal energy (J)
E_{act}	activation energy ($J\,mol^{-1}$)
F	Faraday constant ($96485\,A\,s\,mol^{-1}$)
i_0	exchange current density ($A\,m^{-2}$)
Kn	Knudsen number
k_B	Boltzmann constant ($J\,K^{-1}$)
L	molecular mean free path (m)
M	molar mass ($kg\,mol^{-1}$)
P	power (W)
p	pressure (Pa) unless unit is specified differently
p_0	standard pressure of 101325 Pa
p_i	partial pressure of species i (Pa)
R	gas constant ($8.314\,J\,mol^{-1}\,K^{-1}$)
r_p	mean pore radius (m)
T	temperature (K)
V_i	Fuller diffusion volume of species i (cm^3)
X_i	mole fraction of species i
z	charge number

$\square$	free surface site
ΔG_0	Gibbs reaction enthalpy at p_0 and activities of 1 ($\mathrm{J\,mol^{-1}}$)
ΔH	enthalpy ($\mathrm{J\,mol^{-1}}$)
ϵ	porosity
η_{act}	activation overpotential (V)
η_{conc}	concentration overpotential (V)
η_{ohm}	ohmic overpotential (V)
λ	thermal conductivity ($\mathrm{W\,m^{-1}\,K^{-1}}$)
ν	stoichiometric coefficient
σ_i	collision diameter of species i (m)
τ	tortuosity

1 Introduction

The International Energy Agency (IEA) has predicted an increase in world primary energy demand of 0.7 % per year between 2008 and 2035 [41]. This number is based on the assumption that greenhouse gas concentration in the atmosphere can be limited to 450 ppm CO_2-equivalent. This goal is assumed to keep temperature rise below 2 K compared to preindustrial time. The increase in energy demand is expected to be greatest in newly industrialised countries. Fossil fuels will remain the dominant energy source with an increasing growth in demand for natural gas.

In Germany, the government has published an energy concept promoting the introduction of electric mobility thus increasing the demand for electrical energy [10]. More recently, a law was passed restricting the use of nuclear power up to 2022 [11].

The above examples illustrate the need for new technologies to provide electrical energy reliably and most efficiently. The availability of fossil fuels is limited as is the possibility to use them without exceeding the desired concentration of greenhouse gases in the atmosphere. Increasing the efficiency of electrical power plants can contribute significantly to meet the desired goals.

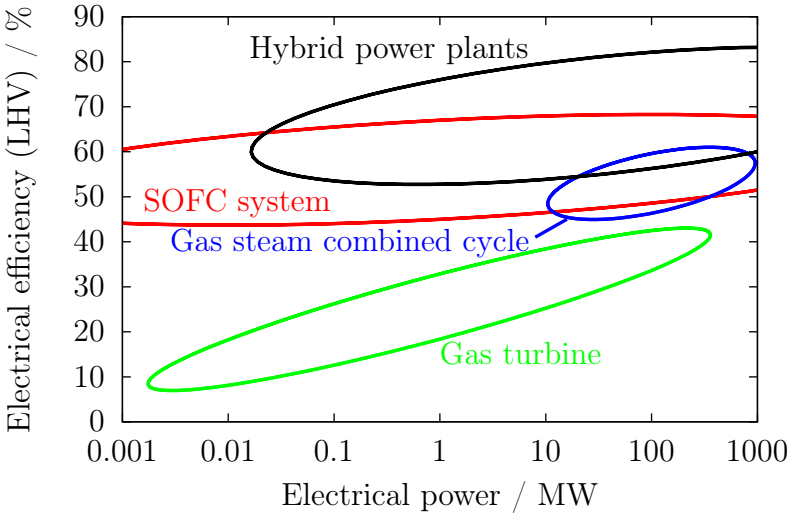

Figure 1.1: Comparison of electrical efficiencies of different power plant types which are fuelled with natural gas.

Figure 1.1 shows electrical efficiencies (based on LHV) that are currently achieved by gas turbines and gas steam combined cycles. Small SOFC systems also have achieved

the efficiencies shown. Larger SOFC systems are likely to reach similar efficiencies. A combination of SOFC and gas turbine promises efficiencies above those of the single components as the hot off gases of the SOFC are used to drive the gas turbine. First demonstrators of such hybrid power plants have reached electrical efficiencies above 50 % at small installed power. At large installed power higher efficiencies around 70 % are expected [39, 93, 106]. A hybrid power plant consisting of an SOFC system coupled with a gas steam combined cycle is only feasible at large installed power but promises to reach even higher efficiency.

Hybrid power plants can generally be operated on all kinds of gaseous hydrocarbon fuels and hydrogen. This flexibility is an important aspect regarding changing energy markets. Hybrid power plants can also supply combined heat and power.

Based on the above listed reasons hybrid power plants offer the potential of reducing cost of electricity and emissions due to high efficiency. Furthermore, they provide long term potential owing to their ability of being operated with renewable gases as well.

The concept of hybrid power plants is being investigated by several companies and research institutions worldwide (see Section 2.3). However, only very few power plants of this kind have actually been build to date. These aspects underline the relevance of this research field.

1.1 Hybrid Power Plant Project at the German Aerospace Center

DLR started the hybrid power plant project in 2006 with the aim of studying, developing, and building a hybrid power plant consisting of a micro gas turbine and an SOFC. Two institutes are cooperating in this project. The Institute of Combustion Technology (VT) is working on the gas turbine whereas the Institute of Engineering Thermodynamics (TT) is responsible for the SOFC. This dissertation was carried out at TT as part of the project.

Today SOFC production capacities are still under development and the production itself is expensive compared with conventional energy conversion technologies. Building a large demonstration power plant is therefore cost intensive and research organisations like DLR investigate the fundamentals of the coupling with reduced power size. First coupled operation of gas turbine and SOFC with an overall electrical power output of 30 kW is scheduled for 2017. The project has been financially supported by the Federal Ministry for Economic Affairs and Energy (BMWi) and the utility EnBW.

1.2 Scope of the Present Dissertation

The scope of this dissertation is to theoretically and experimentally investigate the influence of pressure on SOFC performance and durability. Furthermore, an operating strategy for a hybrid power plant (SOFC+GT) is developed that provides high electrical efficiency over a wide range of electrical power output despite a simple system layout. Moreover, the effect of system component variation on performance, efficiency and operating conditions of a hybrid power plant is analysed.

Compared with numerous works that have previously been published on hybrid power plants, this dissertation is based on very detailed analyses of pressurised operation of SOFC including the experimental validation of an SOFC model prior to system simulations. Furthermore, most of the work found in literature is based on the tubular SOFC concept whereas all investigations in this work are based on planar cells. The main difference here is the operating temperature of planar cells of 950–1125 K compared to 1050–1300 K for tubular cells. Oftentimes, work presented in literature is solely based on theoretical research without the intention to build and operate a hybrid power plant. Work presented in litereature often focuses on system optimisation generally adding additional complexity to the system. The hybrid power plant concept that is discussed in this work includes many aspects that will be important for a future construction and operation of a prototype power plant.

1.3 Outline of the Thesis

This thesis contains five main sections. In Section 2 the scientific and technological background of the thesis subject is described including information on SOFC and gas turbines. Different system architectures of hybrid power plants are presented and publications of various research groups related to this thesis are summarised. Section 3 explains different experimental and theoretical methods that are used in this work. On stack level, these methods include experiments with SOFC stacks as well as the development and validation of an SOFC stack model. Furthermore, the developed system model and system control strategy is described. In section 4, experimental and theoretical results are presented that explain the influence of pressure on different processes inside an SOFC during operation. Furthermore, the combined influence of these effects on performance are analysed. Section 5 presents a short insight into pressure effects

on SOFC durability. In Section 6 results of a sensitivity analysis on system level are presented. In Section 7 an analysis of the operating range of the hybrid power plant is presented.

2 Scientific and Technological Background

This section contains general information about the concept of hybrid power plants, different system architectures, and the need for pressurising SOFC. Furthermore, a literature overview on relevant research and applications is given. General information on SOFC and gas turbines, their design and function can be found in numerous books [51, 88, 93] and is therefore only briefly described here.

Enthalpies of reaction ΔH_R are calculated with

$$\Delta H_\mathrm{R} = \sum \nu_\mathrm{p} H_\mathrm{p} - \sum \nu_\mathrm{r} H_\mathrm{r} \tag{2.1}$$

with the stoichiometric coefficients ν and the enthalpy H of reactants (r) and products (p). All reaction enthalpies are given at STP ($\Delta H_{0,\mathrm{R}}$) and assuming

$$\text{reactants} \rightleftharpoons \text{products} \tag{2.2}$$

although the reactions generally occur in both directions. Thermodynamic data for the calculations is taken from [13, 57, 66].

2.1 Solid Oxide Fuel Cell

Fuel cells are electrochemical devices that directly convert chemically bound energy into electrical energy. Thermal energy is released as a by-product. There are many different types of fuel cells which are more or less suitable for different applications. One type of fuel cell is the SOFC. It consists mainly of three parts as illustrated in Figure 2.1. Hydrogen and oxygen (usually as part of the air) are fed to anode and cathode, respectively. The two electrodes are separated by an electrolyte. At the anode, hydrogen reacts with the oxygen ions which pass through the electrolyte. Electrons are released and conducted to the cathode via an external electric load. There, they react with the oxygen forming oxygen ions. The chemical reaction equations are as follows:

$$\text{Anode :} \quad \mathrm{H_2 + O^{2-} \rightleftharpoons H_2O + 2\,e^-} \qquad \Delta H_{0,\mathrm{R}} = -194\,\mathrm{kJ\,mol^{-1}} \tag{2.3}$$

$$\text{Cathode :} \quad \mathrm{0.5\,O_2 + 2\,e^- \rightleftharpoons O^{2-}} \qquad \Delta H_{0,\mathrm{R}} = -\ 48.0\,\mathrm{kJ\,mol^{-1}} \tag{2.4}$$

$$\text{Global :} \quad \mathrm{H_2 + 0.5\,O_2 \rightleftharpoons H_2O} \qquad \Delta H_{0,\mathrm{R}} = -242\,\mathrm{kJ\,mol^{-1}} \tag{2.5}$$

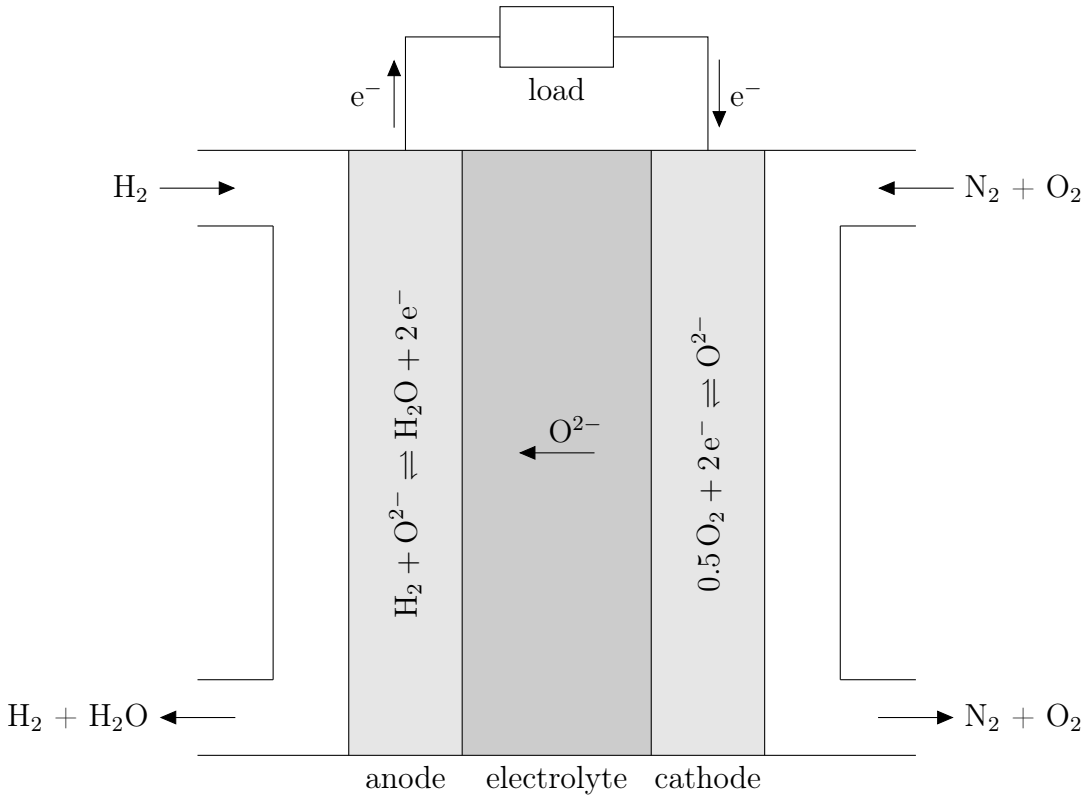

Figure 2.1: General principle of a solid oxide fuel cell operated with hydrogen. Oxygen ions are formed at the cathode and conducted through the electrolyte. At the anode, the ions react with hydrogen forming water. Electrical energy is released which can be used via an external electrical circuit.

SOFC are suitable for hybrid power plant applications due to their high operating temperature. Furthermore, they can be fuelled with hydrogen, carbon monoxide, and hydrocarbons thus enabling an operation with natural gas which contains a high amount of methane. The global chemical reaction equations for carbon monoxide and methane are:

$$\mathrm{CO} + 0.5\,\mathrm{O_2} \rightleftharpoons \mathrm{CO_2} \qquad \Delta H_{0,\mathrm{R}} = -283\,\mathrm{kJ\,mol^{-1}} \tag{2.6}$$

$$\mathrm{CH_4} + 2\,\mathrm{O_2} \rightleftharpoons 2\,\mathrm{H_2O} + \mathrm{CO_2} \qquad \Delta H_{0,\mathrm{R}} = -802\,\mathrm{kJ\,mol^{-1}} \tag{2.7}$$

If an SOFC is operated with methane, it is usually pre-reformed in a separate reformer. In SOFC systems, steam reforming is generally the most suitable reforming type as part of the anode off gas can be recirculated to provide the necessary steam. Steam reforming of methane mainly occurs in two steps via

$$\mathrm{CH_4 + H_2O \rightleftharpoons 3H_2 + CO} \qquad \Delta H_{0,\mathrm{R}} = +206\,\mathrm{kJ\,mol^{-1}} \tag{2.8}$$

and the water gas shift reaction

$$\mathrm{CO + H_2O \rightleftharpoons H_2 + CO_2} \qquad \Delta H_{0,\mathrm{R}} = -41.1\,\mathrm{kJ\,mol^{-1}} \tag{2.9}$$

The reforming process is highly endothermic and the necessary thermal energy can be supplied together with the water vapour via recirculation of the anode off gas which generally increases system efficiency. SOFC are however also capable of internal reforming (thus reforming directly on the cell) which can be used for direct cooling of the SOFC.

In general two different configurations of SOFC exist. Tubular shaped cells are advantageous in terms of sealing of different gas compartments. Planar cells offer higher volumetric power density. From an electrochemical point of view, SOFC could have very thin layers (μm), however, a structural support is needed. Anode (ASC), cathode (CSC), and electrolyte (ESC) supported cells have been built so far with supporting layer thicknesses being 1-2 order of magnitudes larger. Furthermore, metal supported cells (MSC) exist, incorporating a sheet metal as structural support.

A typical material of SOFC electrolytes is yttria-stabilised zirconia (YSZ). SOFC operating temperatures typically range from 950 K to 1300 K. These high temperatures are necessary to ensure the electrolyte's O^{2-}-conductivity. Even higher temperatures are not desirable as it is difficult to find suitable materials for the entire stack. As an alternative electrolyte material scandia stabilised zirconia (ScSZ) is being investigated which promises possible operation at lower temperature. SOFC anodes are usually made of nickel (the catalyst) and YSZ. Cathodes are often made of lanthanum strontium manganite (LSM) or lanthanum strontium cobalt ferrite (LSCF).

Commercialisation of SOFC systems is still under development. In principle, SOFC systems can have small electrical power outputs in the range of 1 kW e.g. for CHP applications for single households and very large power outputs of hundreds of MW for large stationary power plants. An overview of current commercialisation activities is given in [1].

2.2 Gas Turbine

Gas turbines are a type of internal combustion engine. Figure 2.2 shows an ideal gas turbine process. Air is compressed isentropically by the compressor thus increasing gas temperature and pressure (1→2). The air is let into the combustion chamber / combustor where fuel is added and burned thus increasing the temperature of the turbine inlet gas (2→3). Finally, the air is expanded isentropically via the turbine (3→4) which drives the compressor and provides electrical energy via the generator. Gas turbines are being used for various applications e.g. aircraft propulsion or electrical power plants.

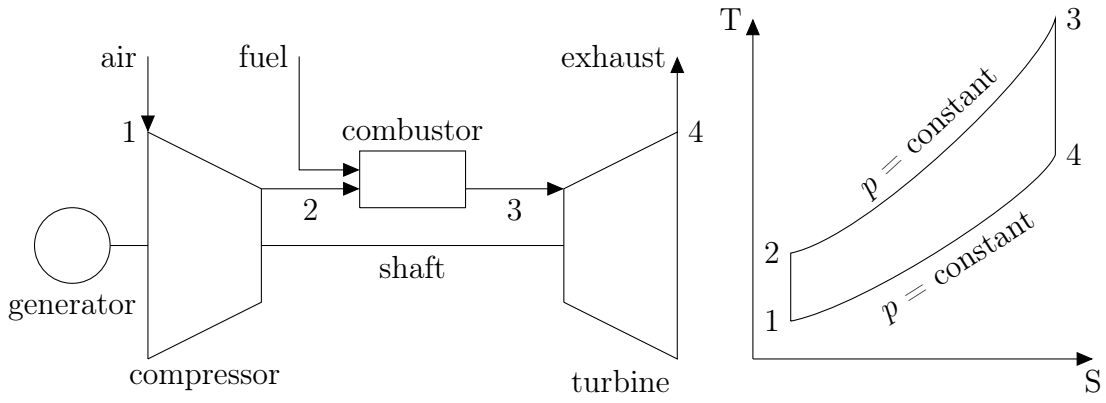

Figure 2.2: General principal of a gas turbine (left) and corresponding ideal temperature versus entropy diagram (right). Air is compressed by the compressor, heated inside the combustion chamber, and expanded via the turbine itself. The turbine drives the compressor as well as an electric generator.

2.3 Hybrid Power Plant

2.3.1 General concept

Hybrid power plants (as referred to in this work) combine a gas turbine and an SOFC. In principle, this is rather simple. The combustion chamber of the gas turbine is replaced by an SOFC therefore replacing combustion with electrochemical conversion. At first, this does not change the total amount of energy released (provided the fuel flow does not change and all fuel is converted). However, a certain amount of the energy is now released as electrical energy. The remaining thermal energy is still used to power the

turbine. The main advantage of this configuration is that the SOFC has a much higher electrical efficiency than the gas turbine. However, if an SOFC is operated separately not all of the fuel can be converted (typically up to 90 % of the fuel is actually used). This gas then leaves the fuel cell as exhaust and is usually burned afterwards. Additionally, the thermal energy that is released inside the SOFC as a by-product cannot be used to provide electricity. By combining gas turbine and SOFC, each system compensates for the others disadvantages. The SOFC provides electricity with already high efficiency and the hot exhaust gases are not wasted but used by the gas turbine to provide additional electricity. In principle, hybrid power plants can be coupled with steam turbines to further increase electrical efficiency and they can also be used for combined heat and power (CHP).

Two different main concepts for coupling of SOFC and gas turbine exist — a direct and an indirect coupling. Figure 2.3 shows an indirect coupling of both components. Fuel cell and gas turbine operate independently from each other. SOFC exhaust gases are conducted through a heat exchanger where they heat up the compressed air of the gas turbine. In this configuration, the SOFC is usually operated at atmospheric pressure.

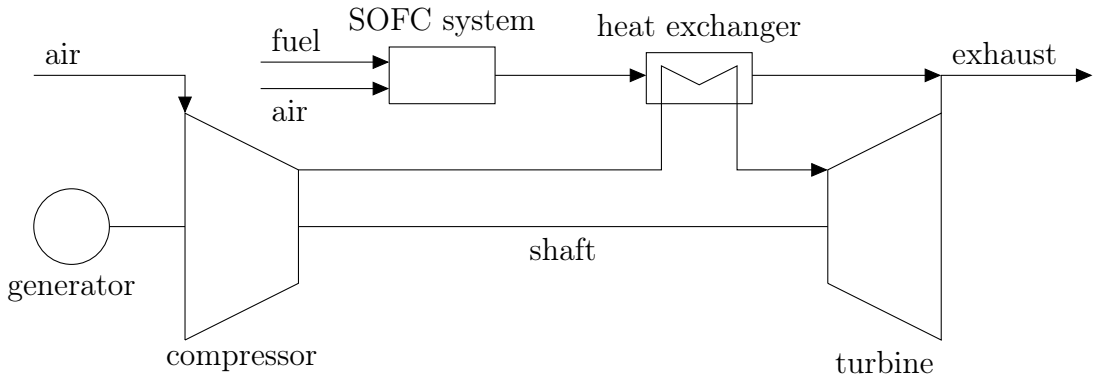

Figure 2.3: Schematic of an indirectly coupled hybrid power plant. Thermal energy is transferred from the SOFC exhaust gases to the gas turbine cycle.

In Figure 2.4 a direct coupling of both components is illustrated. The compressed air is led through the SOFC whose exhaust gases leave the system via the gas turbine. With this configuration, the operating pressure of the fuel cell is mainly determined by the compression ratio of the compressor.

It has been shown that a direct coupling of SOFC and gas turbine is advantageous

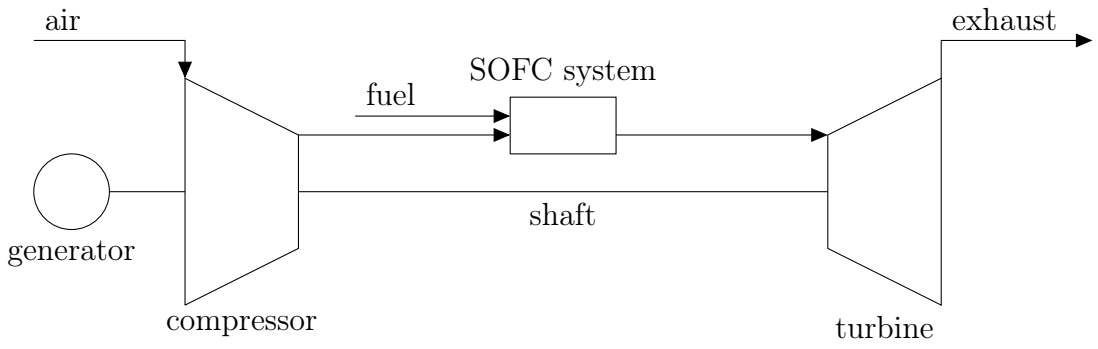

Figure 2.4: Schematic of a directly coupled hybrid power plant. The SOFC is operated at elevated pressure. Its hot exhaust gases are expanded via the turbine before leaving the system.

compared with the indirect coupling [28, 79, 80, 106]. This is mainly due to two reasons. First, a direct use of SOFC exhaust gases is much more efficient than transferring the thermal energy via a heat exchanger. More thermal energy is available at the turbine inlet and thus more electrical energy can be provided by the generator. Second, pressurisation has a positive influence on SOFC performance. A literature overview on pressurised SOFC (PSOFC) is given in Section 2.4. The topic of PSOFC is further discussed in detail in Section 4.

The schematics shown in Figures 2.2–2.4 only illustrate a simplified layout of a gas turbine or hybrid power plant, respectively. In practice, several additional components are usually needed. Heat exchangers can sometimes be used to preheat the air before entering the fuel cell / combustion chamber using exhaust gases. The SOFC system usually incorporates fuel pretreatment (e.g. desulphurisation, pre-reforming) as well as anode and / or cathode gas recirculation. A combustor is usually necessary to burn the remaining fuel of the anode gas or to further heat up the air.

2.3.2 Literature overview

Recently, many research groups worldwide have started investigations on hybrid power plants. Especially within the last decade a vast number of research articles has been published thus making it difficult to evaluate focus and significance of each research group. The predominant amount of work is theoretical, usually evaluating different

system architectures, single power plant components or means of system control. Most of the research is carried out with system simulations which lack experimental validation as operating hybrid power plants are rare.

Analyses are oftentimes carried out by researchers originating from gas turbine groups causing a limitation in scientific approaches. SOFC are often operated at constant conditions which strongly limits the potential operating range of a hybrid power plant concerning electrical power output. Although this work focuses on the SOFC system of a hybrid power plant, the flexibility of both SOFC and gas turbine are regarded in order to achieve high electrical efficiencies within a wide range of electrical power output.

System simulations in literature are often based on the tubular SOFC design of Siemens Westinghouse. Due to the lack of experimental data available in literature, the fuel cell models are in many cases poorly validated. This work is based on planar SOFC which are experimentally examined at different pressures. The SOFC model used in this work is experimentally validated within a wide operating range.

Owing to the large number of publications, this literature overview is limited to the most important research groups and is therefore non-exhaustive. It only includes a short presentation of the general research on hybrid power plants from the companies Siemens Westinghouse, Mitsubishi Heavy Industries, and Rolls-Royce Fuel Cell Systems. Apart from the DLR, research institutions whose work is summarised here as well are the University of Genoa (UG), the Korea Institute of Energy Research (KIER), the National Energy Technology Laboratory (NETL), and the University of California, Irvine (UCI). These companies and research groups intend to or already have built and operated a hybrid power plant. A small focus is set on literature by these groups that covers operating strategies and parameter studies comparable to the analyses presented in Sections 6 and 7 of this work.

Proof of concept was demonstrated by Siemens Westinghouse in 2000 [52, 106]. The 220 kW-system reached an electrical efficiency of 52 % (LHV) using a 200 kW SOFC and a 75 kW gas turbine. Plans for further power plants were published [58]. The system was operated at the UCI [86]. Besides their cooperation, the UCI has been working on hybrid power plants for many years with a focus on transient operation of hybrid power plants including load variation and the operation with different fuels [45, 70–72]. Furthermore, cathode ejectors were analysed [59] and the integration of a hybrid power plant into a locomotive power train was evaluated [62, 63]. Several parametric studies were carried

out [67, 94, 112] including hybrid power plants with a two-stage air compression [112] as well as a study investigating cathode gas recirculation [94].

Detailed theoretical and experimental research has been published by the University of Genoa, Italy who cooperates with Rolls-Royce Fuel Cell Systems. Rolls-Royce Fuel Cell Systems has been intending to build and operate a hybrid power plant for many years [3, 29] but was recently purchased by LG. At the University of Genoa a hybrid power plant test rig has been used for characterisation of various system components of hybrid power plants going along with corresponding theoretical work. Very detailed research has been carried out concerning recirculation of anode off gases [18, 21, 22, 24, 61, 98]. Further research results were published regarding the start-up and shut down of a hybrid system [23], the recuperator of the gas turbine [20], anode-cathode interaction [19] and fuel processing [2, 25]. Another focus is set on the dimensioning of system components and the resulting system behaviour at various load points [15, 17, 60, 64, 96, 97]. In [15] a system operating strategy is presented that is to some extent similar to the operating strategy proposed in this work. By varying turbine rotational speed, high electrical efficiency is achieved over a range of electrical power output from 35 to 100 %.

Extensive analyses regarding hybrid power plants have been carried out around the NETL. Research has been published regarding control strategies [99, 101, 102], coal-based hybrid power plants [104], system start-up [91], and power plant dimensioning [105]. Furthermore, a test facility consisting of a gas turbine, an SOFC simulator, and auxiliary components is being used for experimental analyses of the entire power plant [100, 103].

Mitsubishi Heavy Industries (MHI) has assembled and operated hybrid power plants with an electrical power output of around 75 kW [77] and 200 kW [95] a few years ago. These power plants are equipped with tubular SOFC. The newer and larger plant was operated for a few thousand hours including thermal cycles. A maximum electrical efficiency of 52 % (based on LHV) was achieved. The electrical power ratio of SOFC to GT was around 5 at maximum power with an SOFC power of 204 kW (DC) and a GT power of 41 kW (AC). In the long run, power plants combining SOFC, gas turbine and steam turbine shall be developed in the range of several hundred MW with an efficiency of 70 % (LHV). More recently, MHI has announced the successful operation of a hybrid power plant for 4000 hours in Tokyo [68].

Another hybrid power plant was operated at KIER [56]. A 5 kW anode-supported

planar SOFC was coupled with a 25 kW gas turbine for a short period of time. Difficulties with the gas turbine caused a strong drop of system pressure which damaged the SOFC. No stable long-term operation of the hybrid power plant was achieved and therefore no values for system efficiency were reported.

DLR is currently working on the realisation of a hybrid power plant with an electrical power output around 30 kW. Research activities include experimental investigations of a micro gas turbine with the experimental set-up being adapted to include additional piping as well as an SOFC simulator [39, 40]. This set-up allows for analyses of relevant operating conditions of hybrid power plants prior to the actual coupling of gas turbine and fuel cell. Experiments and simulations concerning the pressurised operation of SOFC are described in Section 2.4. Dynamic simulations of the SOFC sub-system have been carried out in order to evaluate system architectures and control strategies [54, 55]. Stationary hybrid power plant system simulations were performed in order to optimize stack size and other system parameters [78, 79]. A parametric study similar to the work described in Section 3.4.3 was carried out which was — in contrast to this work — based on tubular cells and a different system operating strategy [79]. A dynamic hybrid power plant model was developed in collaboration with the University of Stuttgart [48]. Current activities focus on the development and characterisation of different system components with the aim to realise a coupled operation of SOFC and GT in 2017.

2.4 Operation of Solid Oxide Fuel Cells at Elevated Pressure

It was shown in the section above that pressurisation of the SOFC is essential if highest electrical efficiencies are sought. In order to design and optimise a hybrid power plant, the characteristic behaviour of the fuel cell at all varieties of desired operating conditions has to be known. Whereas the influence of temperature and gas variation on SOFC performance has been researched extensively, the effect of pressure variation has only received more interest by different research groups in the past few years. It is, however, common knowledge that Nernst potential (and thus OCV) increases with rising pressure [51, pp. 35-42].

Research on pressurised SOFC has so far been performed by different companies and research institutions. Companies working on hybrid power plants (see Section 2.3.2) have not published many results of their research. Only some experimental results [83, 92] and theoretical considerations [107] were published by Siemens Westinghouse showing

an improved performance at elevated pressure. This was found to be due to improved transport processes through the electrodes and enhanced Nernst potential.

A 5 kW SOFC stack was operated as part of a hybrid power plant at KIER [56]. The stack was made of planar anode-supported cells and showed a performance increase of 8.5 % with an increase in pressure from atmospheric to 3.5 atm.

Pressurised anode-supported microtubular solid oxide fuel cells are under investigation at the Central Research Institute of Electric Power Industry [33, 34, 76]. Power density was more than doubled by increasing pressure from 0.1 MPa to 0.7 MPa. Power gain was greatest at 0.3 MPa considering the power needed for air compression. It was further found that ohmic resistance of the LSCF cathode and activation overpotentials of the electrodes were reduced.

At Kyoto University impedance measurements of SOFC anode half cells were carried out [47, 65]. It was found that impedance spectra at increased pressure do not qualitatively differ from atmospheric measurements. Furthermore, theoretical considerations suggest that concentration polarisation increases with rising pressure.

At Chinese Academy of Sciences performance of an anode-supported tubular SOFC was investigated under pressurised conditions [113]. It was found that pressure influence on performance is slightly more significant at low temperatures. A maximum increase in power density between 15 and 18 % was measured at temperatures varying from 650 to 800 °C when pressure was increased from 1 to 6 atm.

At Montana State University an SOFC model was developed and used to predict operational behaviour of the cell in fuel cell and electrolysis mode [89]. Predictions show a strong influence of pressure on performance between 1 and 3 bar and a diminishing influence at higher pressure up to 10 bar.

At the Pacific Northwest National Laboratory experimental investigations on pressurised button cells with LSCF cathode were performed with steam reformate of kerosene as fuel [14]. Increasing pressure from 101 to 724 kPa caused an increase in power density by a factor of approximately 2 (temperature dependent) at constant cell voltage of 0.8 V.

Further experimental results of pressurised SOFC were published by the Naval Undersea Warfare Center [12]. The published results did not show a strong or consistent effect of pressure on SOFC performance. This lack in pressure dependency is attributed to significant gas leakages that occurred under pressurised operation.

At the National Institute of Advanced Industrial Science and Technology in Japan,

experiments and simulations were carried out within a pressure range of 0.01 to 1 MPa. Results show that electrode kinetics and diffusion is improved with increasing pressure and ohmic resistance of the LSCF cathode is reduced [69].

Further experiments were carried out at National Central University, Taiwan in a pressure range from 1 to 5 atm. It was found that especially concentration overpotentials decrease strongly with increasing pressure whereas ohmic resistance is pressure independent [111].

Apart from research of direct pressure influence on SOFC performance, investigations on the influence of pressure on reforming and temperature distribution inside the SOFC have been published [2, 42, 84].

Experimental and theoretical research on pressurised SOFC has been carried out at DLR. Experimental results show that performance can be significantly improved by increasing operating pressure up to 0.8 MPa with the strongest effects at low pressure [38, 90, 110]. A detailed elementary kinetic model showed that pressure effects are due to various pressure dependent processes [35]. Experimental results were used to validate a stack model [37]. Some of these results are also presented in this work.

3 Scientific Approach and Methodology

In this section a description of the different scientific methods used throughout this dissertation is presented. The overall approach starts with investigations of pressure related effects on SOFC performance. Experiments are carried out with 5-cell stacks with the aim to acquire a detailed knowledge of SOFC performance in a broad range of operating conditions. Focus of all studies is the effect of pressure on SOFC performance. For the operation of a hybrid power plant other effects (e.g. effects related to temperature or gas composition) are equally important but in general already known. These effects are therefore regarded for system analyses but not studied in detail on stack level. Besides the experiments, a detailed SOFC stack model is developed which allows for a better understanding of experimental results as it offers the possibility to explain various effects from electrochemistry on the electrode surfaces up to temperature gradients on stack level. On the other hand, experiments can be used for validation of the model. This unique combination of detailed modelling and experimental investigations at various pressures allows for a thorough understanding of pressure related effects in SOFC that was previously not available in literature.

In addition to the analysis of SOFC performance at different pressures a study on durability issues is carried out. Calculations concerning nickel oxidation and carbon deposition propensity on the anode are performed. These two aspects are regarded as important for the long term operation of the hybrid power plant. Again, the focus is on the influence of pressure on both degradation mechanisms.

The detailed stack model is slightly adapted and implemented into a model of a complete hybrid power plant. Although, many models of hybrid power plants are already available in literature, they are usually based on tubular cells which are operated in a temperature range of 1100 to 1300 K. Cells regarded in this work can be operated in a temperature range of 950 to 1125 K. This difference has a significant influence on the preferable system design. The system model is designed for system optimisation. Whereas the general system architecture is already determined, the influence of variation in component design and mode of operation on system power and efficiency is investigated at steady state conditions. Results are used for optimisation of system control and design of balance of plant components.

3.1 Experimental Characterisation of SOFC Stacks

3.1.1 Experimental set-up

For performance evaluation of small SOFC stacks, the test rig shown in Figure 3.1 is used. The test rig can be pressurised up to 0.7 MPa (relative to atmosphere). In case of pressurisation, not only the pressure inside the fuel cell (anode and cathode gas channels) is increased but also the pressure of the surrounding atmosphere inside the furnace. In general, pressure inside the anode and cathode gas compartments is adjusted to equal the surrounding pressure. However, pressure differences cannot be eliminated entirely due to pressure losses along the gas channels. With the configuration presented in this work, pressure differences are usually kept below 5000 Pa under conditions similar to the standard operating conditions described in Section 3.2.4. High pressure differences can cause mechanical damage inside the fuel cell stack or the fuel cells itself which can lead to a failure of the whole stack. In order to ensure a precise pressure control, two equalising tanks (for anode and cathode gas, respectively) were installed. They allow for buffering undesired pressure fluctuations. On the downside, measurements at atmospheric pressure cannot be carried out with this test rig due to pressure losses along the gas flow paths and the design of the pressure control. In general, measurements cannot be carried out at absolute pressures smaller than 0.13 MPa.

The furnace of the test rig can be adjusted to temperatures up to 1220 K whereas inlet gases can be preheated up to 1300 K. The anode can be fed with compositions of hydrogen, nitrogen, methane, carbon monoxide, carbon dioxide, and argon. Furthermore, oxygen can be added to the hydrogen for humidification assuming auto ignition at these temperatures. Air, oxygen, nitrogen, and helium can be mixed as cathode gases. Cells and stacks can be analysed via polarisation curves, impedance spectra, and gas chromatography. A schematic of the test rig is shown in Figure 3.2. A description of the test rig was first presented in Ref. [90].

The overall measurement accuracy of the test rig was investigated. The inaccuracy of different measurement devices was estimated based on manufacturer specifications or by comparison with more accurate calibration devices. Measurement inaccuracies of pressure, temperature, gas leakages, anode and cathode gas flows, voltage, and current were considered. An SOFC model which was previously adapted to the tested fuel cells was used to evaluate the influence of measurement errors on SOFC performance.

Figure 3.1: Laboratory with pressurised SOFC test rig including gas distribution (left), pressure vessel (centre), equalising tanks (back), and gas chromatographs (front right) [90].

Results showed an influence of measurement inaccuracies on fuel cell voltage below 5 % with a probability of 95 % for a variety of operating conditions. These investigations were summarised in [53].

3.1.2 SOFC stacks

Anode-supported 5-cell stacks with an active surface area of 84 cm^2 per cell were characterised. The cells consist of a 370 µm nickel mesh, a 285 µm nickel-YSZ anode substrate, a 10 µm nickel-YSZ anode functional layer, a 10 µm YSZ electrolyte, a 10 µm LSM-YSZ cathode functional layer, and a 50 µm LSM cathode current collector. The entire cell is integrated into a cassette. These cassettes are then stacked together with bipolar plates (labelled cathode contact sheet) as visualised in Figure 3.3. The stacks are completed with a gas module (which distributes anode and cathode gases) and a stack top plate.

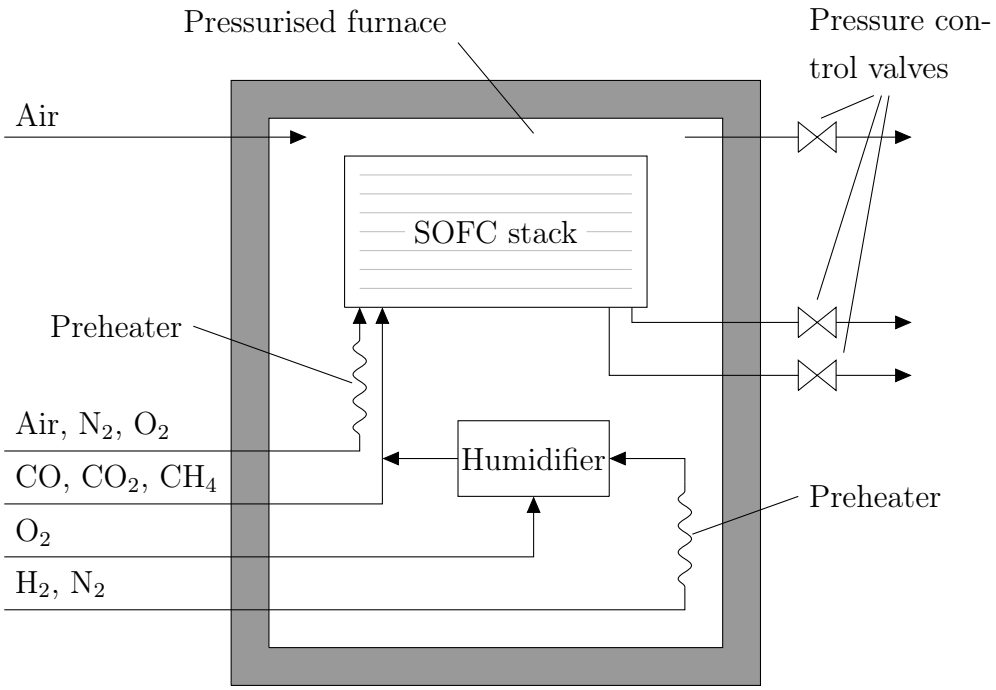

Figure 3.2: Simplified schematic of the pressurised SOFC test rig. The test rig is equipped with numerous thermocouples and pressure gauges. A more detailed schematic can be found in [90].

3.2 Modelling and Simulation on Cell and Stack Level

3.2.1 Aim

Modelling and simulation on cell and stack level are carried out to realise a better understanding of experimental results. Simulations offer the possibility to theoretically explain experimental results which can be influenced by various effects ranging from temperature gradients inside the stack to electrochemistry on the surface of electrodes. On the other hand, experiments are also used for model validation. Only a combined experimental and theoretical investigation allows for a thorough understanding of various phenomena. The models developed here are furthermore used as part of system simulations (see Section 3.4). The cell and stack model described here has previously been published in [37].

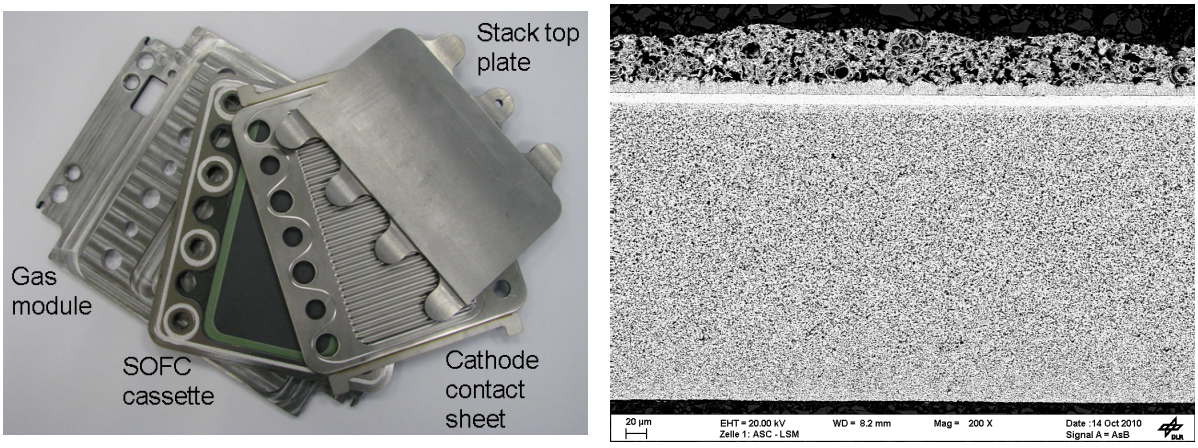

Figure 3.3: Left: Exploded view of the investigated SOFC stack [90]. Several of the SOFC cassettes can be welded together to form a real SOFC stack.
Right: SEM-image of the investigated anode-supported SOFC consisting of two cathode layers (top), electrolyte (centre), and two anode layers (bottom).

3.2.2 Cell model

Modelling and simulation on cell level is carried out within a framework that has first been presented in detail in [7]. It is based on a physical description of various processes inside an SOFC. A detailed two-dimensional description of one single channel of the cell is used as illustrated in Figure 3.4. The model includes gas flow along the gas channels via Navier-Stokes conservation equations. Diffusion of gases through the porous electrodes is described by coupled Fickian/Knudsen diffusion and Darcy flow. Charge transport (e.g. through the electrolyte) is described two-dimensional with Ohm's law. The electrical double layer at the boundary between nickel and YSZ is modelled as an ideal capacitor. All model parameters are summarised in Table 3.1.

Anode electrochemistry is described using elementary kinetics for surface reactions and charge transport on the surfaces of nickel and YSZ. Surface and charge transfer reactions are summarised in Table 3.2. A single hydrogen spillover between nickel and YSZ surface as active charge transfer step is assumed with a symmetry factor of 0.5. Furthermore, reformate gases containing CO, CO_2, and CH_4 were used for some simulations carried out in this work. The reaction mechanism for reformate gases is not shown here but was taken from [43].

Model parameters	Value	Reference
Gas channel		
Length	65 mm	set-up
Channel cross-sectional area	1.07 mm^2	set-up
Channel perimeter	3.8 mm	set-up
Electrodes (mesh anode, anode, cathode, mesh cathode)		
Layer thickness	370 µm, 295 µm, 10 µm, 50 µm	SEM
Porosity	0.6, 0.3, 0.27, 0.5	SEM
Pore diameter	150 µm, 2 µm, 1 µm, 100 µm	SEM
Particle diameter	100 µm, 2 µm, 3.5 µm, 50 µm	SEM
Tortuosity	2, 4*, 2, 2	[16], *fit
Anode		
Active TPB length	4.6e12 $m\,mm^{-3}$	[8]
Specific YSZ surface area	2.0e6 $m^2\,m^{-3}$	[8]
Specific nickel surface area	4.6e6 $m^2\,m^{-3}$	fit
Surface site density nickel	6.1e-9 $mol\,cm^{-2}$	[8]
Surface site density YSZ	1.3e-9 $mol\,cm^{-2}$	[8]
Structural factor el. conductivity	0.3	[8]
Electrolyte		
Thickness	10 µm	set-up
El. conductivity: preexp. factor,	5.15e7 $S\,K\,m^{-1}$,	[8]
activation energy	84 $kJ\,mol^{-1}$	[8]
Additional resistances		
Contact resistances etc.: r_0, α	7.7e-5 $\Omega\,m^2$, -1.1e-3 K^{-1}	EIS
Double layer capacities		
Anode	3.0e5 $F\,m^{-3}$	fit
Cathode	8.5e6 $F\,m^{-3}$	fit

Table 3.1: Electrochemistry model parameters that were used for all simulations shown in this work. Some of the values are further used for other calculations, e.g. layer thicknesses for thermal calculations.

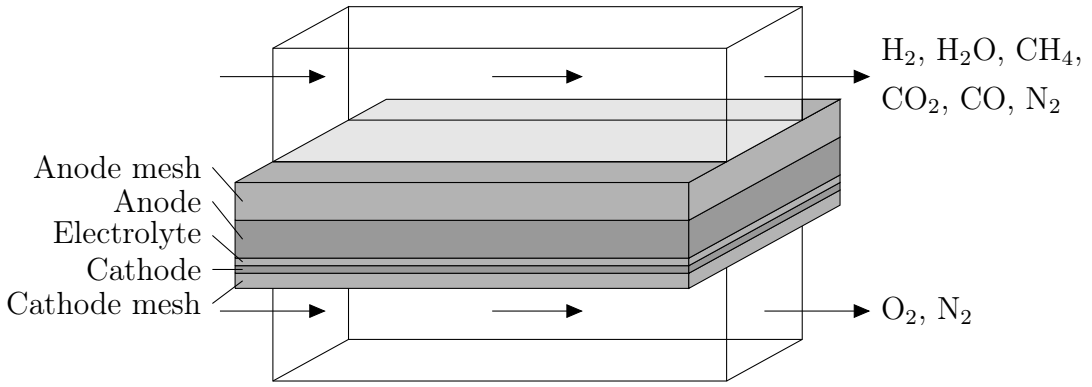

Figure 3.4: Two-dimensional modelling domain for simulations on cell level.

At the cathode the global Butler-Volmer equation

$$i = i_0 \left(\frac{p_{\mathrm{O_2}}}{p_0} \right)^b e^{-\frac{E_{\mathrm{act}}}{RT}} \left(e^{\frac{0.5F\eta_{\mathrm{act}}}{RT}} - e^{\frac{-0.5F\eta_{\mathrm{act}}}{RT}} \right) \tag{3.1}$$

with exchange current density i_0, oxygen partial pressure $p_{\mathrm{O_2}}$, standard pressure p_0, oxygen exponent b and activation energy E_{act} is used to model electrochemistry. Again, a symmetry factor of 0.5 is assumed. Values were obtained by fitting to experimental results (see Table 3.2).

All simulations on cell level are carried out under isothermal conditions. Temperature gradients along the gas channels are neglected. This assumption was made for simplicity. As heat is transported through the cell rather quickly, this assumption is reasonable for small cells. However, deviations between simulation and experiment can be caused by disregarding these inhomogeneities especially at high current densities due to high local heating or under operation with reformate gases due to local reforming processes that cool the cell. Temperature gradients are only taken into account on stack level as described in the following section.

3.2.3 Stack model

The framework of the stack model is visualised in Figure 3.5. Five electrochemistry models (as described in the previous section) are used to describe five entire cells consisting of 34 channels each. Anode and cathode gas flows are evenly distributed to the cells. Gas leakages of the experimental set-up are included in the model and estimated with 10 %.

Anode reaction	Preexponential factor	Activation energy
Charge transfer reaction		
$H_{Ni} + OH^-_{YSZ} \rightleftharpoons \square_{Ni} + H_2O_{YSZ} + e^-$	$6.02e5\,mol\,m^{-1}\,s^{-1}$	$242\,kJ\,mol^{-1}$
YSZ surface reactions		
$H_2O + \square_{YSZ} \rightleftharpoons H_2O_{YSZ}$	$6.6e11\,cm^3\,mol^{-1}\,s^{-1}$	0
$H_2O_{YSZ} + O^{2-}_{YSZ} \rightleftharpoons 2OH^-_{YSZ}$	$1.6e22\,cm^2\,mol^{-1}\,s^{-1}$	$9.6\,kJ\,mol^{-1}$
$O^X_{O_{YSZ}} + \square_{YSZ} \rightleftharpoons V^{\bullet\bullet}_{O_{YSZ}} + O^{2-}_{YSZ}$	$1.6e22\,cm^2\,mol^{-1}\,s^{-1}$	$91\,kJ\,mol^{-1}$
Nickel surface reactions		
$H_2 + 2\square_{Ni} \rightleftharpoons 2H_{Ni}$	$9.8e17\,cm^5\,mol^{-1}\,s^{-1}$	0
$H_2O + \square_{Ni} \rightleftharpoons H_2O_{Ni}$	$1.4e10\,cm^3\,mol^{-1}\,s^{-1}$	0
$H_{Ni} + O_{Ni} \rightleftharpoons OH_{Ni} + \square_{Ni}$	$5.0e22\,cm^2\,mol^{-1}\,s^{-1}$	$98\,kJ\,mol^{-1}$
$H_2O_{Ni} + O_{Ni} \rightleftharpoons 2OH_{Ni}$	$5.4e23\,cm^2\,mol^{-1}\,s^{-1}$	$209\,kJ\,mol^{-1}$
$H_{Ni} + OH_{Ni} \rightleftharpoons H_2O_{Ni} + \square_{Ni}$	$3.0e20\,cm^2\,mol^{-1}\,s^{-1}$	$43\,kJ\,mol^{-1}$

Cathode reaction	Exchange current density i_0	Activation energy E_{act}	b
$\frac{1}{2}\,O_2 + V^{\bullet\bullet}_{O_{YSZ}} + 2e^- \rightleftharpoons O^X_{O_{YSZ}}$	$1.52e10\,A\,m^{-2}$	$136\,kJ\,mol^{-1}$	0.2

Table 3.2: Elementary kinetic reaction mechanism for the anode and global cathode reaction mechanism. Values for the surface reactions are taken from [8]. Values of the anode charge transfer and cathode reaction are fitted to experiments.

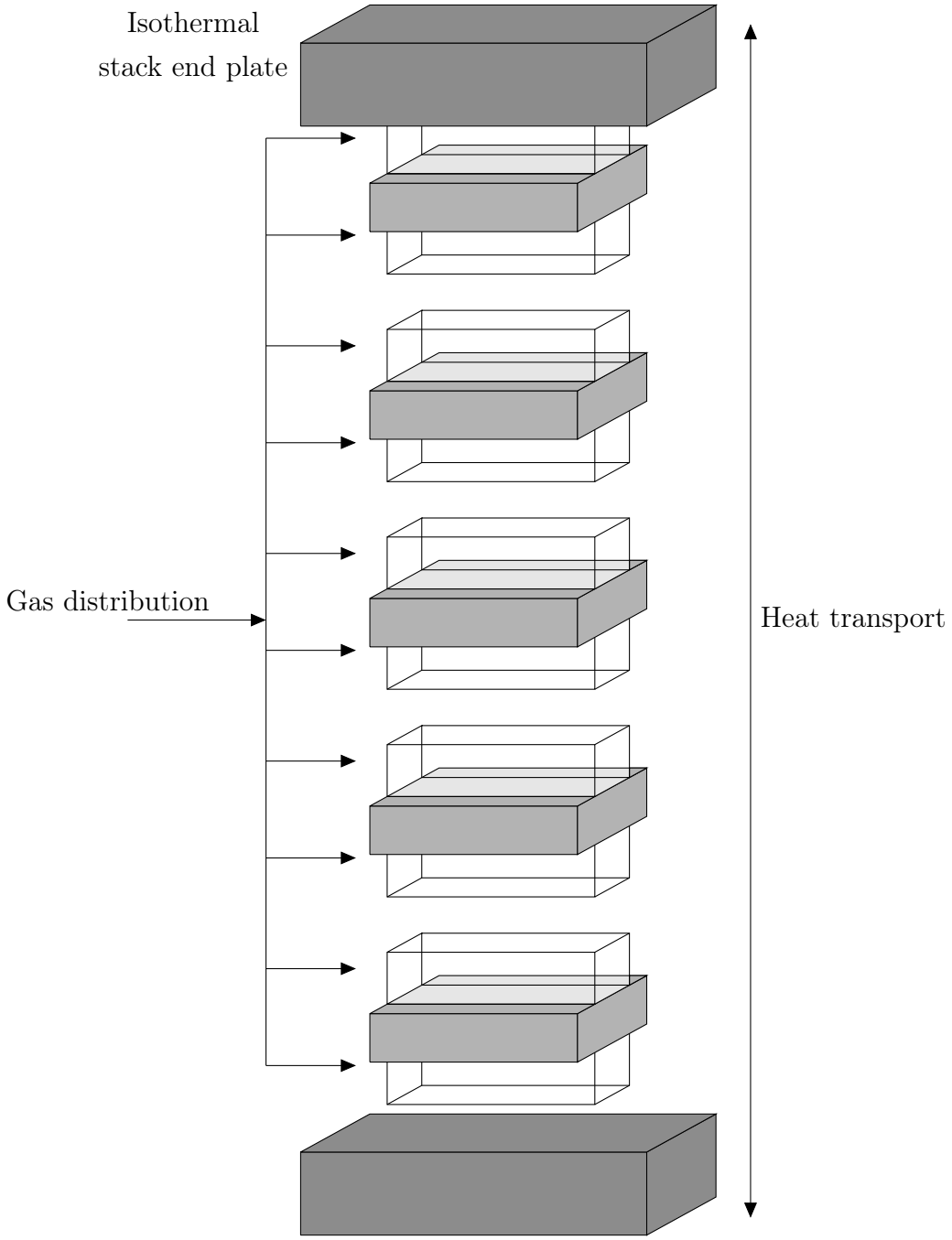

Figure 3.5: Sketch of five-cell stack model. Each cell is modelled using a 2D cell model as described in Section 3.2.2. Gases are evenly distributed to all cells. Thermal energy is transported via conduction to adjacent cells and stack end plates. End plates are assumed to be at constant furnace temperature.

Thermal calculations are the core part of the stack model. Heat capacities of all different stack parts including electrodes, electrolytes, bipolar plates, and cassettes are calculated and added up to the heat capacity of a single cell c_{cell}. Furthermore, cooling and heating due to overpotentials, internal reforming reactions, gas flows through the cells, and heat transfer to adjacent cells / end plates are considered for a global energy balance that is calculated for each cell i with

$$c_{\text{cell},i}\frac{\mathrm{d}T_i}{\mathrm{d}t} = P_{\Delta H,i,\text{an}} + P_{\Delta H,i,\text{ca}} - P_{\text{el},i} + P_{\text{trans},i} \ . \tag{3.2}$$

Enthalpy changes of gas mixtures are caused by changes in gas composition and temperature that are due to fuel consumption and internal reforming reactions. The maximum power $P_{\Delta H,i}$ that is available for heating and cooling of the cells due to these changes is calculated with

$$P_{\Delta H,i} = H(T)_{\text{out}}\dot{n}_{\text{out}} - H(T)_{\text{in}}\dot{n}_{\text{in}} \tag{3.3}$$

with the temperature dependent enthalpy of gas mixture $H(T)$ and the molar gas flow $\dot{n}$ for both anode and cathode gas flows. The power $P_{\Delta H,i}$ needs to be reduced by the electrical power output

$$P_{\text{el},i} = E_i I \tag{3.4}$$

with the cell voltage E_i and the stack current I as $P_{\Delta H,i}$ is only partially releases as thermal energy. Thermal power that is transferred between adjacent cells is calculated with

$$P_{\text{trans},i} = \frac{A\lambda}{d}(\Delta T_{i+1,i} + \Delta T_{i-1,i}) \tag{3.5}$$

with thermal conductivity of the interconnector λ, contact area A, interconnector thickness d and temperature difference

$$\Delta T_{i+1,i} = T_{i+1} - T_i \tag{3.6}$$

between two adjacent cells. Heat transfer between cells and stack end plates is calculated accordingly. Different values for the contact area A are chosen between adjacent cells and between cell and end plate in order to account for different contacting. The two stack end plates are assumed to be isothermal at furnace temperature as their thermal mass and heat conduction to other parts of the test set-up is comparably large. Thermal parameters of the stack model are summarised in Table 3.3.

Simulations of the stack model are carried out using Matlab. The entire stack model is able to simulate polarisation curves at steady-state and dynamic conditions. For

steady-state simulations the equilibrium is found numerically. Dynamic polarisation curves include thermal effects that are caused by varying the current gradient. The model further allows calculation of electrochemical impedance spectra at different load points.

3.2.4 Model validation

The existing model was adapted to reflect the experimentally investigated cells. The anode mesh of the model describes the nickel mesh of the experimental cell. Anode substrate and functional layer are combined in the model anode. Electrolyte, cathode, and cathode mesh of the model represent electrolyte, cathode functional layer, and cathode current collector of the experimental cell, respectively (see Figures 3.3 and 3.4). A large number of different parameters was modified. Geometrical parameters could either be measured directly from the existing set-up (e.g. channel length) or were estimated from SEM images (e.g. electrode porosity). Electrochemical impedance spectroscopy was used to determine ohmic resistances. Some parameters that could not be determined were either taken from existing literature or fitted to experimental results. However, fitting of parameters was carried out only within physically realistic limits. All values including references are summarised in Table 3.1.

Several sets of validation experiments were performed (Figures 3.6–3.10) in order to separately fit unknown parameters. Sensitivity analyses carried out by the author (unpublished) and found in literature [30] were previously used to identify dominating effects. Preexponential factor and activation energy of the anode charge transfer reaction as well as exchange current density and activation energy of the cathode Butler-Volmer equation (Eq. 3.1) are fitted to all sets of experiments as these values have significant influence under all operating conditions. The exponent b of Eq. 3.1 describes pressure dependency of the Butler-Volmer equation and is therefore fitted to polarisation curves at different pressures (Table 3.4, No. 1, 4, 5). Polarisation curves with low H_2 (anode) or O_2 (cathode) content (Table 3.4 No. 7, 9 ,10) are most sensitive to gas diffusion as they are operated close to diffusion limitation (see Section 4.1.4). Tortuosity of both electrodes is therefore adapted to improve agreement between experiments and simulations at these conditions. The active nickel surface area strongly influences the reforming reactions taking place at the anode surface due to its catalytic behavior. This value is therefore fitted to open circuit voltages with reformate gases (Table 3.4, No. 11-12). As double-

Thermal model parameter	Value	Reference
Nickel anode mesh		
Density	$8900\,\mathrm{kg\,m^{-3}}$	[81]
Specific heat capacity	$518\,\mathrm{J\,kg^{-1}\,K^{-1}}$	[81]
Nickel-YSZ anode		
Density	$6870\,\mathrm{kg\,m^{-3}}$	[81]
Specific heat capacity	$595\,\mathrm{J\,kg^{-1}\,K^{-1}}$	[81]
YSZ electrolyte		
Density	$5900\,\mathrm{kg\,m^{-3}}$	[81]
Specific heat capacity	$606\,\mathrm{J\,kg^{-1}\,K^{-1}}$	[81]
LSM cathode and cathode mesh		
Density	$6570\,\mathrm{kg\,m^{-3}}$	[81]
Specific heat capacity	$573\,\mathrm{J\,kg^{-1}\,K^{-1}}$	[81]
Crofer interconnector		
Density	$7700\,\mathrm{kg\,m^{-3}}$	estimated
Specific heat capacity	$630\,\mathrm{J\,kg^{-1}\,K^{-1}}$	estimated
Thickness	0.3 mm	set-up
Thermal conductivity	$0.54\,\mathrm{W\,m^{-1}\,K^{-1}}$	fit
Thermal contact resistance between cells and end plates		
Cell $\Leftrightarrow$ cell contact area	2.7e-3 $\mathrm{m^2}$	estimated
Cell $\Leftrightarrow$ end plate contact area	1.2e-3 $\mathrm{m^2}$	fit
Thickness	0.3 mm	set-up
Thermal conductivity	$0.54\,\mathrm{W\,m^{-1}\,K^{-1}}$	fit
Casette		
Density	$7700\,\mathrm{kg\,m^{-3}}$	estimated
Specific heat capacity	$630\,\mathrm{J\,kg^{-1}\,K^{-1}}$	estimated
Thickness	3 mm	set-up
Area	$0.021\,\mathrm{m^2}$	set-up

Table 3.3: Thermal model parameters of stack model used for all simulations to calculate heat capacities and thermal conductivities of different stack components.

No.	T (K)	p (MPa)	Cathode (%)		Anode (%)					
			N_2	O_2	H_2	N_2	H_2O	CO	CO_2	CH_4
1	1023	0.4	79	21	48.5	48.5	3	0	0	0
2	923	0.4	79	21	48.5	48.5	3	0	0	0
3	1073	0.4	79	21	48.5	48.5	3	0	0	0
4	1023	0.135	79	21	48.5	48.5	3	0	0	0
5	1023	0.8	79	21	48.5	48.5	3	0	0	0
6	1023	0.4	40	60	48.5	48.5	3	0	0	0
7	1023	0.4	94	6	48.5	48.5	3	0	0	0
8	1023	0.4	79	21	90	7	3	0	0	0
9	1023	0.4	79	21	15	82	3	0	0	0
10	1023	0.4	79	21	15	35	50	0	0	0
11	1023	0.4	79	21	58.4	0	20	12.2	5.5	3.9
12	1023	0.4	79	21	18	0	34	2	27	19

Table 3.4: Overview of operating conditions for measured and simulated polarisation curves that were used for model validation. In general, values were measured at steady state. Conditions No. 3 were also used for a dynamic polarization curve with a current increase / decrease of $0.07\,\mathrm{A\,s^{-1}}$. Electrochemical impedance spectroscopy was carried out at conditions 1, 4, and 5. Cathode volume flows were set to 21 nlpm for the entire stack. Anode flows were set to 10 nlpm for No. 1-10, 5.63 nlpm for No. 11, and 5.05 nlpm for No. 12.

layer capacities of anode and cathode are only relevant for dynamic processes, they are fitted to match the phase of impedance spectra. Heat conduction between cells and stack end plates is fitted to the reference polarisation curve (Table 3.4, No. 1) in order to correctly calculate different cell temperatures at various current densities. Note that thermal conductivity is rather low compared to realistic values for metals. However, this value also includes the thermal contact resistance.

Simulated and experimental polarisation curves are plotted in Figures 3.6 and 3.7. Reference conditions (Table 3.4, No. 1) are compared to polarisation curves with different pressure, temperatures, and gases. Results generally show good qualitative agreement between model and experiment. The top diagram of Figure 3.6 shows a comparison be-

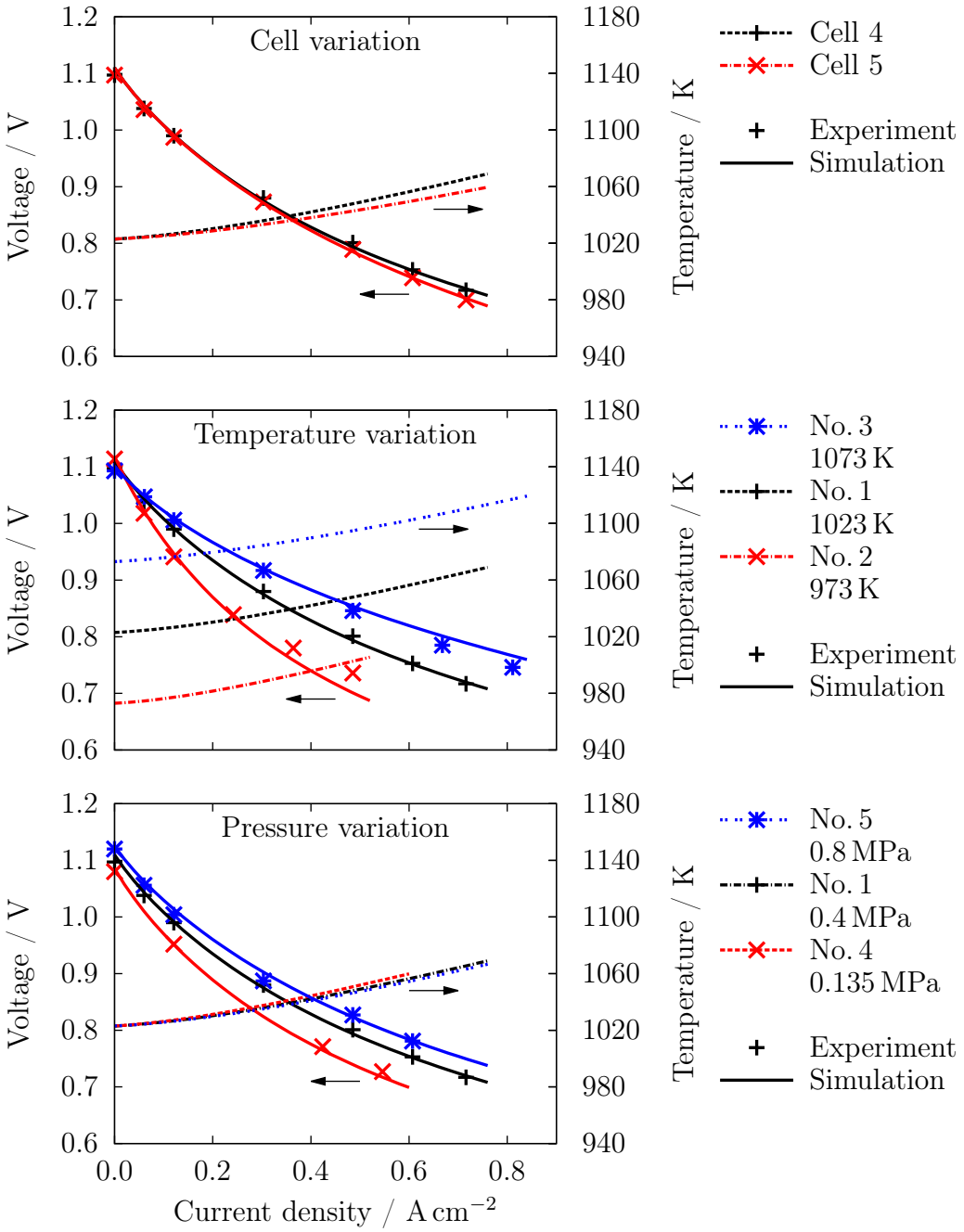

Figure 3.6: Comparison of experimental and simulated polarisation curves. The top diagram shows a comparison of the upper two cells of the stack at reference conditions (Table 3.4, No. 1). The lower two diagrams show the influence of temperature and pressure on polarisation curves. The legend indicates the operating conditions according to Table 3.4.

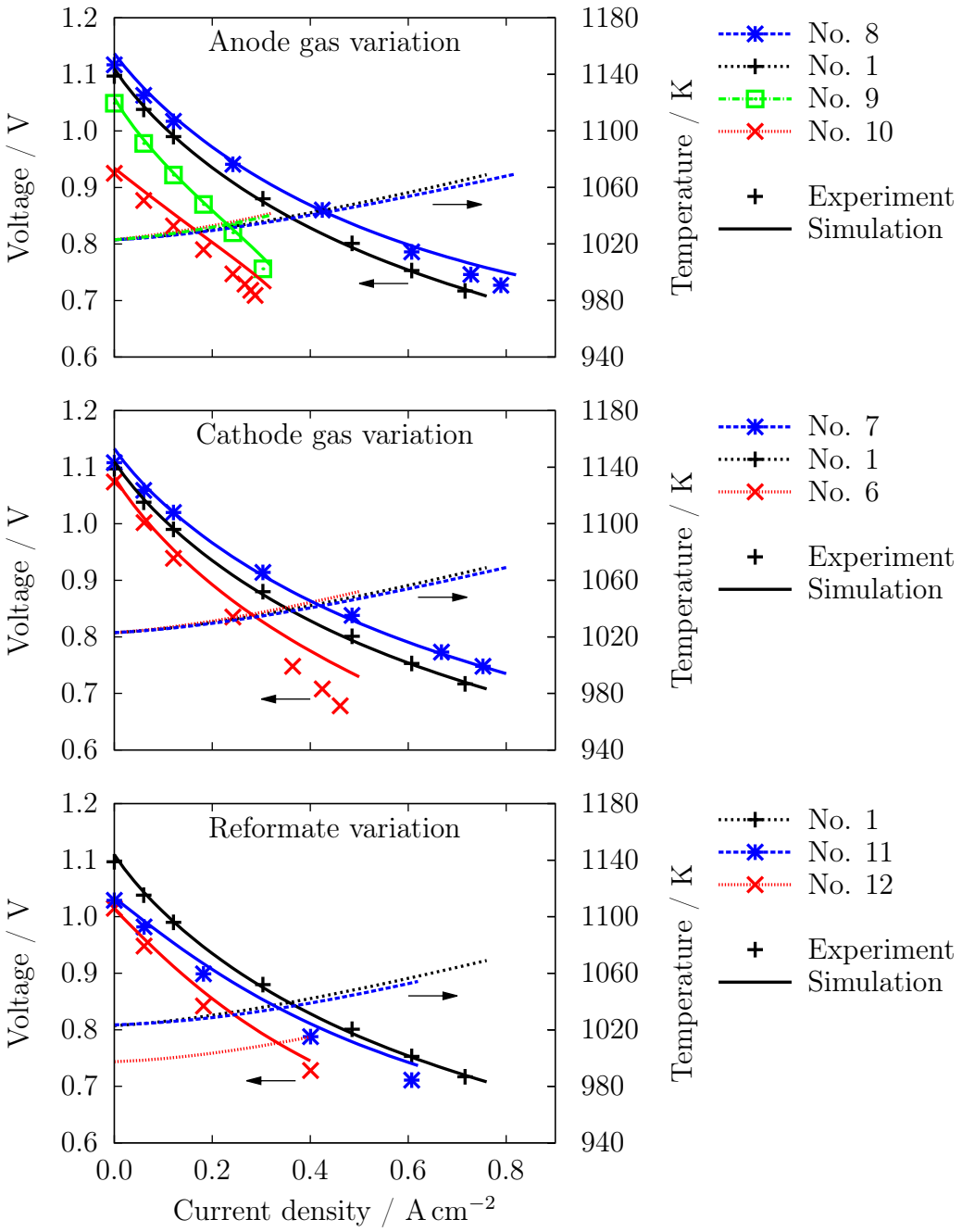

Figure 3.7: Comparison of experimental and simulated polarisation curves with different gas compositions. The legend indicates the operating conditions including the different gas compositions according to Table 3.4.

tween cells 4 and 5. Performance difference is attributed to differences in cell temperature of up to 10 K at these conditions. The increase in cell temperature with increasing current density is validated by analysing ohmic resistance using electrochemical impedance spectroscopy (Re Z at Im $Z = 0$) as shown in Figure 3.8. An increase in current density causes the stack to heat up thus reducing ohmic resistance.

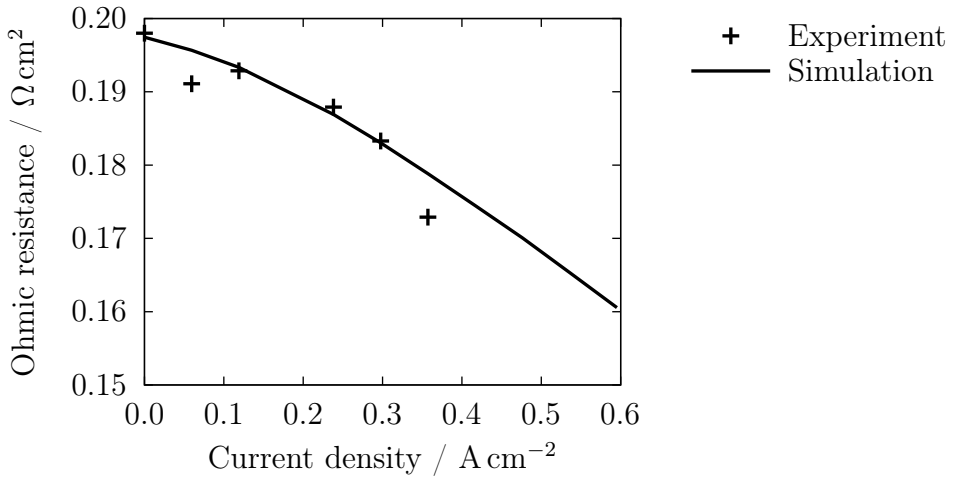

Figure 3.8: Comparison of experiment and simulation of area specific ohmic resistance of a single SOFC cassette during a polarisation curve at reference conditions (Table 3.4, No. 1). Experimental values are obtained using electrochemical impedance spectroscopy. Ohmic resistance decreases with increasing current density due to a load induced temperature increase.

Figure 3.6 further shows a variation of temperature and pressure. Temperature shows a strong influence on cell performance. Whereas OCV decreases with increasing temperature, polarisation resistance is reduced resulting in a generally better performance at high temperature. This behaviour also causes a stronger temperature increase with increasing current density at low temperatures due to higher overpotentials. Results for pressure variation are shown in the bottom diagram of Figure 3.6. An increase in pressure generally causes an increase in performance. Pressure related effects are described in detail in Section 4.

Figure 3.7 shows model validation with different gas compositions. The top diagram shows a variation of anode gas composition. High hydrogen concentrations cause higher OCV and significantly better performance than gas compositions with less hydrogen. High water vapour content further decreases performance. A similar effect is

visible from the middle diagram for variations in oxygen concentration at the cathode although the influence is not as strong. The bottom diagram compares different anode gas mixtures containing reformate gases (CO, CO_2, CH_4). For these measurements anode volume flows were reduced providing the same theoretical maximum current density compared to reference conditions. Operation with reformates causes lower OCV due to high product concentrations in the anode gas. For low methane concentrations (3.9 % CH_4, No. 11) this performance difference decreases with increasing current density especially when regarding simulation results. Higher methane concentration (19 %, No. 12) causes endothermic reforming reactions inside the cell, cooling it to 30 K below furnace temperature. This drop in temperature is the main reason for the observed performance differences. Detailed analyses of SOFC operation with reformate fuels including temperature effects have been presented here [109, 110].

Figure 3.9 presents a measured and simulated dynamic polarisation curve. Current density is increased / decreased with a rate of $0.07\,\mathrm{A\,s^{-1}}$. Increasing current density causes the cell to heat up slowly. Simulations show that cell temperature further increases while current density is decreasing already before the cell finally cools down slowly. This temperature development results in a better performance of the cell during the backward polarisation curve. After the full cycle, cell temperature is still 15 K higher compared to furnace temperature.

Figure 3.10 shows Nyquist and Bode plots of impedance spectra for three different pressures. Impedance spectra are very useful for model validation as they allow for experimental separation of different processes that are dominant at different excitation frequencies. Three different arcs are distinguishable from the Nyquist plot. For the investigated cells, these are generally attributed to polarisation resistance at the anode (low frequencies) [49, 50], polarisation resistance at the cathode (intermediate frequencies) [49, 50], and gas conversion resistance (high frequency) [5, 82]. Ohmic and overall resistance are given at Im $Z = 0$ at low and high frequency, respectively. Experiment and simulation generally show good agreement with only small deviation in the phase. The model correctly reproduces pressure related effects. Overall impedance is significantly reduced with pressure. This improvement is mainly due to a reduction of anode and cathode polarisation resistance whereas gas conversion impedance is hardly affected.

All simulation results are obtained with the same set of paramters. Most of these were either obtained experimentally or else estimated from literature values. All fitted

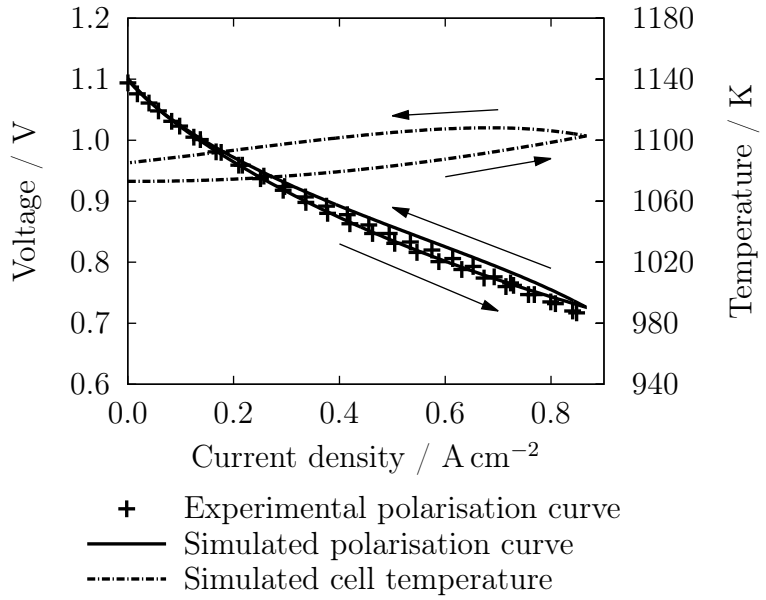

Figure 3.9: Experimental validation of simulated dynamic polarisation curve. The diagram shows the temperature related difference in performance while increasing and decreasing current density during measurement of a polarisation curve. Operating conditions are listed in Table 3.4 No. 3.

parameters are within physically realistic limits. Experiments and simulations show good agreement within a broad range of operating conditions. Furthermore, comparison of experimental and simulated electrochemical impedance spectra prove that the dominating pressure related effects are correctly predicted by the model. The model can therefore be used to theoretically analyse pressure effects and to accurately predict SOFC performance for system simulations.

3.3 Thermodynamic Simulations

Thermodynamic simulations with the software package Cantera were carried out in order to assess the tendency to carbon formation at elevated pressure. Chemical equilibrium of anode feed gas in a range of temperature, pressure, and oxygen to carbon ratio (O/C) was calculated regarding 53 C-N-O-H gas phase species including up to C_3 hydrocarbons and solid graphite. Thermodynamic equilibria are calculated via the minimisation of Gibbs energy. More detailed information about the equilibrium calculations can be found in [32] and on the project website [31].

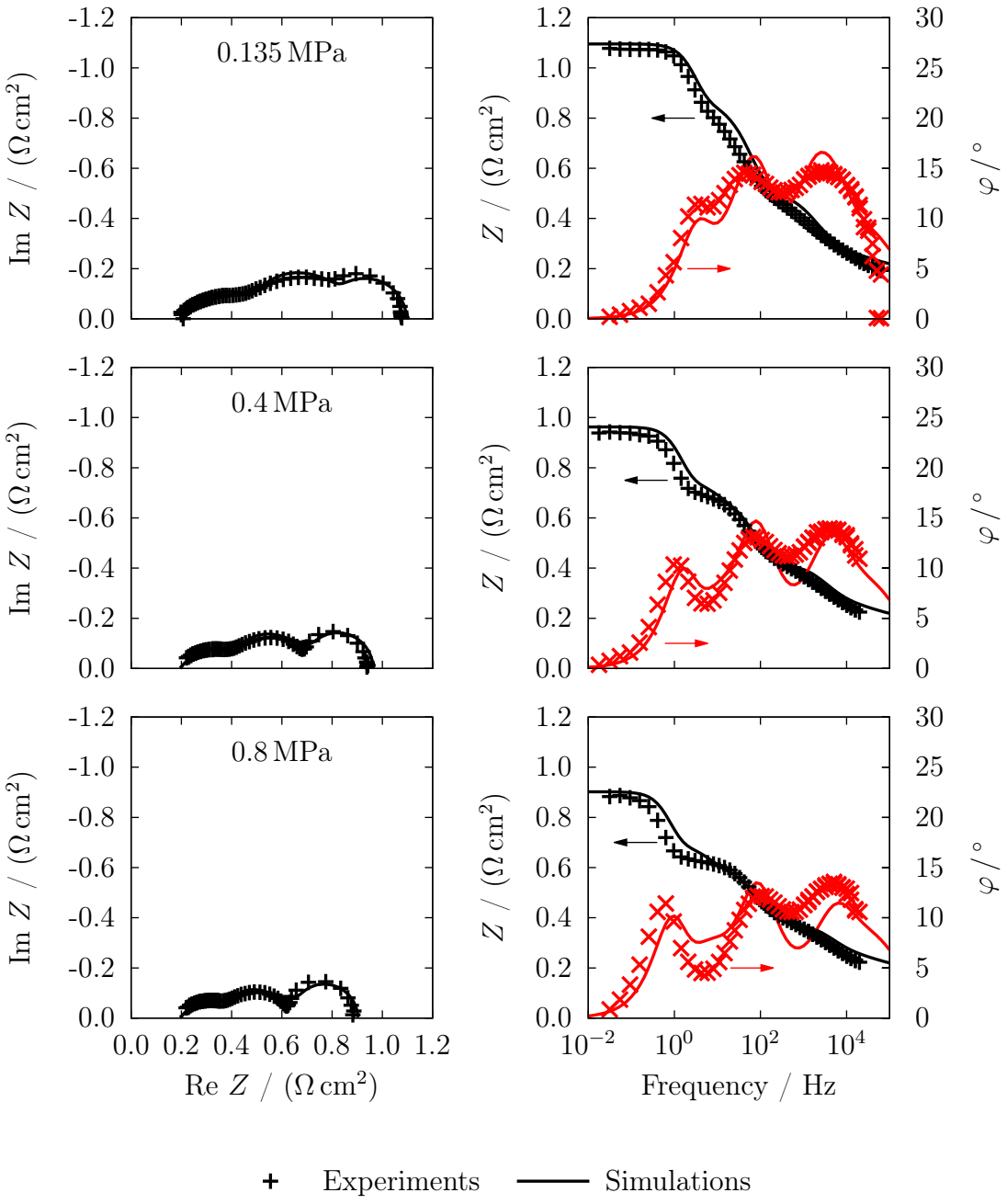

Figure 3.10: Comparison of measured and simulated impedance spectra for three different pressures. All operating conditions are listed in Table 3.4 (No. 4,1 and 5).

3.4 Modelling and Simulation on System Level

3.4.1 Model structure

The structure of the hybrid power plant model is illustrated in Figure 3.11. Air enters the compressor and is led through the pressure vessel. This configuration is chosen to prevent hydrogen accumulation inside the pressure vessel in case of gas leakages. Furthermore, it helps to prevent large pressure differences between pressure vessel and cathode gas compartment. Additionally, thermal energy that leaves the SOFC (and other system components located inside the vessel) is not lost but used to preheat the fresh air. After leaving the pressure vessel, the air is preheated via two heat exchangers (labelled 'Recuperator' and 'Heat exchanger'). A pressure loss caused by the SOFC system can be added if desired before the air enters the SOFC.

Cold fuel entering the system is mixed with hot recirculated anode gas. The fuel is pre-reformed inside the reformer and then enters the SOFC. Part of the anode off-gas is recirculated to provide steam for the reforming process. The remaining part is led into the combustor where it is burned. Cathode off-gas is led through a heat exchanger and into the combustor providing the oxygen for the combustion process. The hot gases are then expanded via the turbine and leave the system after preheating fresh air. The turbine drives the compressor as well as a generator that provides electrical energy apart from the fuel cell. A detailed description of all components and important operating conditions is given below.

Ambient conditions Ambient conditions influence the compression ratio and air mass flow that is provided by the compressor and thus influence the entire system. For this work the surrounding air is assumed to have a constant temperature of 298.15 K and to consist of 79% N_2 and 21% O_2 (molar fractions). Ambient pressure is assumed to be 0.1 MPa.

Model of Micro Gas Turbine The model of the micro gas turbine includes generator, compressor, turbine, combustor, and recuperator and is based on a model developed at the DLR Institute of Combustion Technology [78, 79]. The model represents a Turbec T100 micro gas turbine. A detailed description of all components is given in [79]. The model accounts for temperature and pressure losses. Compressor and turbine output

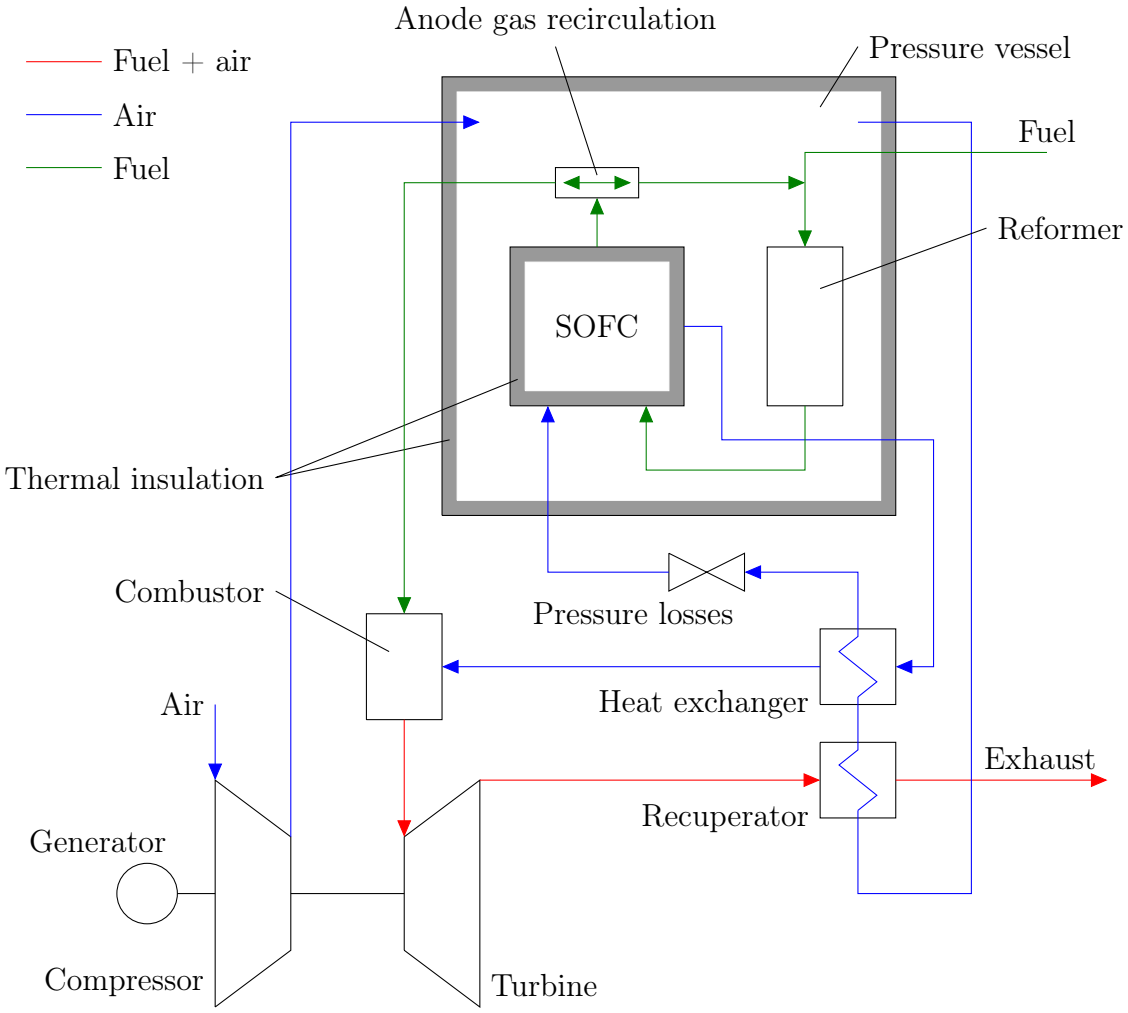

Figure 3.11: Hybrid power plant system model showing all different components that are included. A sensitivity analysis is carried out by varying the characteristics of different components.

is calculated using corresponding maps. Thermal effectiveness of the recuperator is adapted to the experimental device. The model was validated with experimental data.

Pressure losses Pressure losses are implemented in the model of the micro gas turbine depending on mass flow, temperature, and pressure of the fluid. However, pressure losses are not included in any part of the SOFC system (e.g. SOFC stack, piping). An additional absolute pressure loss can therefore be added as indicated in Figure 3.11 to account for these losses.

Thermal losses Thermal losses to the surroundings are generally not included in the parts of the system that do not belong to the model of the micro gas turbine. Besides those parts, only the model of SOFC and pressure vessel account for thermal losses. Please see the corresponding sections below for details.

Heat exchanger The heat exchanger transfers thermal energy from the cathode outlet gas to the fresh air. A value between 0 and 1 can be given where 0 means that no energy is transferred at all whereas 1 means that the maximum possible amount of thermal energy is transferred. The transfer is limited as the cold gas can only be heated up to the temperature of the hot gas, while the hot gas can only be cooled to the temperature of the cold gas.

Fuel supply A mixture of 94% CH_4 and 6% N_2 (molar fractions) is provided as fuel for all calculations presented in this work. This gas composition represents a typical mixture of natural gas. Further components that may be needed for fuel treatment (e.g. desulphurizer) are not regarded in this study.

Steam reformer The steam reforming process is modelled assuming thermodynamic equilibrium at the reformer outlet. Calculations are performed using the software package Cantera [31]. Results are simplified to only contain the gases H_2, N_2, H_2O, CO, CO_2, and CH_4. Anode gas entering the reformer contains both the fresh natural gas and the recirculated anode off gas from the SOFC. Due to mainly endothermic reactions, the gas mixture is cooled during the reforming process.

SOFC The SOFC is modelled as a variable number of SOFC stacks with 60 cells per stack. All cells are operated at equal conditions. The model presented in Section 3.2 is used. Unlike the model described there, temperature gradients inside the stack are neglected. This is reasonable as the stacks will be thermally insulated when operated in a system. Therefore, temperature differences between inner and outer cells are much smaller. Thermal losses to the surrounding pressure vessel are regarded via heat conduction through the stack insulation. It is assumed that the outer surface of every stack insulation is at average pressure vessel temperature and that all thermal energy that is conducted through the stack insulation is transferred to the pressure vessel gas. Each stack has a surface area of $0.11\,\mathrm{m}^2$ that is exposed to the pressure vessel air which corresponds approximately to the surface area of a 60-cell stack.

The SOFC stacks can be operated at varying electrical power output depending on the operating conditions. In this study power output and number of stacks are therefore analysed as separate independent parameters.

Anode gas recirculation The anode gas recirculation is modelled as a variable splitting device. A given part of the anode off gas is recirculated whereas the remaining part is led into the combustor. In theory, the fraction of recirculated gas can be varied between 0 (no recirculation) and 1 (everything is recirculated). However, very high recirculation rates would result in unacceptable high anode gas mass flows through the cell. Very low recirculation rates are also not possible as not enough steam would be provided for reforming which is likely to cause deposition of solid carbon inside different system components.

It is assumed that recirculation is realised via an ejector. The necessary energy for the recirculation is provided by pressurisation of the fuel inlet gas. It is assumed that a pressure of 1 MPa above SOFC pressure is sufficient. Changing this value does not influence any simulation results except for the system efficiency.

Pressure vessel The pressure vessel contains the reformer, the SOFC stacks and the anode gas recirculation. Air from the compressor flows through the pressure vessel. It is heated via thermal losses from the SOFC. Thermal energy leaves the pressure vessel via heat conduction to the surrounding atmosphere. It is assumed that heat conduction is determined by an average vessel gas temperature and a constant surrounding temperature of 298.15 K. In the model, an absolute value for thermal losses is given at a

temperature of 500 K. This value is used for a linear temperature dependency down to no losses at atmospheric temperature inside the vessel.

3.4.2 System control

The system control concept assumed for this work is based on a few simple assumptions. The general idea of the hybrid power plant is to use the high efficiency of the fuel cell to convert as much chemically bound energy into electrical energy as possible / reasonable and to use the energy that would normally be released as waste heat inside the gas turbine to generate additional electrical energy. Only due to this combination, exceptionally high electrical efficiencies are realised. In order to achieve highest efficiencies it is therefore not desirable to install separate cooling (or heating) cycles to keep certain system components like the SOFC at a constant temperature. The proposed system architecture therefore only includes cooling that is due to heat losses to the surroundings.

A second assumption is regarding the provision of fuel. Fuel is needed inside the SOFC and the combustion chamber but only a single fuel supply (entering the reformer) is regarded in this work. The combustion chamber does not have a direct fuel supply. This limitation is reasonable as extra fuel that may be needed inside the combustion chamber should always be provided via the SOFC if possible. Extra fuel — although unused — will increase the efficiency of the fuel cell and is therefore preferable to a direct feed to the combustion chamber. For steady-state operation this assumption is reasonable. In real system operation which will include dynamic processes like start-up, a direct feed of fuel may be necessary but should not be used in stationary operation.

A further assumption is concerning the operation of the turbine. For this study the turbine outlet temperature is set to 920 K. A rotation speed of the turbine is given to determine the operating point. This is in accordance with the stand-alone operation of the Turbec T100. SOFC power output is determined via an external power demand. As the SOFC will provide the major part of electrical energy this value will have to be changed in order to significantly change the power output of the entire system.

The only variable (assuming a given rotation speed of the turbine and a given power output of the SOFC) that remains for the control of the system is the fuel mass flow. This is controlled via the turbine outlet temperature. Additional fuel is provided if it is too cold and the amount of fuel is reduced if it becomes too hot. This approach

will always keep the gas turbine at the desired operating point. In this case, the SOFC will be operated at varying conditions depending on the current power demand. This variation should not yield considerable problems as long as the variation is kept within certain limits.

This control approach will limit the operating range of the system in terms of power variation. A larger range could be accomplished with additional cooling in case of high SOFC power and additional heating in case of low SOFC power. Temperature can only be controlled by indirect means e.g. via variable heat transfer within the system (see section above on heat exchanger) or by adjusting air flow via compressor rotational speed. Apart from its simplicity, the presented configuration offers the advantage that no unnecessary energy flows leave the system during normal operation which offers high potential for optimisation. Unlike other system configurations the ability of the fuel cell to operate under different conditions is used. This offers the possibility of good system performance over a wide range of electrical power.

3.4.3 Sensitivity analysis and operating range of a hybrid power plant

The aim of the sensitivity analysis on system level is to evaluate how changes of key characteristics of different components and changes in mode of operation will influence performance and efficiency of the hybrid power plant. Furthermore, the effect of these changes on the operating conditions of the SOFC is analysed. The evaluation is carried out based on the system control described in Section 3.4.2. Based on these results a system configuration is developed which offers high electrical efficiency over a wide power range while keeping operating conditions of the SOFC within acceptable limits.

A sensitivity analysis is carried out varying several of the components described in Section 3.4.1. These variations include the number of SOFC stacks, SOFC power output, the rate of anode gas recirculation, the fraction of heat transfer from the cathode off-gas to the fresh air, changes in SOFC and pressure vessel thermal insulation, additional pressure losses, and the operating point of the gas turbine. A set of standard conditions is determined based on the expected system behaviour. All parameters are separately varied within a certain range. Reference conditions and range of variation are summarised in Table 3.5.

Based on the results of the sensitivity analysis, fixed values for most parameters are chosen and variation is limited to SOFC power and rotational speed of the gas turbine.

Component variation	Reference value	Range
Number of stacks	400	350–450
SOFC Power (kW)	500	450–550
Anode gas recirculation rate	0.75	0.7–0.8
Heat exchanger transfer rate	0.4	0–0.8
Thermal losses of pressure vessel at 500 K average pressure vessel temperature (kW)	10	0–20
SOFC stack insulation thickness (m)	0.3	0.2–0.4
Pressure losses (Pa)	15000	0–30000
Rotational speed of gas turbine (1/min)	65000	63000–67000

Table 3.5: Reference conditions and variation range of different components used for sensitivity analysis.

These parameters should also be varied in the real operation of a hybrid power plant. The operating range of the power plant is investigated and electrical efficiencies are calculated over the entire power range. Electrical efficiencies are calculated with

$$\eta_{\mathrm{el}} = \frac{P_{\mathrm{el,GT}} + P_{\mathrm{el,SOFC}} - P_{\mathrm{el,aux}}}{\dot{n}\Delta H_{\mathrm{r,STP}}} \tag{3.7}$$

with the electrical power output of gas turbine ($P_{\mathrm{el,GT}}$) and SOFC ($P_{\mathrm{el,SOFC}}$), the electrical power demand of auxiliary devices ($P_{\mathrm{el,aux}}$), the molar fuel flow $\dot{n}$ and the molar enthalpy of reaction of the fuel $\Delta H_{\mathrm{r,STP}}$ assuming full conversion of methane to H_2O and CO_2 at standard conditions based on HHV and LHV. In this model, auxiliary power demand only includes the electrical power demand of a fuel compressor that has an efficiency of 70 %. Fuel is compressed to a pressure of 1 MPa above SOFC pressure thus providing the necessary energy to ensure functionality of the anode gas recirculation via an ejector. Power needed for the the system control is not regarded.

4 Influence of Pressurisation on SOFC Performance

This section consists of two main parts. In the first part, pressure effects are investigated from a theoretical point of view. The influence of pressure on thermodynamics, reaction kinetics, and gaseous transport in porous electrodes is analysed in order to understand different phenomena influenced by pressure. These findings are used in the second part to analyse experimental results. All simulations were carried out with the model presented in Section 3.2. Experiments were performed using the set-up presented in Section 3.1. Theoretical and experimental investigations were previously published in similar manner [35, 38]. All gas compositions in this section are given in mole-%. The enthalpies of reaction $\Delta H_{0,\mathrm{R}}$ are calculated with Equation 2.1 and thermodynamic data from [13, 66].

4.1 Theoretical Investigation of Pressure Effects

4.1.1 Numerical simulation results

In order to theoretically analyse SOFC behaviour at different pressures, isothermal 1D-simulations through the thickness of the MEA are carried out. This simplification allows for focussing on pressure effects that are not related to the gas flows. Changes in fuel concentration along the gas channels are neglected. Simulation results show MEA potential as if unlimited fuel were provided. Fuel cell performance is therefore overestimated compared with more realistic 2D-simulations or experimentally measured data. However, 1D-simulations help to clearly distinguish different physical effects.

For theoretical investigations a pressure range from 0.05 to 2 MPa is chosen. This helps to highlight pressure related effects that might be too small to be clearly visible within the experimental range (0.135 to 0.8 MPa). Simulations are performed with two different gas mixtures at the anode (Hydrogen mixture: 50% H_2, 50% H_2O; Reformate mixture: 58.4% H_2, 20.0% H_2O, 12.2% CO, 5.5% CO_2, 3.9% CH_4) and air (79% N_2, 21% O_2) at the cathode at an isothermal temperature of 1150 K. At these conditions different pressure effects are clearly distinguishable.

Results for both gas mixtures are shown in Figure 4.1. Three main pressure effects are obvious from both diagrams. First, open circuit voltage is higher at higher pressure. Second, the slope of the polarisation curve levels with increasing pressure. Third, the limiting current density is higher at elevated pressures. These three phenomena will be explained and analysed in more detail in the following three sections.

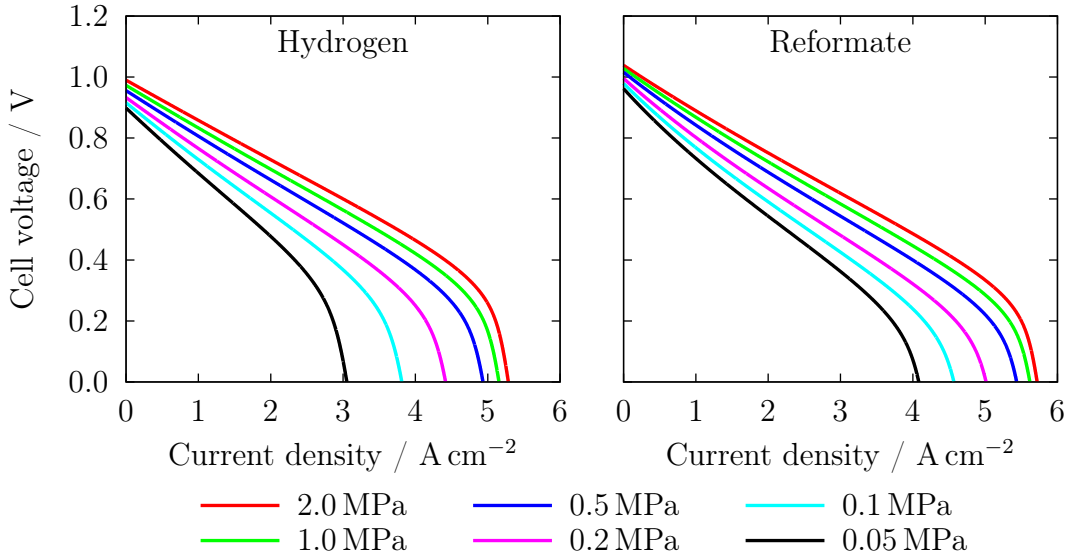

Figure 4.1: Results of isothermal 1D-simulations for two different gas mixtures (Hydrogen mixture: 50% H_2, 50% H_2O; Reformate: 58.4 % H_2, 20.0 % H_2O, 12.2 % CO, 5.5 % CO_2, 3.9 % CH_4). These results directly reflect the performance of the MEA. Results are shown for different pressures between 0.05 and 2 MPa at a temperature of 1150 K.

4.1.2 Thermodynamics

The increase in OCV caused by pressurisation is due to thermodynamics which is discussed in more detail in this section. At equilibrium conditions, the OCV of SOFC can be accurately approximated using the Nernst equation,

$$E = -\frac{\Delta G_0}{zF} - \frac{RT}{zF} \ln \prod a_i^{\nu_i} \ , \tag{4.1}$$

with Gibbs reaction enthalpy ΔG_0 (at standard pressure p_0, temperature T, and activities of 1) as well as activities a_i and stoichiometric coefficients ν_i (negative for reactants and positive for products) of all reactants and products. Numerical simulations are required for systems that are not in electrochemical equilibrium, e.g. fuel cells operated with reformate gases.

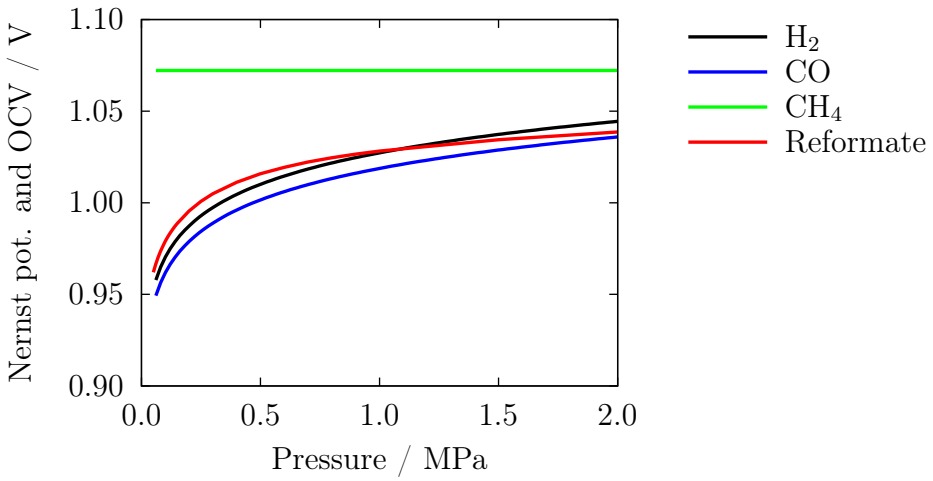

Figure 4.2: Influence of pressurisation on Nernst potential and OCV. Nernst potentials are calculated for different gases using Equations 4.5-4.7 assuming molar fractions of 0.25 for products (0.125 each for H_2O and CO_2 in case of methane) with air (21 % O_2) as oxidiser at a temperature of 1150 K. OCV of the reformate gas is given for the results shown in Figure 4.1.

The Nernst equation was applied to the oxidation of H_2, CO, and CH_4.

$$H_2 + 0.5\,O_2 \rightleftharpoons H_2O \qquad \Delta H_{0,R} = -242\,\mathrm{kJ\,mol^{-1}} \tag{4.2}$$

$$CO + 0.5\,O_2 \rightleftharpoons CO_2 \qquad \Delta H_{0,R} = -283\,\mathrm{kJ\,mol^{-1}} \tag{4.3}$$

$$CH_4 + 2\,O_2 \rightleftharpoons 2\,H_2O + CO_2 \qquad \Delta H_{0,R} = -802\,\mathrm{kJ\,mol^{-1}} \tag{4.4}$$

Using the definition of the mole fraction $X_i = p_i/p$ and assuming ideal gases ($a_i = p_i/p_0$), Equation 4.1 yields

$$E = E_0 + \frac{RT}{2F} \ln\left(\frac{X_{H_2} X_{O_2}^{0.5}}{X_{H_2O}}\right) + \frac{RT}{4F} \ln\left(\frac{p}{p_0}\right) \ , \tag{4.5}$$

$$E = E_0 + \frac{RT}{2F} \ln\left(\frac{X_{CO} X_{O_2}^{0.5}}{X_{CO_2}}\right) + \frac{RT}{4F} \ln\left(\frac{p}{p_0}\right) \tag{4.6}$$

and

$$E = E_0 + \frac{RT}{8F} \ln\left(\frac{X_{CH_4} X_{O_2}^2}{X_{H_2O}^2 X_{CO_2}}\right) \tag{4.7}$$

for H_2, CO, and CH_4 oxidation, respectively. The results of these equations at varying pressure are shown in Figure 4.2. Nernst potential is calculated for each gas with 25 % products and air (21 % O_2) as oxidiser. Values for ΔG_0 are calculated with data from Ref.

[57]. Hydrogen and carbon monoxide oxidation yield similar voltages both being pressure dependent. Pressure effects are greatest at very low pressures but still clearly visible at higher pressure. Nernst potential of methane oxidation is pressure independent. Open circuit voltages of the results shown in Figure 4.1 show qualitatively similar behaviour to the Nernst potentials of H_2 and CO as CH_4-concentration is very low or zero.

4.1.3 Kinetics

In this section the effect of pressurisation on reaction kinetics is discussed. Figure 4.3 shows the simulated polarisation resistance at a constant current density of $1\,\mathrm{A\,cm^{-2}}$. Polarisation resistance is significantly reduced with pressure for both gas mixtures. Improvement is most significant up to 0.5 MPa. The reduction in polarisation resistance is due to different overpotentials that are reduced with increasing pressure. Figure 4.4 shows activation (η_{act}), concentration (η_{conc}), and ohmic overpotentials (η_{ohm}) versus pressure at a constant current density of $1\,\mathrm{A\,cm^{-2}}$. Ohmic losses depend on temperature and current density but are constant with pressure. Concentration overpotentials depend on gas transport processes inside the cell and are discussed in the next section. Activation overpotentials are related to electrochemical reactions that occur inside the cell. In the present model, the kinetics of the anode are described by an elementary kinetic reaction mechanism [7] including adsorption, reaction and desorption processes.

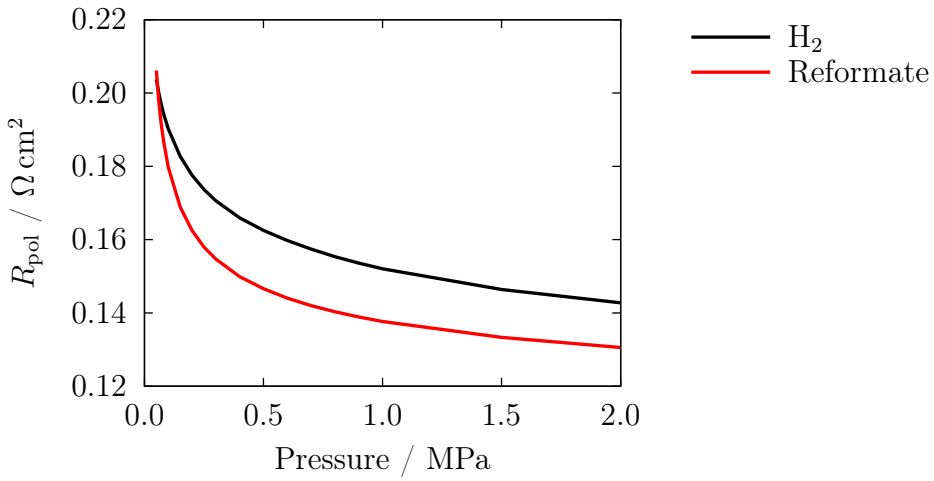

Figure 4.3: Influence of pressurisation on polarisation resistance at a constant current density of $1\,\mathrm{A\,cm^{-2}}$ for the polarisation curves shown in Figure 4.1.

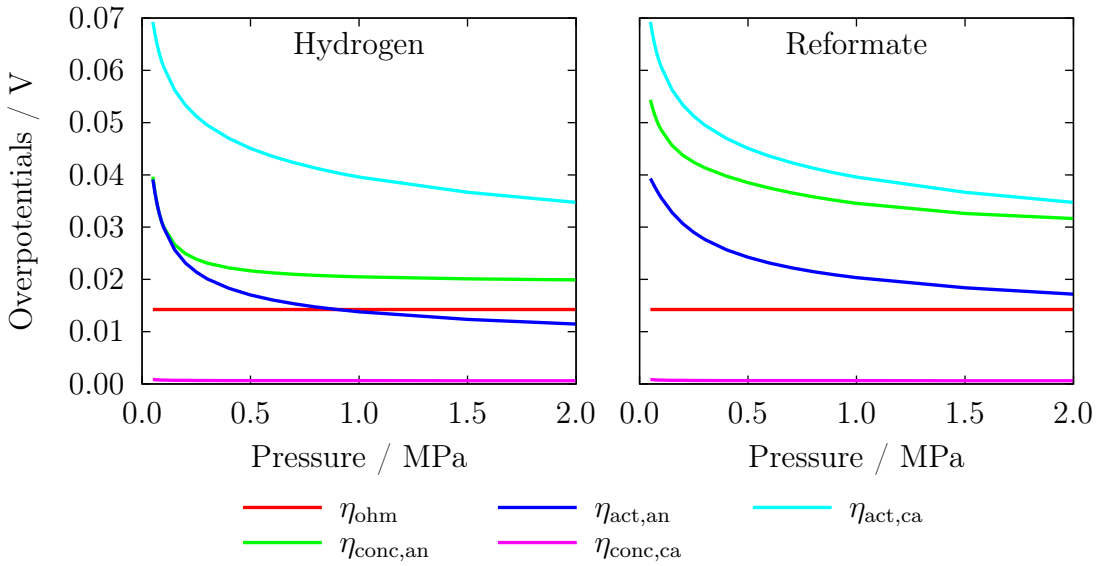

Figure 4.4: Pressure dependence of various overpotentials shown at a constant current density of 1 A cm^{-2} for the polarisation curves presented in Figure 4.1.

Activation overpotentials show a similar qualitative behaviour for both anode and cathode. They significantly decrease with pressure at low absolute pressure (up to about 1 MPa) whereas higher pressurisation has a considerably smaller effect. Activation overpotentials at the cathode are higher than those at the anode. The reduction due to pressurisation can be explained by enhanced surface coverage (number of surface sites that are occupied relative to the total number of surface sites) with reactant species as shown in Figure 4.5 for the anode nickel surface. Higher partial pressures of reactants (due to higher overall pressure) cause higher adsorption rates. At very low pressure, surface coverage with reactants is very low thus preventing the charge transfer reaction. This effect is more pronounced with the hydrogen gas mixture. The greatest change in surface coverage is calculated up to about 0.5 MPa. Further pressurisation yields a much smaller but still significant effect. This behaviour is directly reflected in the reduction of anode activation overpotentials as charge transfer is assumed to take place via spillover of adsorbed H atoms from the nickel surface to the YSZ surface [9, 108].

Cathode kinetics are modelled using a global Butler-Volmer equation in which the exchange current density depends on partial pressure of oxygen. This behaviour is reflected in the results of Figure 4.4. It is assumed that the reduction of cathode activation overpotentials are caused by effects similar to those at the anode.

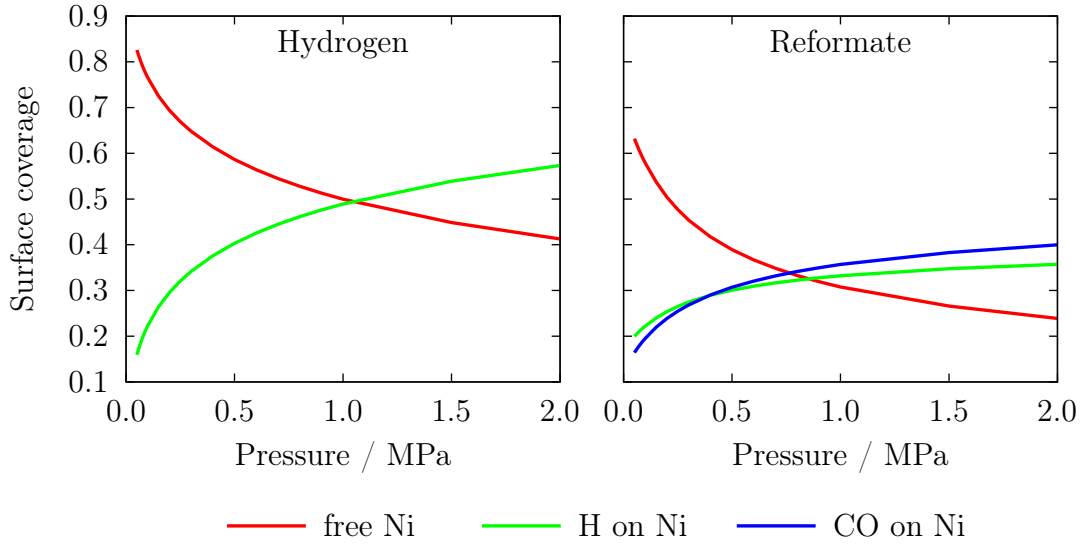

Figure 4.5: Pressure dependence of anode surface coverage with reactant species at a constant current density of 1 A cm^{-2} for the polarisation curves presented in Figure 4.1. Furthermore, free nickel sites are given. Surface coverage with other species is negligible.

4.1.4 Gas transport through porous electrodes

When gas flow rates through the gas channels are high enough (thus fuel utilisation is very low), the limiting current density is determined by the maximum diffusion of gases through the electrodes. For the investigated cells, the anode is about 10 times as thick as the cathode. Therefore diffusion of fuel generally is the limiting process. In this section the influence of pressure on gas transport through porous electrodes is discussed. For the following discussion it is assumed that diffusion takes place via Knudsen and ordinary diffusion mechanism as is the case in the present model.

The limiting current density $i_{\max}$ for diffusive transport through a porous media of thickness d is given by [4]

$$i_{\max} = zFD_{\text{eff}}(p)c_0(p)/d \ , \tag{4.8}$$

with c_0 being the concentration gradient of the diffusive species through the anode and D_{eff} being the diffusion coefficient inside the anode. In the following, both pressure dependent terms D_{eff} and c_0 are discussed.

The effective binary diffusion coefficient (here described as a combined Bosanquet

diffusion coefficient) is calculated via [6]

$$D_{\mathrm{eff}}^{ij} = \frac{\epsilon}{2\tau^2}\left[\left(\frac{1}{D_{\mathrm{K}}^{i}} + \frac{1}{D_{\mathrm{ord}}^{ij}}\right)^{-1} + \left(\frac{1}{D_{\mathrm{K}}^{j}} + \frac{1}{D_{\mathrm{ord}}^{ij}}\right)^{-1}\right] \tag{4.9}$$

with the porosity ϵ and tortuosity τ. The Knudsen diffusion coefficient D_{K} is given by

$$D_{\mathrm{K}} = \frac{2}{3} r_{\mathrm{p}} \sqrt{\frac{8RT}{\pi M}} \tag{4.10}$$

with the mean radius r_{p} of the electrode pores and the molar mass M of the diffusive gas. Knudsen diffusion coefficient is independent of pressure. Many different expressions are available for the calculation of the ordinary binary diffusion coefficient of gases D_{ord}^{ij} [46, 85]. Here as well as for the model an empirical expression derived by Fuller et al. [26, 27] is used,

$$D_{\mathrm{ord}}^{ij} = \frac{0.001 T^{1.75}\left(M_i^{-1} + M_j^{-1}\right)^{0.5}}{p\left(V_i^{\frac{1}{3}} + V_j^{\frac{1}{3}}\right)^2} \ , \tag{4.11}$$

with the molar masses M ($\mathrm{g\,mol^{-1}}$) of both gases, the Fuller diffusion volumes V ($\mathrm{cm^3}$) of both gases, temperature T (K), and pressure p (atm). The ordinary binary diffusion coefficient is therefore reciprocally proportional to pressure.

The concentration gradient is assumed to equal the concentration inside the anode gas channel. This assumption is adequate for 1D-simulations with constant fuel concentration inside the gas channel. It is assumed that all hydrogen that diffuses through the anode is consumed. Therefore, the hydrogen concentration at the three phase boundary equals zero. The concentration gradient $\mathrm{c_0}$ is directly proportional to pressure according to the ideal gas law,

$$c_0 = \frac{p}{RT} \ . \tag{4.12}$$

The relative importance of Knudsen and ordinary diffusion can be expressed via the Knudsen number Kn. It is calculated as

$$\mathrm{Kn} = \frac{L}{2r_{\mathrm{p}}} \tag{4.13}$$

with the molecular mean free path [46]

$$L = \frac{k_{\mathrm{B}} T}{\sqrt{2}\pi\sigma_{ij}^2 p} \tag{4.14}$$

with Boltzmann constant k_B and collision diameter

$$\sigma_{ij} = \frac{\sigma_i + \sigma_j}{2} \ . \tag{4.15}$$

Data for these values is taken from [85]. Combining Equations 4.8–4.12 considering pressure dependent terms only (all other parameters are assumed constant), results in a general form for the limiting current density,

$$i_{max} = \frac{p}{a_K + a_{ord} p} \ , \tag{4.16}$$

where a_K is a measure for the Knudsen diffusion resistance and a_{ord} a measure for the ordinary diffusion resistance. At very low pressure the term $a_{ord}p$ is negligible yielding

$$i_{max} \sim \frac{p}{a_K} \sim p \ . \tag{4.17}$$

At these pressures diffusion is governed by Knudsen diffusion mechanism thus collisions between molecules and wall are dominating (Kn >> 1). Knudsen diffusion mechanism itself is pressure independent and therefore the diffusive mass flux is governed by the concentration gradient c_0 which is proportional to pressure. Limiting current density i_{max} is therefore proportional to pressure as well. At very high pressures Equation 4.16 yields

$$i_{max} \sim \frac{p}{a_{ord} p} \tag{4.18}$$

as a_K is negligible. In this case diffusion is governed by ordinary diffusion mechanism thus inter-molecular collisions are dominating (Kn << 1). Ordinary diffusion is reciprocally proportional to pressure and thus cancelling out the pressure dependence of the concentration gradient. In this case, limiting current density i_{max} is therefore pressure independent.

Knudsen number is plotted in Figure 4.6 together with various diffusion coefficients for the anodic binary diffusion of H_2 and H_2O. The effective diffusion coefficient D_{eff} is smaller than all other diffusion coefficients due to the additional factor of $\frac{\epsilon}{2\tau^2}$. At low pressure diffusion takes place within the transition region of Knudsen and ordinary diffusion shifting to ordinary diffusion mechanism as pressure is increased.

The shift from Knudsen to ordinary diffusion mechanism with increasing pressure causes an increase in limiting current density as illustrated in Figure 4.7. Limiting current density is calculated analytically using Equations 4.8–4.12 (an.) and compared to

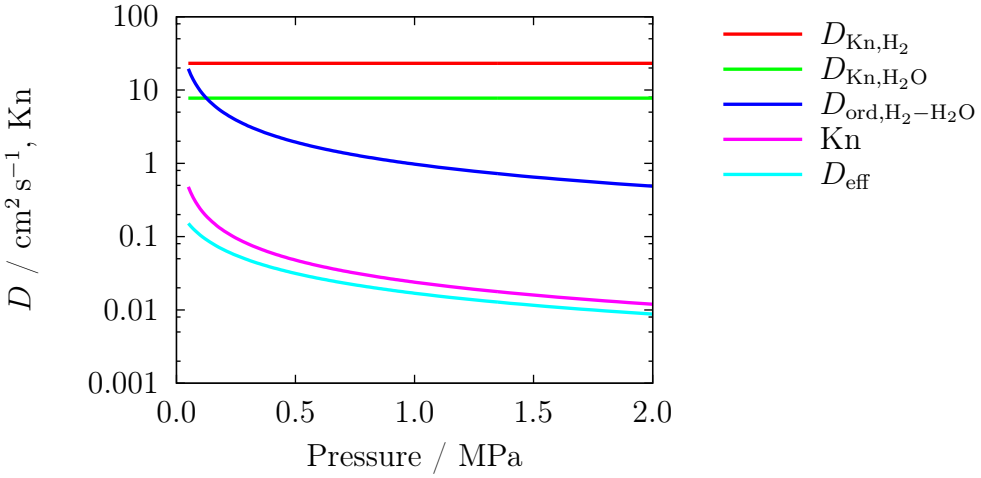

Figure 4.6: Influence of pressure on diffusion coefficients and Knudsen number.

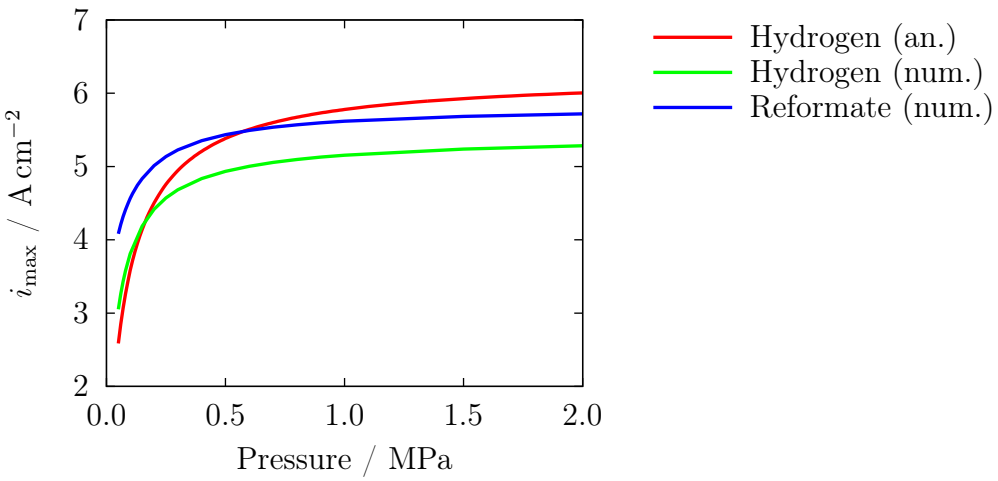

Figure 4.7: Influence of pressure on limiting current density calculated analytically (an.) and numerically (num.).

simulated results (num.). Both results are in good qualitative agreement, especially showing a strong pressure influence only up to about 0.5 MPa. The quantitative differences between analytical calculations and numerical simulations are due to simplifications in the analytical calculations. Here, the diffusion through the anode mesh is neglected. Furthermore, the numerical simulations consider that electrochemical reactions can take place within the anode volume. Diffusion therefore does not always have to take place through the entire anode. Simulated results for the reformate gas mixture include diffusion of all reactants and products. Qualitatively, pressure effects are very similar to the hydrogen gas mixture. Absolute values differ due to the higher portion of reactants in the fuel and different diffusive properties of the different gases.

4.2 Effect of Pressure on Power Density and Efficiency

In the previous section, pressure effects on different phenomena are analysed separately, under isothermal conditions and with unlimited reactant supply in order to clearly distinguish between different effects. This approach is very useful to understand the theory of different effects. However, is does not yield results that can be used to quantify pressure effects in real operation.

For this purpose, experimental results and more realistic 2D-simulations are used in order to analyse pressure influence on power density and efficiency both accounting for temperature effects within the stack as well as hydrogen and oxygen consumption along the gas channels. Both experiments and simulations were performed (see Section 3 for a detailed description of model and experimental set-up) at equal conditions. Furnace temperature was set to 1073 K. Air was used as cathode gas with a constant oxygen utilisation of 15 %. A mixture of 30 % hydrogen and 70 % nitrogen was chosen as fuel with a constant fuel utilisation of 40 %. For the simulations, a slight humidification of the fuel (3 % H_2O) was added in order to avoid numerical instabilities. All results reflect the performance of one of the inner cells of the five cell stack.

In Figure 4.8 polarisation curves at five different pressures are shown. In both diagrams the dots mark the same experimentally measured data. In the left diagram the polarisation curves are interpolated using exponential functions in the form of

$$E(i) = B\mathrm{e}^{Ci} \tag{4.19}$$

with voltage E, current density i and two fitting parameters B and C. Exponential

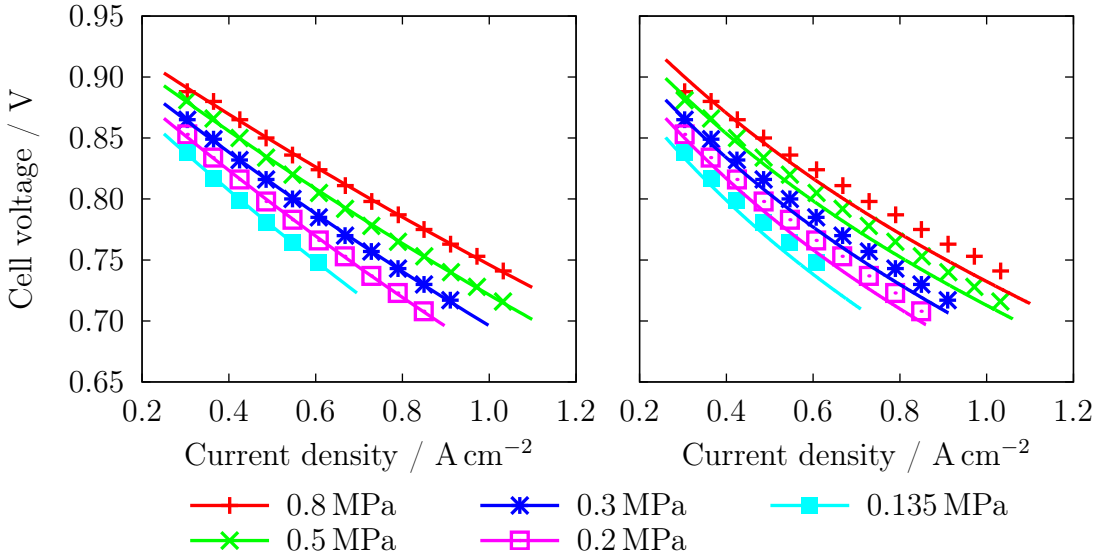

Figure 4.8: Polarisation curves at different pressure with constant fuel utilisation of 40 % and constant air utilisation of 15 %. In both diagrams, the dots mark the same experimentally measured data. In the left diagram, the lines are an interpolation according to Equation 4.19. In the right diagram, the lines are simulated polarisation curves.

functions are chosen as they offer excellent agreement with measured values. The exponential functions are used to calculate values for Figures 4.9 and 4.10 where experimental data was missing. The right diagram of Figure 4.8 shows measured data together with simulation results. Of course, simulation results do not reproduce experimental data as accurately as interpolation does but still show good agreement. Simulated values are generally lower due to the higher water content of the fuel.

Figure 4.9 shows the effect of pressure on power density at three different cell voltages. Electrochemical conversion efficiency is propotional to cell voltage. High voltages yield high conversion efficiencies whereas lower cell voltages result in lower conversion efficiencies. A strong increase in power density with pressure is obvious from experiments and simulations. Based on the experimental data, power density increases between 61 % at lowest voltage and 83 % at highest voltage with a pressure increase from 0.135 MPa to 0.8 MPa. Simulations yield similar increases. Results furthermore show that performance increase is strongest at low pressure and somewhat weaker at higher pressure. Nevertheless, pressure effects are significant over the entire range of pressure that is in-

vestigated. This effect is due to logarithmic pressure dependencies of various phenomena as discussed in Section 4.1. Concluding, Figure 4.9 shows that pressure can be used to significantly increase power density of an SOFC while keeping its efficiency constant.

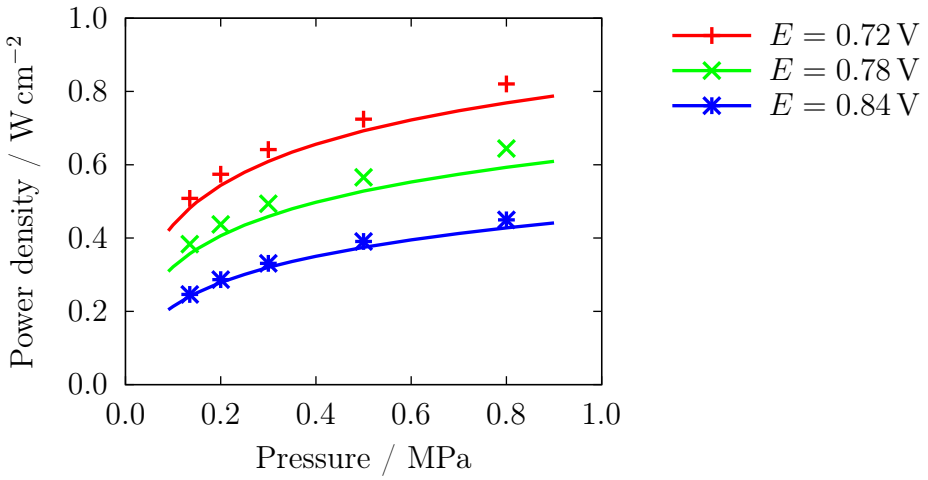

Figure 4.9: Influence of pressure on power density for the polarisation curves shown in Figure 4.8. The dots represent experimental data that was calculated using the interpolation. The lines are simulation results. Results are shown for three different cell voltages.

Figure 4.10 illustrates the increase in cell voltage (and thus electrochemical efficiency) with increasing pressure if power density is kept constant. Experiment and simulation show similar results for all three power densities that are considered. Cell voltage increases with pressure. Pressure effects are strongest at low pressure and weaken towards higher pressure. The overall increase from 0.135 MPa to 0.8 MPa was measured to be between 8 and 14 % with the highest relative increase at high power density. Simulation results yield similar values. Again, the increase in efficiency with increasing pressure is due to the pressure dependency of Nernst potential, kinetics, and diffusion as described in Section 4.1. Concluding, Figure 4.10 shows that pressure can be used to increase the electrochemical efficiency of an SOFC while keeping power output constant.

4.3 Conclusions

In this section the influence of pressure on SOFC performance was analysed in detail. It was shown that SOFC performance is significantly increased by elevating pressure.

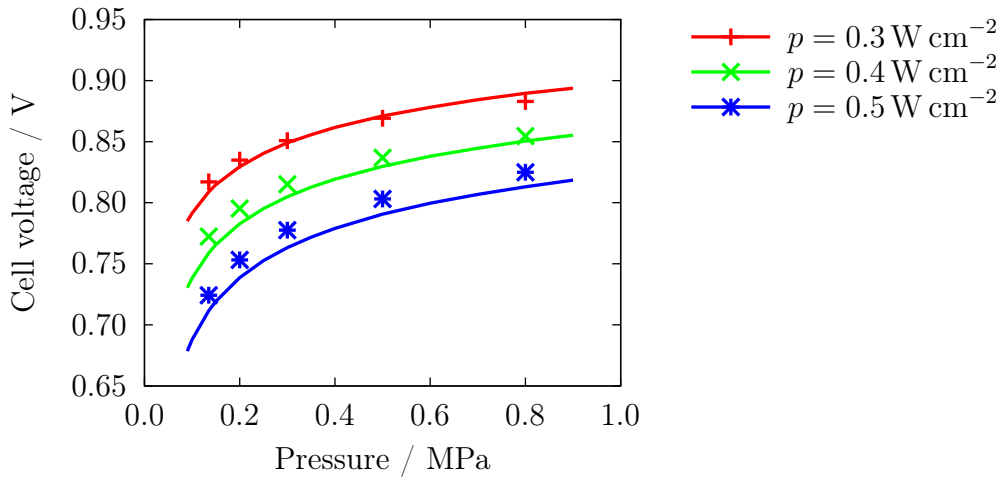

Figure 4.10: Influence of pressure on cell voltage at constant electrical power for the polarisation curves shown in Figure 4.8. Dots represent experimental data that was calculated using Equation 4.19. Lines are simulation results. Results are shown for three different power densities.

Experimental results show an increase in power output of up to 83 % (from 0.135 MPa to 0.8 MPa) while keeping electrochemical efficiency constant. This value strongly varies with operating conditions. On the other hand, while keeping power output constant, electrochemical efficiency was measured to increase up to 14 %, again in the pressure range from 0.135 MPa to 0.8 MPa. The increase in efficiency also depends on operating conditions. All results showed that pressure effects are strongest at low pressure and weaken towards higher pressure. However, improvement was significant within the entire pressure range.

The increase in performance caused by pressure is attributed to different phenomena. Open circuit voltage increases with pressure due to an increase in Nernst potential. Reaction kinetics at the electrodes are enhanced which is caused by an increase in electrode surface coverage with reactants. Diffusion of reactants and products is improved by increasing pressure which is due to a change in diffusion mechanism from Knudsen diffusion to ordinary diffusion. Again, these three effects are strongest at low pressure and weaker at higher pressure.

It is important to note, that the results presented in this section can vary significantly for different types of cells. Qualitatively, pressure effects are likely to be similar. Quantitatively, pressure effects are highly dependent on cell characteristics and perfor-

mance. Electrolyte supported cells, for example, have thin electrodes thus gas diffusion resistance of the electrodes is small. An increase in pressure would improve diffusion but its influence on overall cell performance were negligible. On the other hand, the ohmic resistance of the electrolyte is pressure independent and strongly contributes to the overall resistance of the cell. The performance increase caused by pressurisation is therefore likely to be smaller than for anode-supported cells. These aspects always have to be considered when estimating a performance increase caused by pressure. As a general rule (with some exceptions), an increase in pressure has a stronger influence on cells with a generally weaker performance or on cells that are operated at less favourable conditions.

The results presented in this section should be considered when designing SOFC systems. Pressurisation of a SOFC system would allow for smaller systems as less cells will be able to generate the same amount of electrical power without reducing efficiency. This option seems most interesting for mobile applications. On the other hand, enhanced electrochemical efficiency could be used to improve system efficiency while keeping power output constant. In large stationary power plants, even small increases in efficiency sum up to a large amount of saved fuel. However, usually additional auxiliary system components are necessary for operation at elevated pressure (e.g. a gas compressor) which can again reduce the overall system power output and efficiency. Therefore, an overall system layout has to be regarded for optimisation. In Section 6 the results presented here are used for further interpretation on system level.

5 Influence of Pressurisation on SOFC Durability

For the long term operation of an SOFC (e.g. in power plants like the hybrid power plant), durability is an important topic that needs to be addressed. Nickel oxidation and carbon deposition are two important degradation mechanisms. The influence of pressure on these mechanisms is discussed in this chapter. Results concerning the pressure dependency of SOFC durability have previously been published [35]. The enthalpies of reaction $\Delta H_{0,\mathrm{R}}$ are calculated with Equation 2.1 and thermodynamic data from [13, 66].

5.1 Nickel Oxidation

Formation of nickel oxide (NiO) at the anode is a well-known degradation mechanism in SOFC [73, 74, 87]. It can occur chemically via

$$\mathrm{Ni} + 0.5\,\mathrm{O_2} \rightleftharpoons \mathrm{NiO} \qquad \Delta H_{0,\mathrm{R}} = -133\,\mathrm{kJ\,mol^{-1}} \tag{5.1}$$

or electrochemically via

$$\mathrm{Ni} + \mathrm{O^{2-}} \rightleftharpoons \mathrm{NiO} + 2\mathrm{e^-} \qquad \Delta H_{0,\mathrm{R}} = -85.0\,\mathrm{kJ\,mol^{-1}}\ . \tag{5.2}$$

In this work, only chemical oxidation of nickel is discussed. A more detailed theoretical study including electrochemical oxidation of nickel is available from [75]. The equilibrium constant of Equation 5.1 can be calculated with

$$\ln K = \ln\left(\frac{a_{\mathrm{NiO}}}{a_{\mathrm{Ni}}\sqrt{a_{\mathrm{O_2}}}}\right) = -\frac{\Delta G_0}{RT} \tag{5.3}$$

where ΔG_0 is the Gibbs reaction enthalpy of Equation 5.1 at standard pressure and activities of 1. For the following calculations a temperature dependent value for ΔG_0 is taken from [44]. The activity of solids equals one, whereas the activity of oxygen is calculated with

$$a_{\mathrm{O_2}} = \frac{p_{\mathrm{O_2}}}{p_0} \tag{5.4}$$

assuming ideal gases. The equilibrium partial pressure of $\mathrm{O_2}$ for the simultaneous presence of Ni and NiO is therefore given by

$$p^{\mathrm{eq}}_{\mathrm{O_2}} = p_0 \mathrm{e}^{\frac{2\Delta G_0}{RT}}\ . \tag{5.5}$$

For $p_{O_2} < p_{O_2}^{eq}$, the reduced species Ni is thermodynamically favoured, else the oxidised species NiO.

At electrochemical equilibrium, oxygen activities at anode and cathode are related via the cell voltage,

$$E^{eq} = \frac{RT}{zF} \ln\left(\frac{a_{O_2,ca}}{a_{O_2,an}}\right) . \tag{5.6}$$

Considering Equation 5.4, the partial pressure of oxygen at the anode can be calculated with

$$p_{O_2,an} = p_{O_2,ca} e^{-\frac{zEF}{RT}} . \tag{5.7}$$

Figure 5.1 shows the equilibrium partial pressure of oxygen for the chemical oxidation of nickel (Equation 5.5) as well as the equilibrium partial pressure of oxygen at different cell voltages (Equation 5.7) for a temperature of 1000 K. If oxygen partial pressure is higher than $p_{O_2}^{eq}$, the formation of NiO is thermodynamically favoured. This will result in a degradation of the anode. Oxygen partial pressure $p_{O_2,an}$ shows a similar pressure dependency at all voltages. It generally shows a strong increase at very low pressure and only a weaker increase at higher pressure. For cell voltages higher than 0.8 V the oxygen partial pressure at the anode is low enough to prevent nickel oxidation. At a cell voltage of 0.7 V, nickel oxidation will occur in almost the entire pressure range. Note, that the diagram only accounts for the non-polarised cell thus at OCV. It is very unlikely that OCV will fall below a voltage of 0.8 V. However, it is shown that pressure generally increases the partial pressure of oxygen at the anode and therefore facilitates the formation of nickel oxide also in case of polarised cells.

It should be noticed that $p_{O_2}^{eq}$ and $p_{O_2,an}$ are temperature dependent. For a detailed analysis of the formation of NiO, temperature aspects have to be regarded. In order to quantify the nickel oxidation propensity in a polarised cell, the above presented thermodynamic calculations are combined with the model described in Section 3.2 generally accounting for pressure and temperature dependencies. The model calculates the local O_2 partial pressures inside the anode which are than compared to $p_{O_2}^{eq}$. For the system simulations (Section 6), this comparison is used to prevent operating conditions where nickel oxidation is likely to occur.

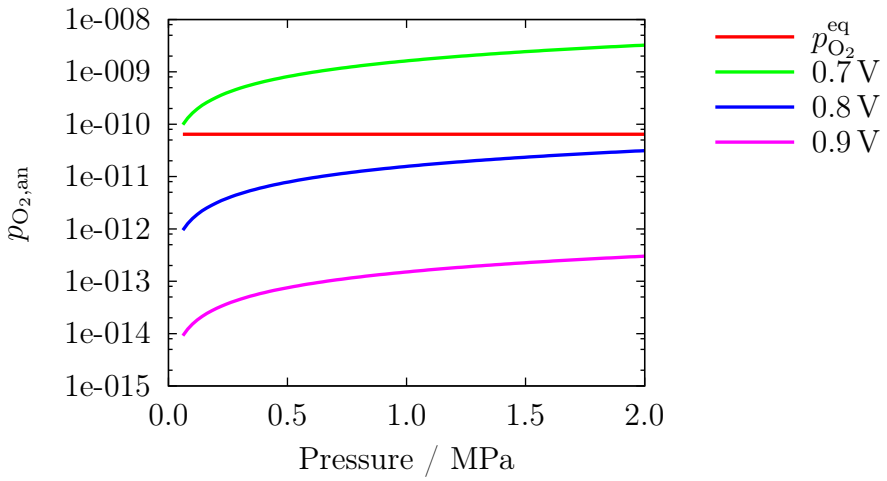

Figure 5.1: Influence of pressure on the oxygen partial pressure at the anode at electrochemical equilibrium for a temperature of 1000 K. Chemical oxidation of nickel is thermodynamically favoured at anode gas oxygen partial pressure greater than $p_{O_2}^{eq}$.

5.2 Carbon Deposition

Carbon deposition at the anode can be an important degradation mechanism that may occur if the SOFC is fuelled with hydrocarbons. The hybrid power plant will preferably be operated with natural gas that contains large amounts of methane. Carbon deposition is therefore a relevant topic and pressure effects on this degradation mechanism are analysed in this section.

Carbon deposition can occur via

$$CH_4 \rightleftharpoons C + 2H_2 \qquad \Delta H_{0,R} = 74.6\,\mathrm{kJ\,mol^{-1}} \tag{5.8}$$

and after formation of carbon monoxide via the Boudouard reaction

$$2CO \rightleftharpoons C + CO_2 \qquad \Delta H_{0,R} = -172\,\mathrm{kJ\,mol^{-1}}\ . \tag{5.9}$$

In order to prevent carbon deposition, hydrocarbon fuels are usually mixed with product gases (H_2O, CO_2) which are used for reforming processes. For the hybrid power plant, steam reforming is the most promising option, as large amount of hot water vapour leave the SOFC and can be recirculated to provide heat and water that are needed for these reforming processes. In this study, the propensity for carbon deposition is therefore

investigated in a range of temperature, pressure and oxygen to carbon ratios (O/C). The investigated temperature range not only includes operating temperatures of SOFC but is extended to cover temperatures in other relevant system components (e.g. piping, reformer) as well. Thermodynamic simulations starting with H_2O-CH_4-mixtures (see Section 3.3) are carried out which calculate thermodynamic equilibrium while considering the formation of solid carbon.

Results of these simulations are shown in Figure 5.2. The diagram indicates threshold O/C for different temperatures. At O/C lower than indicated, solid carbon formation is thermodynamically favoured. This O/C is temperature independent at pressures tending towards 0 Pa. At this pressure, threshold O/C tends towards 1. At low temperatures (600 K and 800 K), O/C shows a distinct peak at low pressure with a rather sharp drop in O/C towards higher pressure. Note, that for 600 K this peak is hardly visible from the diagram (O/C of 2.6 at 150 Pa). Towards higher temperatures, this peak becomes less pronounced and pressure effects are much smaller in general. At 1200 K pressure dependency is almost linear. Note, that these results are not only valid for H_2O-CH_4-mixtures but also for other gas compositions (e.g. pre-reformed gas mixtures) with the same atomic composition.

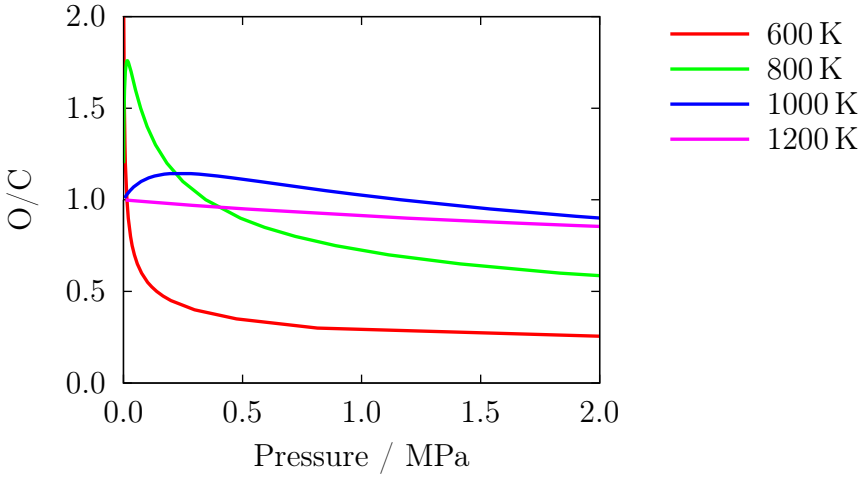

Figure 5.2: Pressure dependence of carbon deposition. The lines show oxygen to carbon ratios of H_2O-CH_4-mixtures below which the formation of solid carbon is thermodynamically favoured.

5.3 Conclusions

In this section, the influence of pressure on SOFC durability was discussed concerning the oxidation of the nickel anode and the deposition of solid carbon inside the anode. It was found that nickel oxidation is more likely to occur at elevated pressure because the equilibrium partial pressure of oxygen in the anode gas increases with increasing pressure under the assumption of constant cell voltage and thermodynamic equilibrium. These results however do not consider electrochemical oxidation of nickel. Further investigations of pressure effects on nickel oxidation are therefore necessary for detailed prediction of nickel oxidation during real operation of SOFC. In the meantime, it is advisable to slightly increase the operating voltage of SOFC at elevated pressure compared to atmospheric pressure. For a hybrid power plant that will be operated in a pressure range between 0.3 and 0.5 MPa an operating voltage of the SOFC greater than 0.75 V (see Figure 5.1) is reasonable at an operating temperature of 1000 K.

Carbon formation propensity was found to be a complex function of temperature and pressure. In the hybrid power plant, carbon deposition is most likely to occur at pressures below 0.3 MPa, especially inside the reformer and the piping where temperatures are usually lower than inside the fuel cell. However, carbon deposition can be prevented by adequate recirculation of anode gas which can easily increase O/C to favourable values within the entire relevant temperature and pressure range.

6 Hybrid Power Plant Sensitivity Analysis

In this section, some results of the hybrid power plant system simulations are presented. A sensitivity analysis (see Section 3.4.3) is carried out in order to evaluate the influence of different system components on electrical efficiency and SOFC operating conditions. The aim of this analysis is to determine and optimise key components of the system with regard to electrical efficiency and SOFC operating conditions. First results of the sensitivity analysis have been published in [36].

Results of the sensitivity analysis are presented in standardised form in Figures 6.1a to 6.8b. Important operating conditions at crucial points of the system as well as performance data is presented. Anode and cathode volume flows are important as experiments have shown unstable behaviour of the SOFC if gas flows become too small. For a safe operation, volume flow per cell should not be below 0.5 nlpm. Fuel mass flow is important as it strongly determines electrical efficiency of the power plant. Electrical output powers are given as these are essential characteristics of a power plant. Furthermore, important operating characteristics of the SOFC are shown like voltage, current density, fuel utilisations, air utilisation and molar gas composition of the anode gas entering the SOFC. Gas composition is important as it strongly affects the performance of the SOFC. Temperature and operating pressure are other operating conditions that can have a strong influence on SOFC performance. Furthermore, the temperature of the air leaving the SOFC system towards the combustion chamber is shown. This parameter is a good indicator for system efficiency. If air temperature is high, little fuel needs to be burned inside the combustor to reach the desired turbine inlet temperature. Finally, electrical efficiencies of the power plant are shown based on lower and higher heating value (LHV and HHV).

6.1 Number of Stacks

The number of SOFC stacks is a very important aspect in the design of a hybrid power plant. Cells are one of the most expensive parts of the power plant but also contribute the largest amount of output power. If the number of cells is too small, the desired electrical power can only be reached by increasing current density to high values which can cause degradation of the cells. On the other hand, the number of cells is limited by the air flow that is provided via the compressor. Experiments have shown that stable

SOFC operation can be critical if gas flows fall below 0.5 nlpm. For this analysis it is assumed that the number of cells is varied by varying the number of 60-cell stacks. The number of stacks is varied in a range of 350 to 450 stacks. A reference value of 400 is selected for all other simulations of the sensitivity analysis. Range and reference values were selected based on previous estimations with respect to adequate gas flows through the cells and the expected electrical power demand.

In this analysis, changing the number of SOFC stacks does not affect the power output of the stack. Power ouput is another parameter that is varied separately from the number of stacks (see Section 6.2). As SOFC offer great potential for part load operation it is very important to distinguish between stack number and power output.

6.1.1 Results and discussion

The results of this analysis are presented in Figures 6.1a and 6.1b. Diagram I shows how a variation in stack number influences volumetric flows on anode and cathode (shown for a single cell) as well as the fuel mass flow entering the SOFC system. Volumetric flows are significantly smaller at high stack count. At the cathode, the available air is simply distributed to a larger number of cells. The same applies to the anode where the small increase in natural gas mass flow does not have a significant influence. Overall, volumetric flows are small, especially at the anode. From this point of view, a smaller number of stacks would be preferable.

Diagram II illustrates the influence of stack number on voltage and current density as well as fuel and air utilisation. Current density decreases substantially as the number of stacks is increased because power demand is distributed over a larger number of cells. This effect should cause cell voltage to increase accordingly, however, the decrease in cell temperature (Diagram III) counteracts a significant increase. Air utilisation hardly changes. Constant turbine speed results in nearly constant overall air flow. Constant power demand and only slightly varying cell voltage result in a nearly constant overall current and thus air utilisation. For similar reasons, fuel utilisation both of cell and SOFC system is not effected strongly. Increasing fuel flow with increasing stack number causes a small decrease in fuel utilisation. Fuel utilisation of cell and system decreases by 4 and 2 percentage points, respectively, when increasing stack number from 350 to 450.

Diagram III shows stack temperature and pressure over number of stacks. Pressure

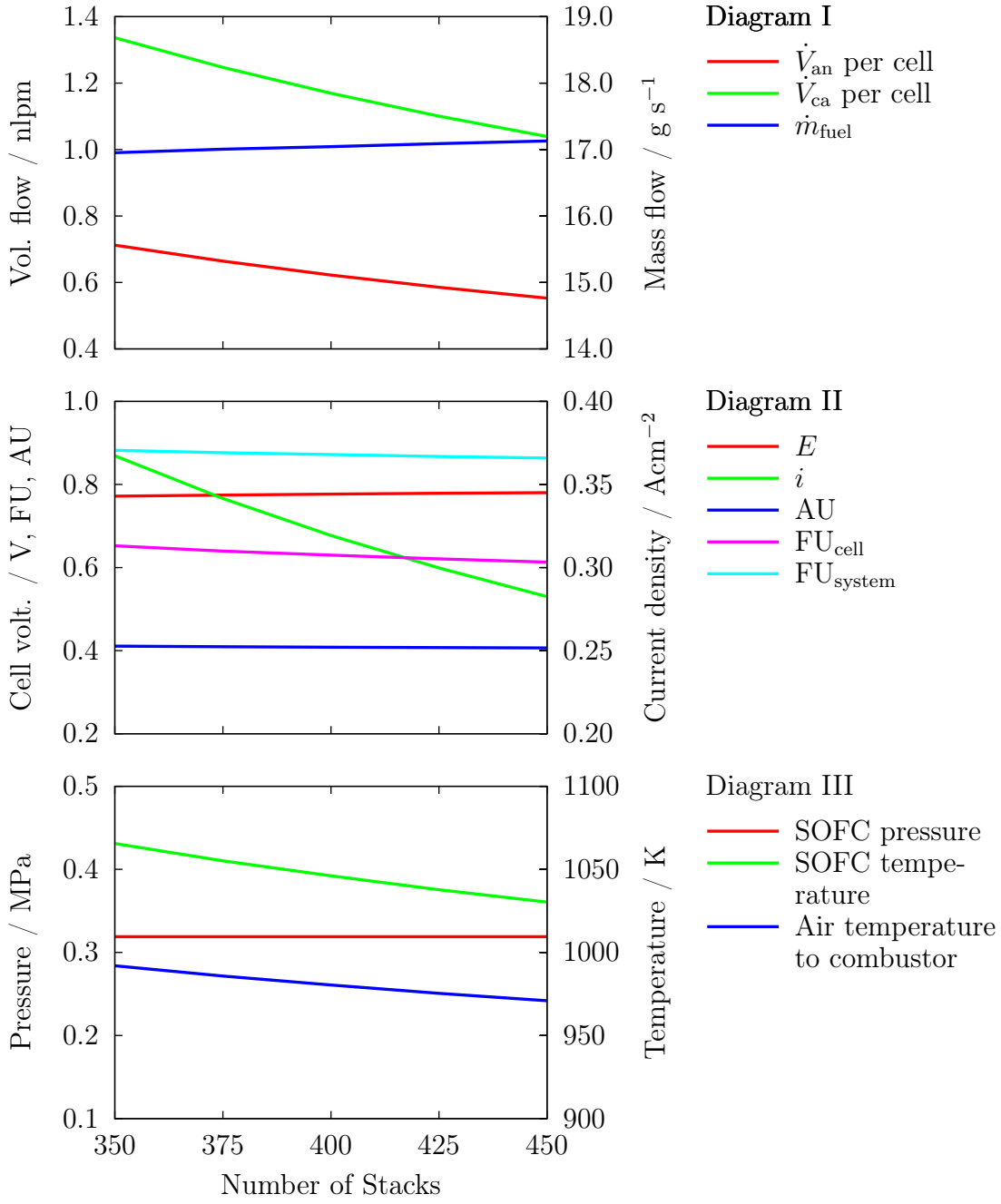

Figure 6.1a: Influence of varying stack count on the performance of the hybrid power plant (Diagrams I–III).

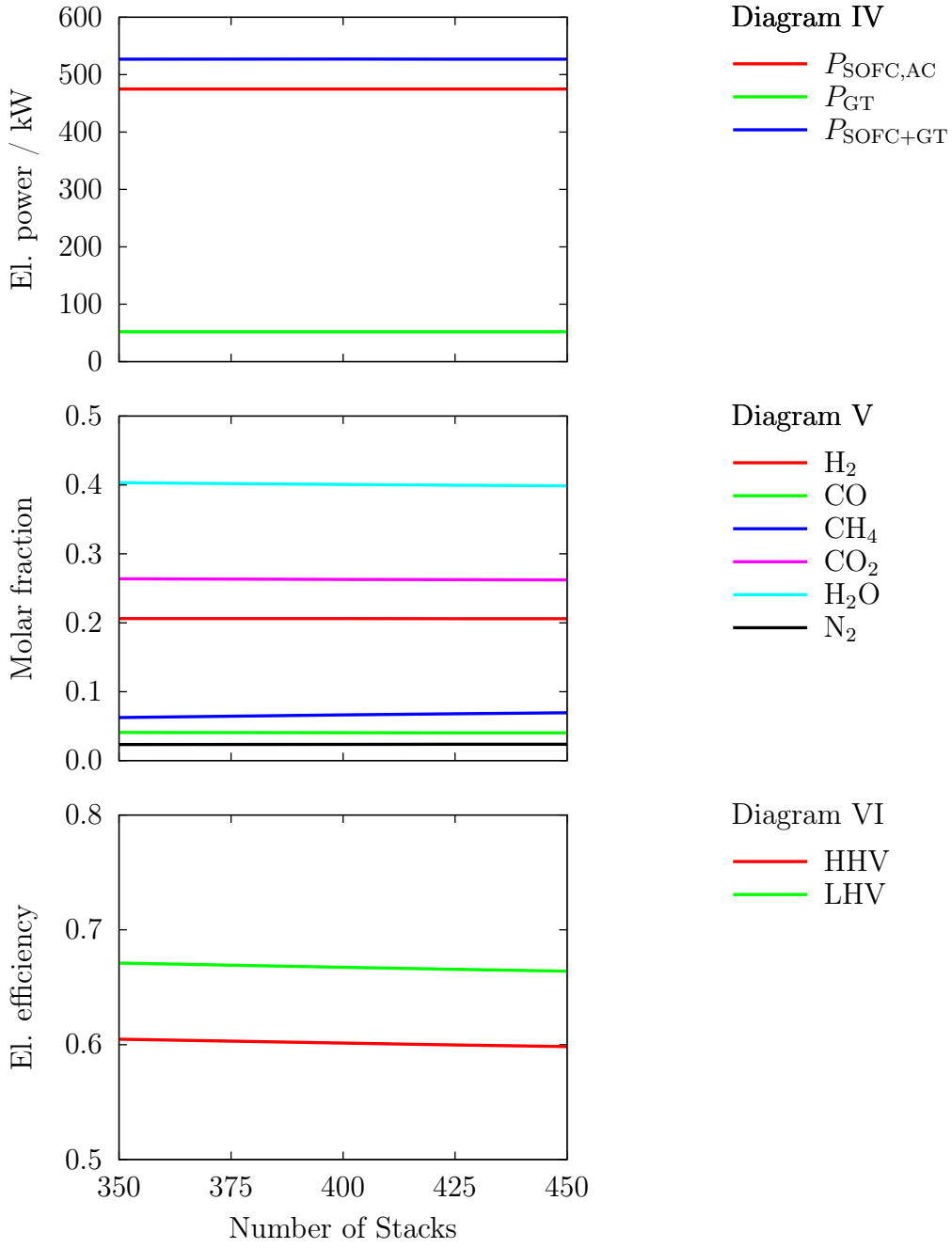

Figure 6.1b: Influence of varying stack count on the performance of the hybrid power plant (Diagrams IV–VI).

inside the stack is dominated by the compression ratio of the compressor. The pressure drop caused by the SOFC system is not changed thus pressure is only marginally influenced by small changes of the gas flows through the turbine piping system. SOFC temperature drops significantly when stack number is increased. The reason for the reduction in temperature is not the decrease in power output per cell as could be assumed. The smaller power output does reduce the internal heating of the cell, however gas flows are also reduced decreasing the cooling effect especially that of air. Overall about the same thermal energy is released in all stacks regardless of stack number as electrical power output is kept constant and cell voltage (and thus electrochemical efficiency) hardly varies. The reason for the reduced cell temperature is the increase in stack surface area with increasing number of stacks (linear dependency is assumed). An increasing number of stacks therefore increases the flow of thermal energy from stacks to the pressure vessel gas. The stacks are located inside the pressure vessel which has an average temperature of 506 K at reference conditions.

A lower SOFC temperature causes a reduced gas temperature of the air that leaves the SOFC system towards the combustion chamber. The difference between SOFC temperature and air temperature to the combustor is due to the transfer of thermal energy from the SOFC off gas to the air entering the SOFC system.

Diagram IV shows the influence of stack number on electrical power output of the system. SOFC power is set to a constant value as boundary condition. Gas turbine power output is indirectly affected by changes in stack number. Changes in stack number have an effect on temperatures and mass flows through the system thus influencing the power output of the turbine. However, these effects are only marginal. Note that a possible change of pressure losses caused by an increase in stack count is not regarded in this sensitivity analysis.

Diagram V shows the variation of molar anode gas composition entering the SOFC stacks. The effect of stack number on gas composition is small. Changing the number of stacks slightly changes the reformer temperature (not shown) via the recirculation of anode gas and thus influences the equilibrium gas composition entering the SOFC.

Diagram VI shows the variation of electrical efficiency with varying number of SOFC stacks calculated with both higher (HHV) and lower heating value (LHV). Electrical efficiency decreases slightly with increasing number of SOFC stacks. This effect is due to the increase in thermal losses with increasing stack count and thus stack surface

area as described previously. The thermal energy is lost to the air inside the pressure vessel which therefore enters the recuperator with higher temperature. The thermal energy which can be recuperated is reduced and the system's exhaust gas temperature increases. By increasing the stack number from 350 to 450, exhaust gas temperature rises from 594 K to 602 K which corresponds to a thermal power increase of 6 kW. Thermal energy that leaves the system via the exhaust gas is lost and has to be compensated by an increase in fuel mass flow. This reduces the electrical efficiency of the system.

6.1.2 Conclusion

The number of SOFC stacks is an important parameter in the design of a hybrid power plant. However, simulation results show that for the presented system concept the number of SOFC stacks does not have a strong influence on the performance of the hybrid power plant within the investigated range. Mainly, the current density decreases if more stacks are used. Thermal losses increase with additional SOFC stacks thus slightly reducing the overall electrical efficiency of the hybrid power plant. In real systems these losses could be minimised by adequate packaging of different components. SOFC stack number can however not be reduced arbitrarily as this would cause high current densities which lead to increased degradation of the cells.

6.2 SOFC Electrical Power

In this section the effect of SOFC electrical power variation on system behaviour and SOFC operating conditions is analysed. Electrical power of the fuel cell is varied between 450 and 550 kW. A reference value of 500 kW is used for all other simulations throughout this sensitivity analysis. SOFC power needs to be matched to gas turbine power in order to reach high electrical efficiency. Ideally, electrical SOFC power output is chosen to provide the right amount of thermal energy for the gas turbine without directly feeding additional fuel to the combustion chamber.

6.2.1 Results and discussion

Simulation results are presented in Figure 6.2a and 6.2b. Fuel mass flow (Diagram I) strongly increases with increasing electrical power as more fuel is needed to provide the desired power output. The increase in fuel mass flow similarly affects anode volume flow.

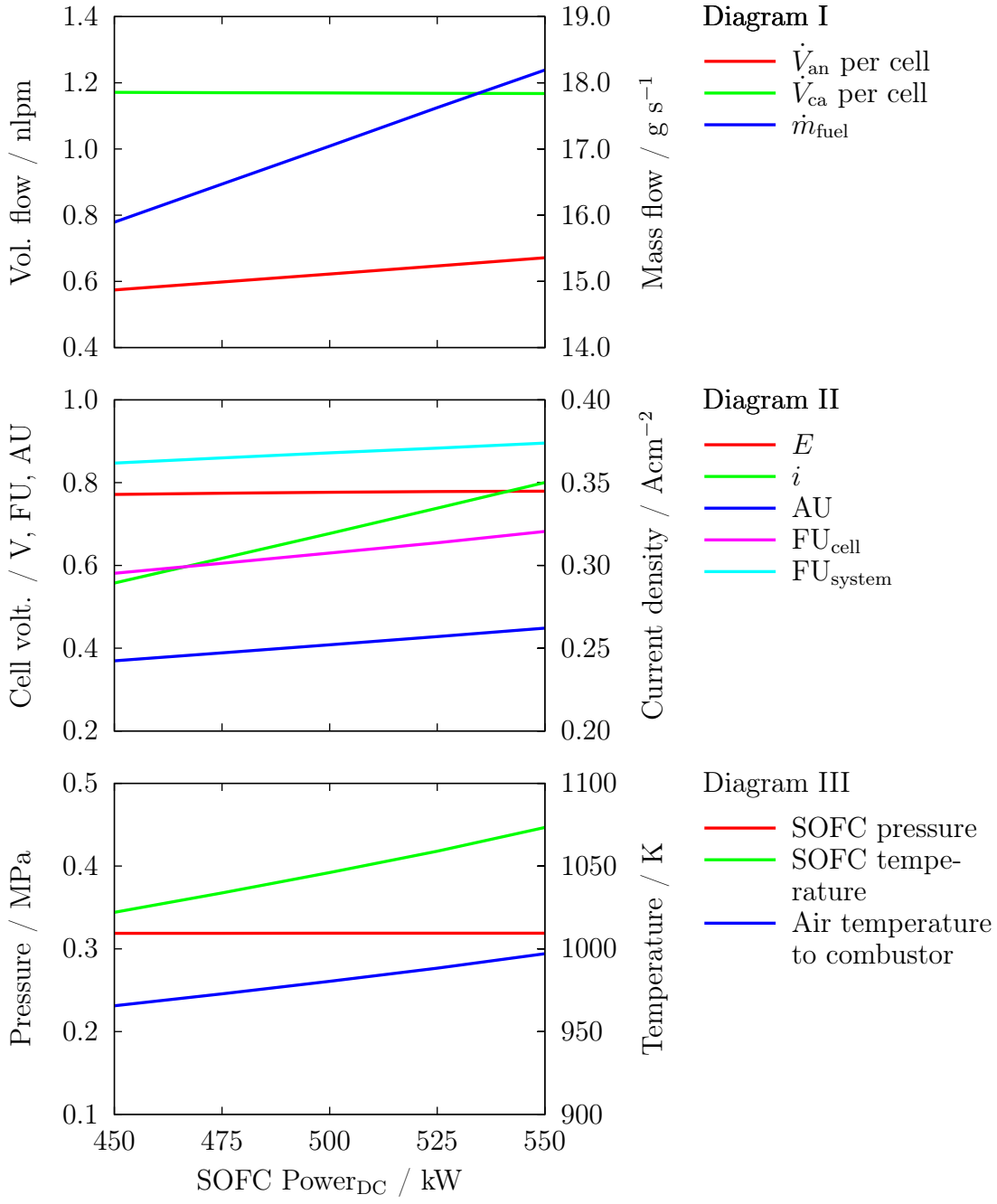

Figure 6.2a: Influence of varying stack power on the performance of the hybrid power plant (Diagrams I–III).

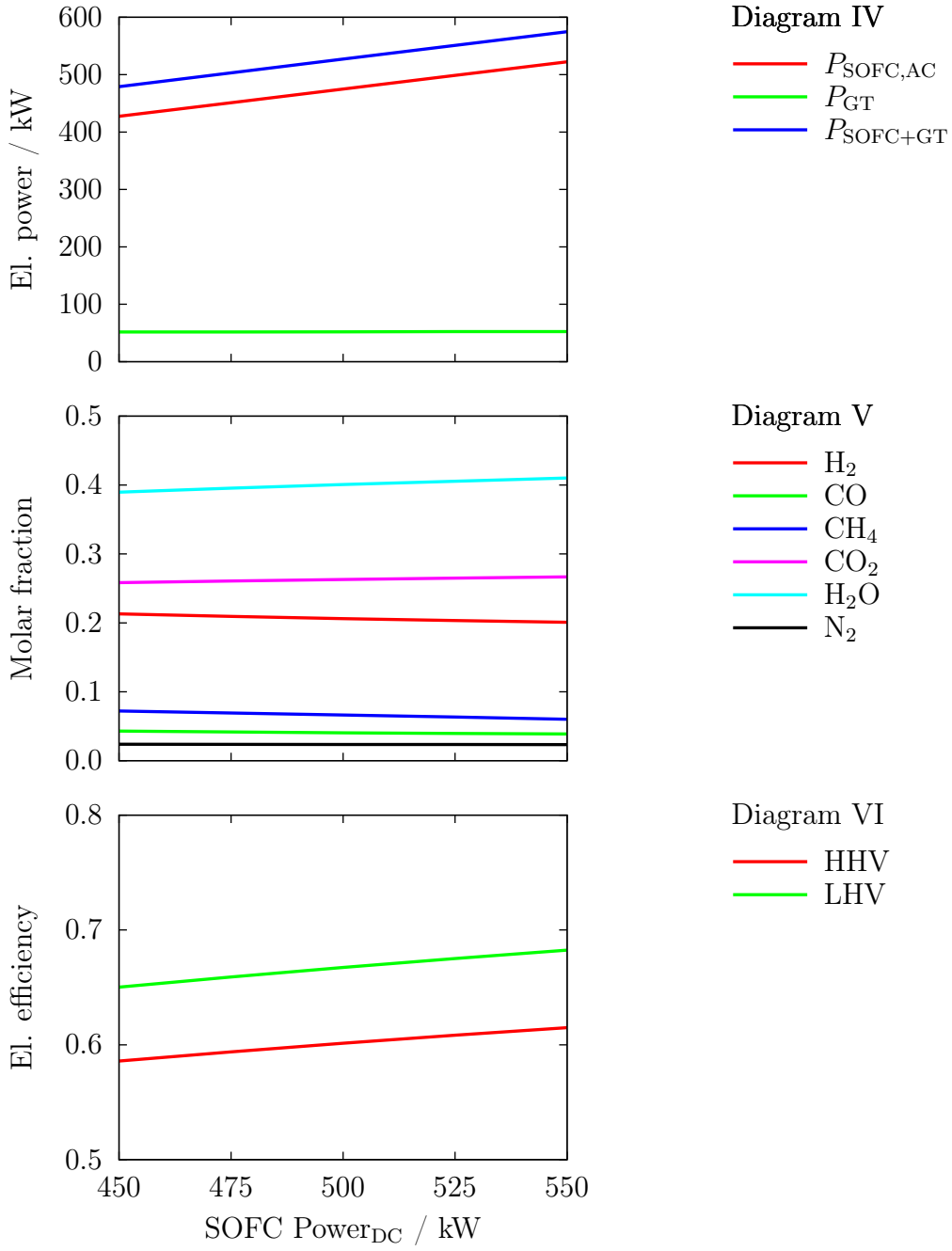

Figure 6.2b: Influence of varying stack power on the performance of the hybrid power plant (Diagrams IV–VI).

Cathode gas flow hardly changes as turbine rotational speed is kept constant. Different operating conditions within the entire system cause a slight reduction in cathode flow.

Diagram II shows current density, voltage, fuel utilisations, and air utilisation versus SOFC electrical power. As a constant number of cells has to provide a larger electrical power, current density increases with power demand. This would usually cause a decrease in cell voltage. However, cell voltage stays nearly constant which is due to a strong temperature increase (Diagram III). Air flow is almost independent of SOFC power (Diagram I) and therefore air utilisation increases proportionally with current density according to Faraday's law. Fuel utilisations increase with electrical power output of the SOFC as the air temperature to the combustor (Diagram III) increases. Less additional fuel is needed inside the combustor to reach the desired turbine inlet temperature.

Diagram III shows operating pressure and temperature of the SOFC. Pressure does not change significantly as it is determined by the gas turbine operating point. Temperature increases with SOFC power output by 51 K within the investigated range. Increasing the electrical power output of the SOFC also increases the thermal power output. With nearly constant cell voltage (Diagram II) thermal power output is proportional to electrical power output. Increasing electrical power from 450 to 550 kW (+22 %) also results in an increase in thermal power to a similar extent. Despite the substantial temperature variation, absolute temperature does not yet reach critical values suggesting that a broader range of SOFC power variation would be feasible without changing other parameters. Air temperature to the combustor increases with increasing SOFC temperature. However, changes are attenuated by the cathode gas heat exchanger.

Diagram IV shows the influence of electrical power output if SOFC power is varied. Please note the difference between alternating (AC) and direct current (DC). As the SOFC provides DC (as shown on the x-axis), this value is varied between 450 and 550 kW. Nevertheless, the number of SOFC stacks is kept constant. On the y-axis the power provided to the electrical grid is shown based on AC. For all simulations a conversion efficiency from DC to AC of 95 % is chosen resulting in smaller values for AC power. AC Power output of the SOFC is proportional to desired DC power changes. Gas turbine power nearly stays constant as its operating point is hardly affected by changes in SOFC power. The overall electrical power output of the hybrid power plant therefore increases according to SOFC power output.

Diagram V illustrates the gas composition entering the fuel cells. The increase in cell fuel utilization (Diagram II) reduces the amount of fuel in the recirculated anode off gas and thus reduces hydrogen, methane and carbon monoxide molar fractions. On the contrary molar fractions of carbon dioxide and water increase.

Diagram VI shows the influence of SOFC power on the electrical efficiency of the hybrid power plant. Electrical efficiency increases with increasing electrical power output by about 3 percentage points within the investigated power range. For low SOFC electrical power of 450 kW 85 % of the fuel is used by the fuel cell system and air leaves the fuel cell with a temperature of 966 K. For high SOFC electrical power of 550 kW 90 % of the fuel is used and air leaves the SOFC with a temperature of 997 K. High efficiency of the hybrid power plant is only reached if most of the fuel is used by both SOFC and gas turbine meaning that ideally the SOFC converts the fuel electrochemically at high efficiency and further provides the remaining thermal power for the gas turbine. A high system fuel utilization is therefore preferable. However, a high fuel utilization is only advantageous if enough thermal energy is supplied to power the turbine. High fuel utilization would not improve overall electrical efficiency if additional fuel were fed directly to the combustion chamber in order to reach the desired turbine inlet temperature. An increase in SOFC power results in a significantly higher SOFC temperature as more fuel is used thus the gases that are fed to the combustion chamber are hotter. Less remaining fuel (enhanced fuel utilization) is necessary to further heat up the SOFC off gases before they enter the turbine.

A further increase in SOFC power would further enhance electrical efficiency of the hybrid system, however increasing SOFC power is limited. If SOFC temperature exceeds its maximum value, sealings inside the fuel cell are likely to be destroyed.

6.2.2 Conclusion

Power output of the SOFC strongly influences the electrical efficiency of the hybrid power plant. For highest efficiency SOFC power output and GT power output need to be attuned to each other. A variation in power output further has a strong influence on SOFC temperature. Fuel utilization increases with increasing SOFC power.

6.3 Anode Gas Recirculation Rate

In this section the influence of anode gas recirculation rate on the hybrid power plant is discussed. Recirculation rate is varied between 0.7 and 0.8 meaning that 70 to 80 % of the anode exhaust gas is recirculated. A recirculation rate of 0 would mean that no recirculation exists at all, while a value of 1 would mean that all exhaust gas is recirculated. Anode gas recirculation is necessary in order to pre-heat fresh fuel, to increase fuel utilisation, and to provide steam for the reforming reactions. Rather high values of recirculation (in the range of the values chosen here) are needed in order to safely prevent carbon deposition inside the reformer and the SOFC (see also Section 5.2). If values are too high, recirculation will cause a strong increase in anode flow up to unlimited flow if all offgas is recirculated.

6.3.1 Results and discussion

Results of the simulations are presented in Figures 6.3a and 6.3b. Diagram I shows the influence of anode gas recirculation rate on gas flows through the cells. Fuel mass flow is hardly affected by changes in recirculation rate as neither electrical power output of SOFC and gas turbine (Diagram IV) nor thermal losses inside the system are changed. Cathode volume flow per cell also stays constant as the gas turbine operating point is not affected. The anode volumetric flow rises exponentially if anode recirculation rate is increased. A larger recirculation rate primarily increases the gas flow entering the cells but by this means also increases the gas flow leaving the cell which again leads to a further increase in recirculated gas flow.

Diagram II shows that the operating point of the SOFC is only slightly affected by changes in anode gas recirculation rate. Current density stays nearly constant. Cell voltage is slightly reduced due to the larger concentration of product gases entering the anode (Diagram V). This effect is weakened by a small increase in cell temperature (Diagram III). Fuel utilisation on cell level is reduced with increasing recirculation rate. Increasing recirculation rate causes a larger amount of fuel being supplied to the cells. As current density stays constant, fuel utilisation is reduced. A lower fuel utilisation on the cell usually has a positive effect concerning the degradation of SOFC. System fuel utilisation is hardly affected as the overall amount of fuel that is used stays approximately the same. Air utilisation also stays constant as neither air supply nor current density change.

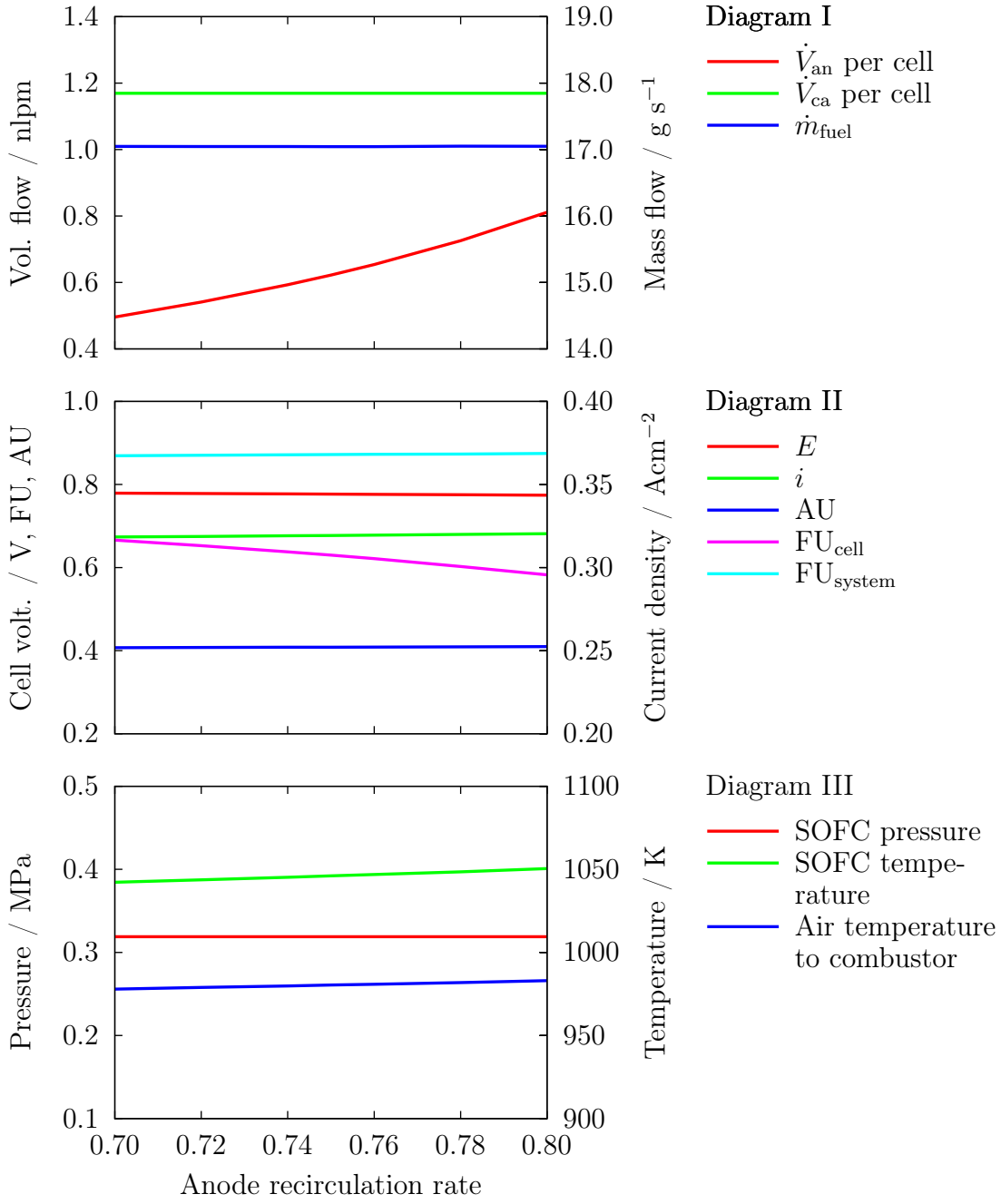

Figure 6.3a: Influence of varying anode recirculation on the performance of the hybrid power plant (Diagrams I–III).

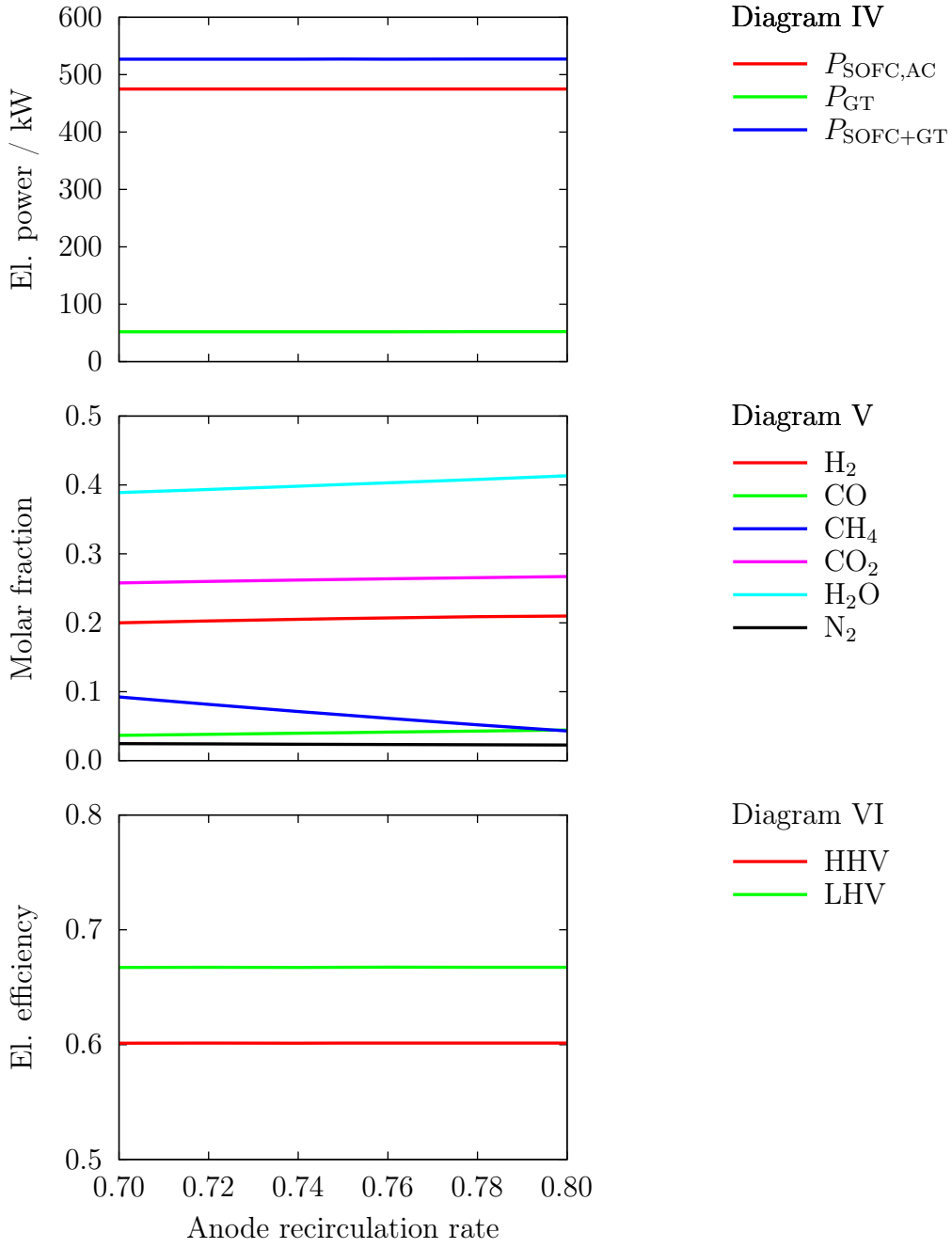

Figure 6.3b: Influence of varying anode recirculation on the performance of the hybrid power plant (Diagrams IV–VI).

Diagram III shows operating pressure and temperature of the SOFC. Operating pressure is mainly depending on the compression ratio of the compressor which is not affected by the anode gas recirculation. SOFC temperature increases if more anode exhaust gas is recirculated. A higher recirculation rate increases the SOFC anode gas inlet temperature and therefore causes an increase in SOFC temperature. Another reason for a change in temperature is the operating voltage of the SOFC. With increasing recirculation rate, operating voltage is slightly reduced thus reducing electrical efficiency of the SOFC and increasing its thermal power output. Air temperature to the combustor increases slightly with increasing SOFC temperature.

Electrical power output (Diagram IV) of both gas turbine and SOFC does not change with variable anode gas recirculation rate. SOFC power is set as a boundary condition and the turbine is kept at constant speed which results in a nearly constant power output.

Diagram V shows how the anode inlet gas composition depends on anode gas recirculation rate. Increased recirculation rate causes a higher concentration of product gases (H_2O and CO_2) entering the reformer. A higher product gas concentration shifts the equilibrium compositions towards lower methane concentrations (thus towards the right side of Equation 2.8) reducing it from 9 to 4 %. This limits the increase in water vapour content and results in an increase in H_2 and CO concentration.

Diagram VI shows electrical efficiency versus anode gas recirculation rate. Electrical efficiency is nearly unaffected by recirculation rate within the investigated range. Varying the recirculation rate mainly results in minor changes in operating conditions of the SOFC. These only have a minor indirect influence on electrical efficiency of the hybrid power plant.

6.3.2 Conclusion

Changes in anode gas recirculation rate only have a minor effect on performance and operating conditions of the hybrid power plant within the investigated range. An adequate recirculation rate needs to be found ensuring that no carbon deposition occurs inside the power plant. High recirculation rates can be used if higher anode flow per cell is desired and in order to reduce fuel utilisation on the cells. Furthermore, methane concentration of the anode gas entering the SOFC can be varied.

6.4 Cathode Heat Exchanger Transfer Rate

A heat exchanger transferring heat from the cathode outlet gas towards the cathode inlet gas provides an option for controlling the temperature of the SOFC. Simulation results in this section are shown in Figures 6.4a and 6.4b for heat transfer rates between 0 and 0.8. A value of 0 means that no heat is transferred at all whereas a value of 1 means that as much thermal energy is transferred as theoretically possible. In real applications, transfer rates of heat exchangers can be high (above 90 %). Variable heat transfer rates are possible by bypassing some of the gas.

6.4.1 Results and discussion

Diagram I shows that volumetric and mass flows through the SOFC are hardly affected by the cathode heat exchanger transfer rate. Only a slight increase in fuel and anode gas flow is observed.

Several changes in operating conditions are visible from Diagram II. Cell voltage increases in response to an increase in cell temperature (Diagram III). In order to keep power output stable, current density is reduced. With slightly increasing fuel flow but decreasing current density, cell and system fuel utilisation are reduced considerably. With air flow being constant, air utilisation is not affected as strongly and only decreases due to the reduced current density.

Cell temperature (Diagram III) is directly affected by an increase in heat transfer rate. Cell temperature increases with more heat being recirculated. However, the effect is not very large (23 K within the investigated range) as the increase in cell voltage enhances electrochemical efficiency of the cells and reduces their thermal power output. Operating pressure of the SOFC is not affected by changes in heat transfer rate. Air temperature to the combustor equals SOFC temperature at a heat transfer rate of 0 and is reduced strongly with increasing transfer rate.

Electrical power output neither of SOFC nor GT is significantly affected by changes in heat transfer rate as they are given as boundary condition (SOFC) or mainly determined by the turbine speed (GT).

Diagram IV shows the composition of the anode gas that enters the cells. With decreasing fuel utilisation, fuel gas concentrations at the SOFC outlet increase. More fuel is recirculated and fuel concentration at the SOFC inlet increases as well.

Simulation results show a slight decrease in electrical efficiency with increasing heat

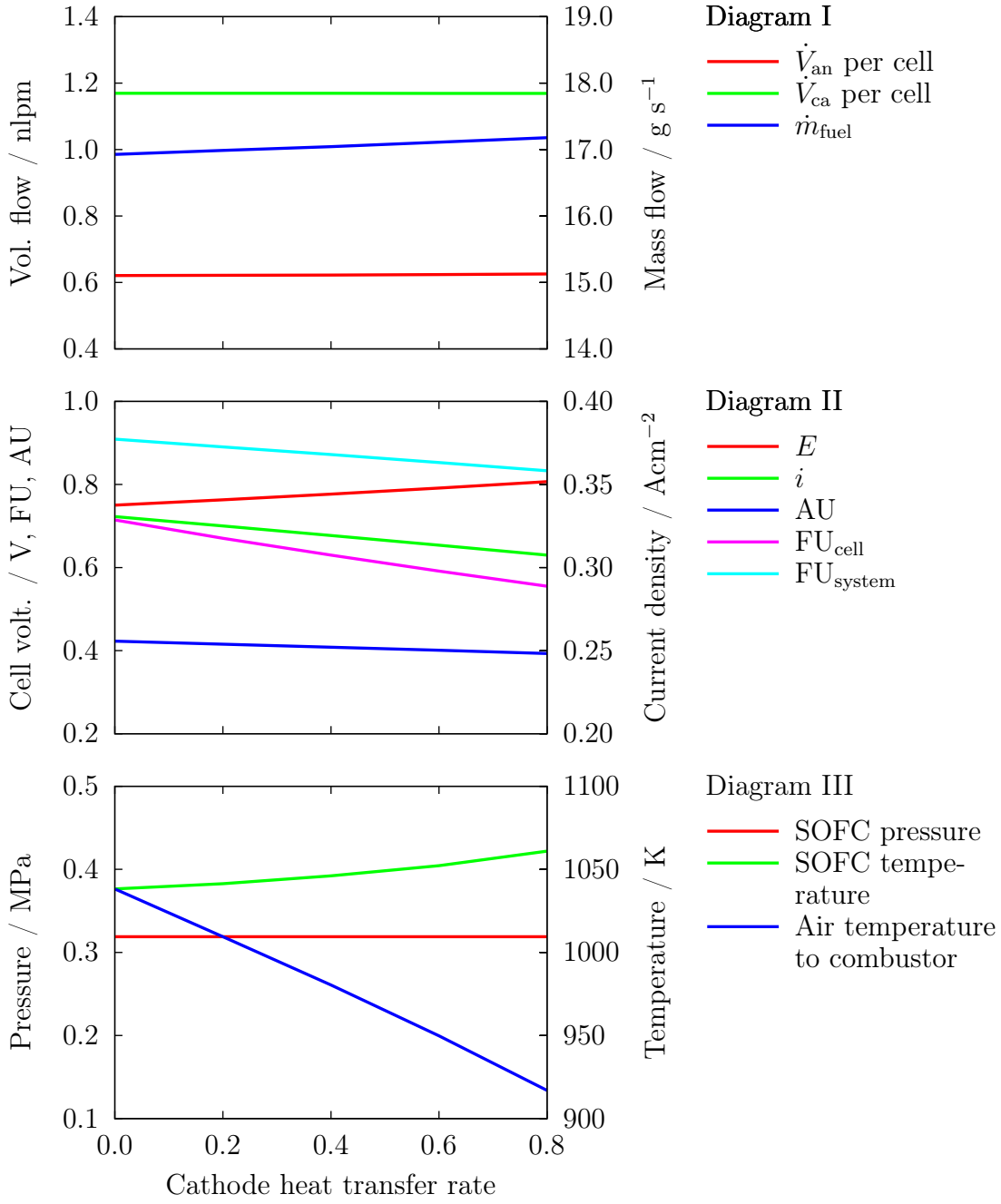

Figure 6.4a: Influence of varying cathode heat transfer on the performance of the hybrid power plant (Diagrams I–III).

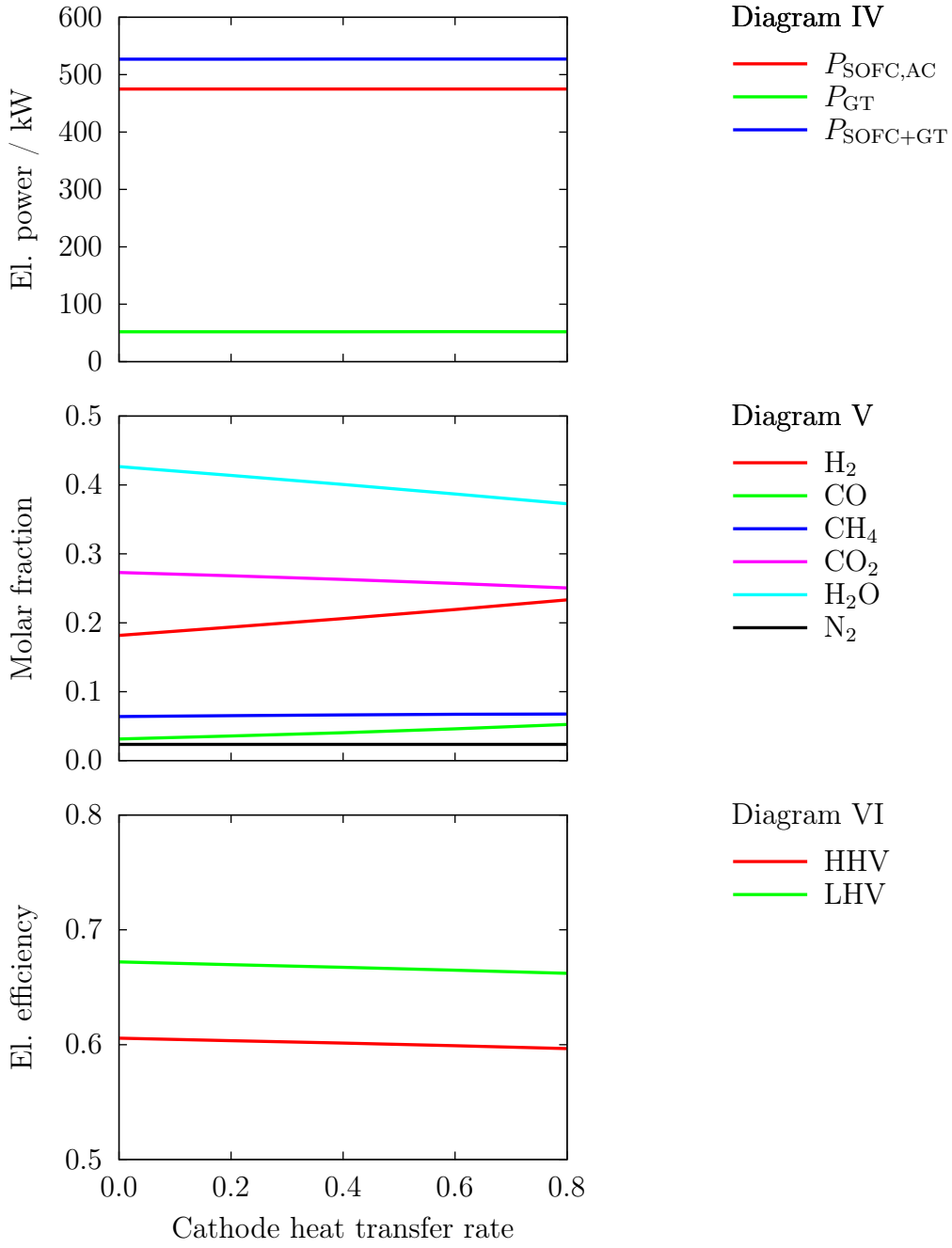

Figure 6.4b: Influence of varying cathode heat transfer on the performance of the hybrid power plant (Diagrams IV–VI).

transfer rate. The decrease is caused by the increase in fuel mass flow entering the hybrid power plant while keeping its electrical power output constant. Cell voltage of the SOFC increases due to the increase in temperature which results in a smaller current density and thus a reduction of used fuel inside the SOFC. The electrical efficiency of the electrochemical conversion inside the SOFC increases. However, regardless of the SOFC operation, the gas turbine requires the same amount of energy thus in this case a constant turbine inlet temperature. Temperature of the air leaving the SOFC system towards the combustor strongly decreases with increasing heat transfer rate and therefore more fuel has to be burned inside the combustion chamber. This causes an increase in thermal losses from the combustion chamber to the surroundings thus increasing the overall fuel demand.

6.4.2 Conclusion

Varying cathode heat transfer rate only slightly influences SOFC temperature. Simulation results show that temperature varies by 23 K within the investigated range. A higher cathode heat transfer rate positively influences SOFC operating conditions (higher cell voltage and lower FU) but has a small detrimental effect on system efficiency.

6.5 Thermal Losses of Pressure Vessel

A pressure vessel is needed in order to avoid large pressure differences between inside the SOFC and the surrounding atmosphere. In the presented system layout of the power plant, the pressure vessel is kept at intermediate temperature (average temperature of 506 K at reference conditions). Thermal losses of the pressure vessel (or other parts) to its surroundings can be critical as the energy ultimately leaves the system. In this section the influence of these thermal losses are elucidated. Note, that the thermal losses given here (in kW) are not absolute values but the thermal power leaving the pressure vessel at average pressure vessel temperature of 500 K (see Section 3.4).

6.5.1 Results and discussion

Figures 6.5a and 6.5b show the influence of thermal losses of the pressure vessel to the surrounding atmosphere on system performance and SOFC operating conditions. Thermal losses of the pressure vessel do not have a significant influence neither on

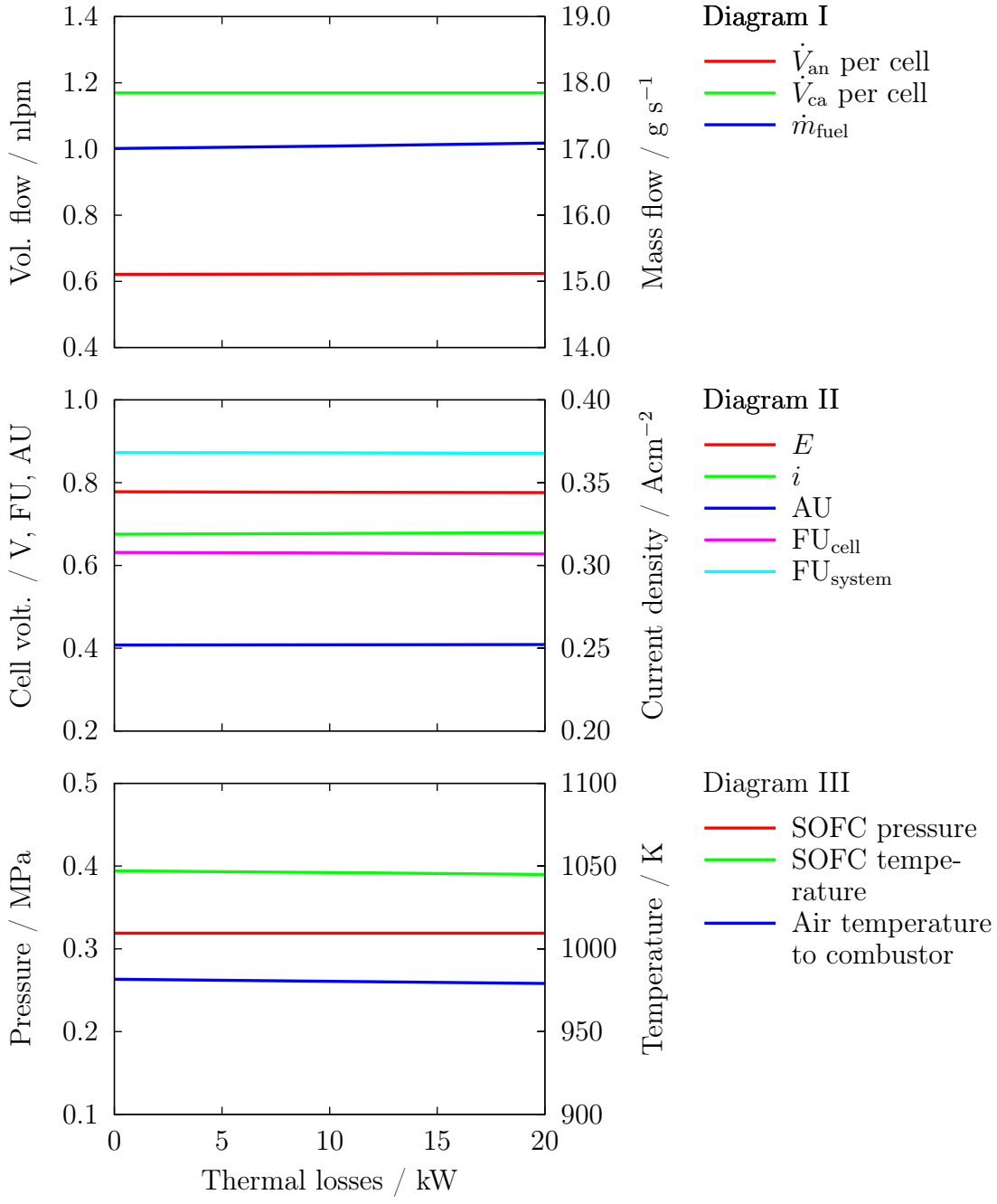

Figure 6.5a: Influence of varying thermal losses on the performance of the hybrid power plant (Diagrams I–III).

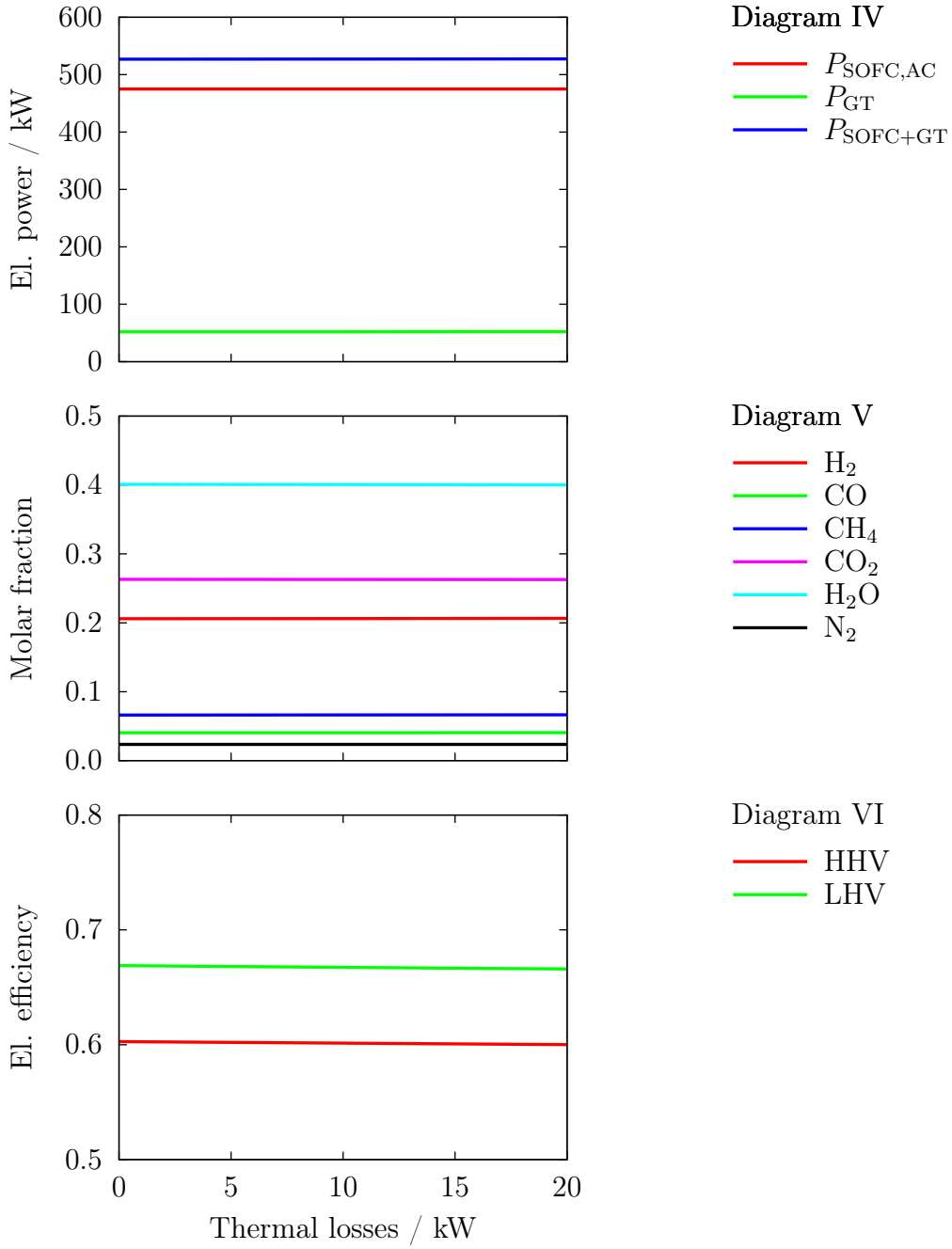

Figure 6.5b: Influence of varying thermal losses on the performance of the hybrid power plant (Diagrams IV–VI).

operating conditions of the SOFC nor on the performance of the hybrid power plant. An increase in thermal losses slightly reduces SOFC temperature due to an increased heat conduction from stacks to pressure vessel. Average pressure vessel temperature and stack temperature are reduced from 515 to 499 K and 1047 to 1045 K, respectively within the investigated range. Electrical efficiency of the system is reduced by 0.27 percentage points (HHV).

Influence of thermal losses are in this case only marginal because they occur before the air flow reaches the recuperator. An increase in thermal losses results in cooler air entering the recuperator where it is heated again with thermal energy that is about to leave the system. An increase in thermal losses of the pressure vessel therefore reduces system exhaust temperature (611 K at 0 kW and 586 K at 20 kW). The temperature of the air leaving the recuperator towards the SOFC only changes by 3 K. Within the investigated range the thermal losses at one part of the system (pressure vessel) can be compensated by reducing the thermal losses at another part of the system (exhaust).

6.5.2 Conclusion

Thermal losses of the pressure vessel do not have a strong influence on system performance. They can be compensated if they occur upstream of the recuperator resulting in lower exhaust gas temperatures. Results for variation in thermal losses differ strongly if these occur downstream of the recuperator (see Section 6.6).

6.6 Thermal Insulation of SOFC Stacks

In the current system layout, the SOFC stack is located inside a comparatively cool pressure vessel. The temperature of the pressure vessel is approximately 500 K depending on the current system operation. In order to keep SOFC operating temperature sufficiently high, the SOFC stacks need to be thermally insulated. In this section the thickness of the stack insulation is varied. Results are presented in Figures 6.6a and 6.6b. Similar results would be obtained by influencing stack insulation by other means such as variation in thermal conductivity of the insulation material or by reducing the area of hot surfaces that are exposed to the cooler pressure vessel atmosphere.

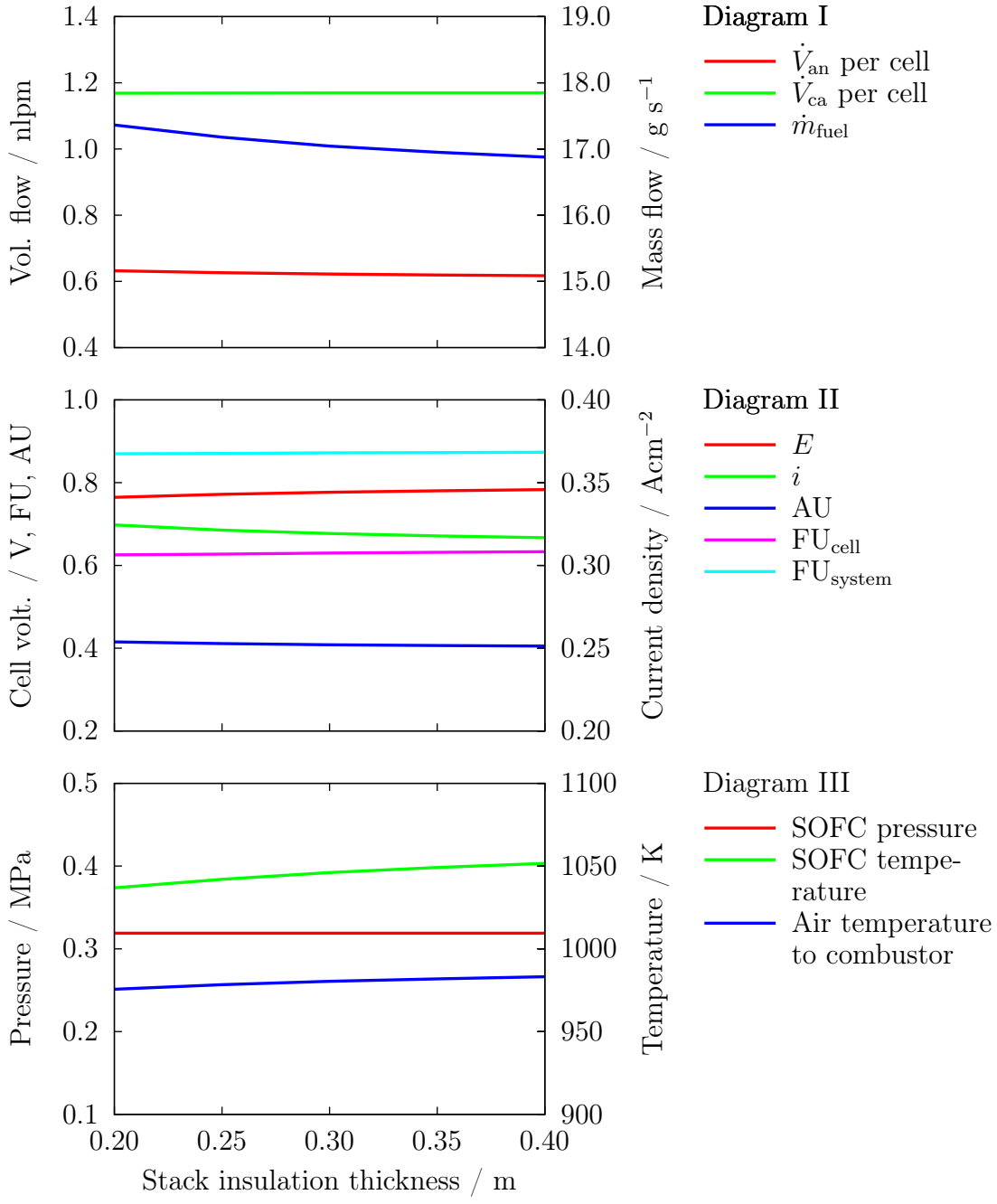

Figure 6.6a: Influence of varying stack insulation thickness on the performance of the hybrid power plant (Diagrams I–III).

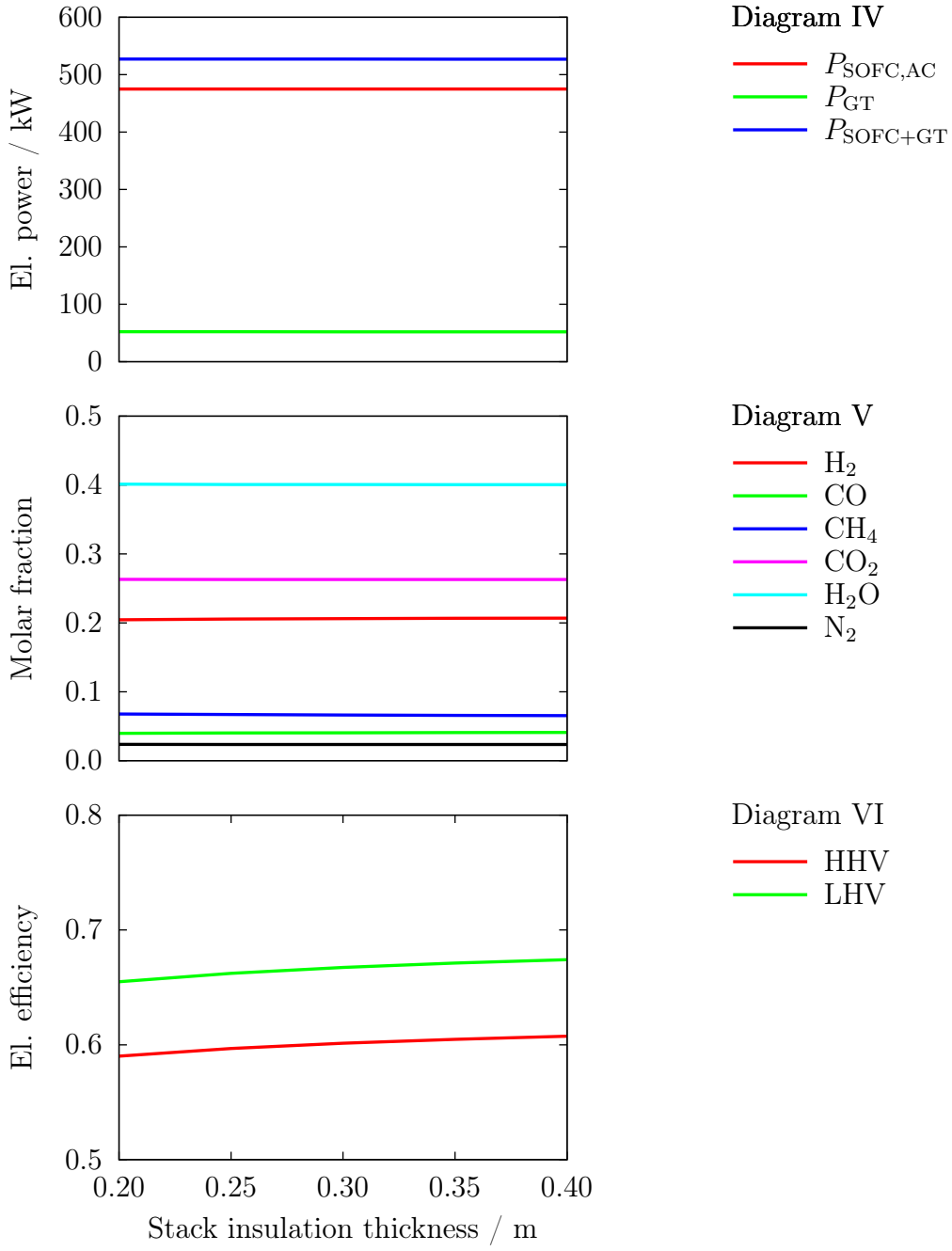

Figure 6.6b: Influence of varying stack insulation thickness on the performance of the hybrid power plant (Diagrams IV–VI).

6.6.1 Results and discussion

Diagram I shows that volumetric flows through the cell are hardly influenced. Fuel mass flow clearly decreases if stack insulation is improved. The influence is strongest at low insulation thickness.

Cell voltage slightly increases with stack insulation thickness (Diagram II) due to the increase in SOFC temperature (Diagram III). Current density is reduced accordingly in order to keep the electrical power of the SOFC constant. Fuel utilization is affected in two ways. On the one hand the decrease in current density decreases fuel utilization whereas on the other hand the reduction in fuel mass flow (Diagram I) increases it. These two affects mainly compensate each other leaving an only slight increase in cell and system fuel utilization with increasing insulation thickness. Overall airflow stays constant thus air utilization is reduced according to the reduction in current density.

SOFC pressure and temperature are shown in Diagram III. Temperature increases by 15 K if stack insulation is thickened from 0.2 to 0.4 m as thermal losses to the pressure vessel are reduced. The temperature increase is much higher between 0.2 and 0.3 m (9 K) compared to a further increase of 6 K up to 0.4 m. This behaviour is reasonable as the conductive heat flux through the insulation is proportional to insulation thickness resulting in a stronger influence at lower absolute values. SOFC pressure does not change noticeably as the gas turbine operating point is kept constant.

Electrical power output of the hybrid power plant stays constant. SOFC power is not varied and turbine operation is hardly influenced by SOFC stack insulation.

The influence of stack insulation on molar gas composition (Diagram V) is negligible. The small changes in cell voltage and fuel utilization do not strongly affect gas composition. Only the cell temperature increase (and thus increase of the recirculated anode gas) slightly shifts equilibrium composition towards lower methane concentrations inside the reformer.

Electrical efficiency is positively influenced by increasing stack insulation thickness as shown in Diagram VI. Increasing stack insulation causes an increase in SOFC temperature and thus hotter exhaust gases leaving the SOFC towards the combustion chamber (Diagram V). Less additional fuel is needed in order to reach the desired turbine inlet temperature and therefore fuel mass flow can be reduced (Diagram I). The effect here is very similar to reducing stack number as described in Section 6.1. The thermal energy that leaves the SOFC via conduction through the thermal insulation does not yet

leave the system entirely as it heats up the air inside the pressure vessel. It is, however, still lost as the air subsequently enters the recuperator at higher temperature and is preheated by far less. Comparing insulation thicknesses of 0.2 and 0.4 m the air enters the recuperator with 547 and 511 K while leaving it with 880 and 877 K, respectively. In case of 0.2 m insulation thickness the recuperator exhaust gas temperature is 31 K higher compared with an insulation of 0.4 m. Thermal energy that leaves the stack towards the pressure vessel thus indirectly leaves the system via the recuperator exhaust. This behaviour results in an overall increase in electrical efficiency of the system with increasing stack insulation thickness.

6.6.2 Conclusions

Improving stack insulation positively influences electrical efficiency of the hybrid power plant. Heat losses are reduced and therefore less fuel is needed to reach the desired turbine inlet temperature. Similar effects can be expected for other system components (e.g. piping) that are located behind the recuperator (in air flow direction). Heat losses that occur before the recuperator (e.g. as described in 6.5) can be compensated to a large extent.

6.7 Pressure Losses

Pressure losses are an important parameter for the layout of a hybrid power plant. Whereas pressure losses are not critical for the operation of the SOFC they can strongly effect the operation of a gas turbine. An increase in pressure losses changes the operating point. This can be problematic concerning the air compressor. High pressure losses can cause reverse air flow through the compressor. This behaviour can result in strong pressure fluctuations and continuous changes in air flow direction and can cause the destruction of several parts of the system. It is therefore essential to operate the compressor sufficiently far away from this operating region. In compressor maps, the region of possible operation is usually limited by a surge line. In this work, this problem is not discussed in detail. Pressure losses of the SOFC system are varied up to 30 kPa which does not yet cause a compressor surge. Results are presented in Figures 6.7a and 6.7b.

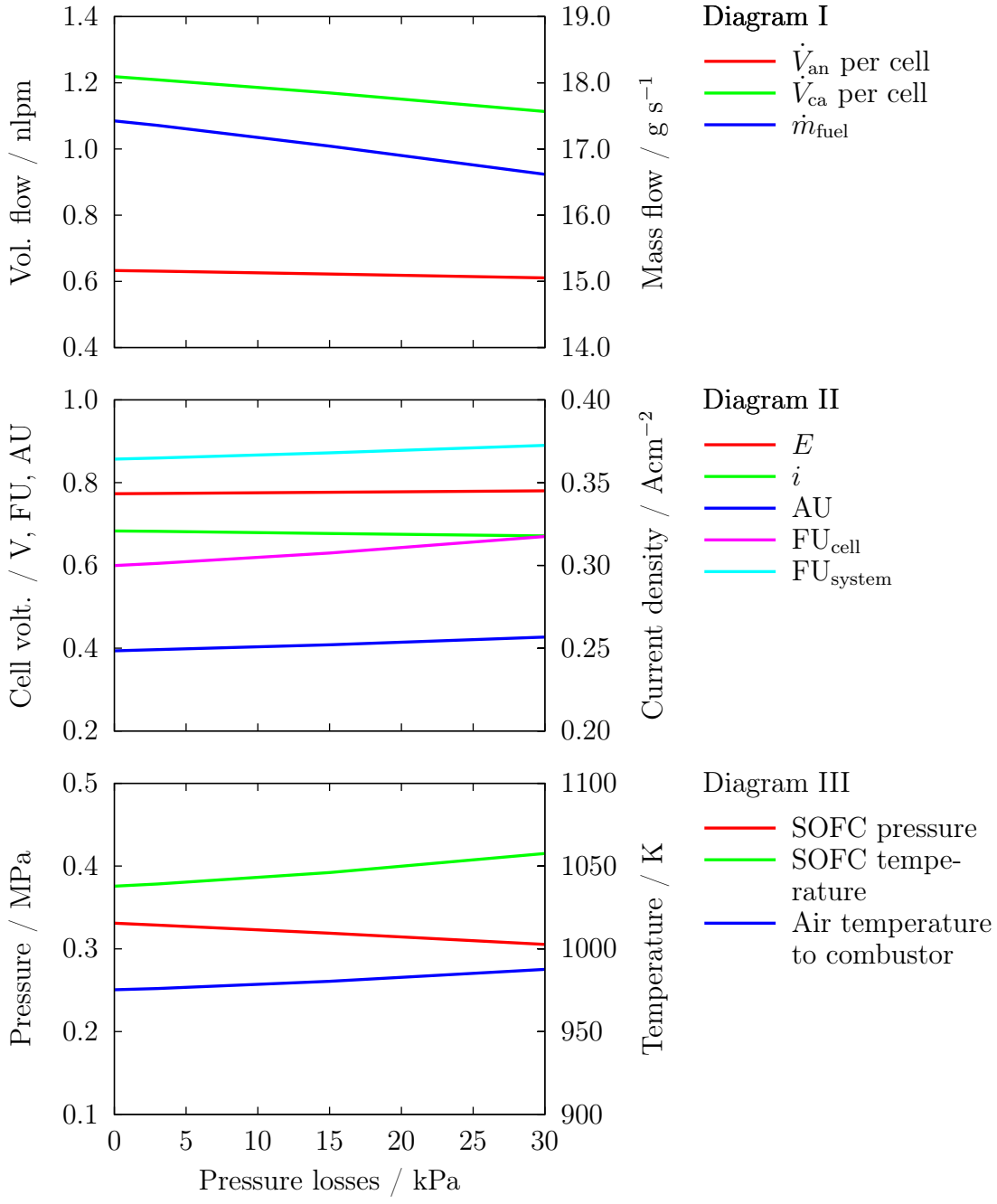

Figure 6.7a: Influence of varying pressure losses on the performance of the hybrid power plant (Diagrams I–III).

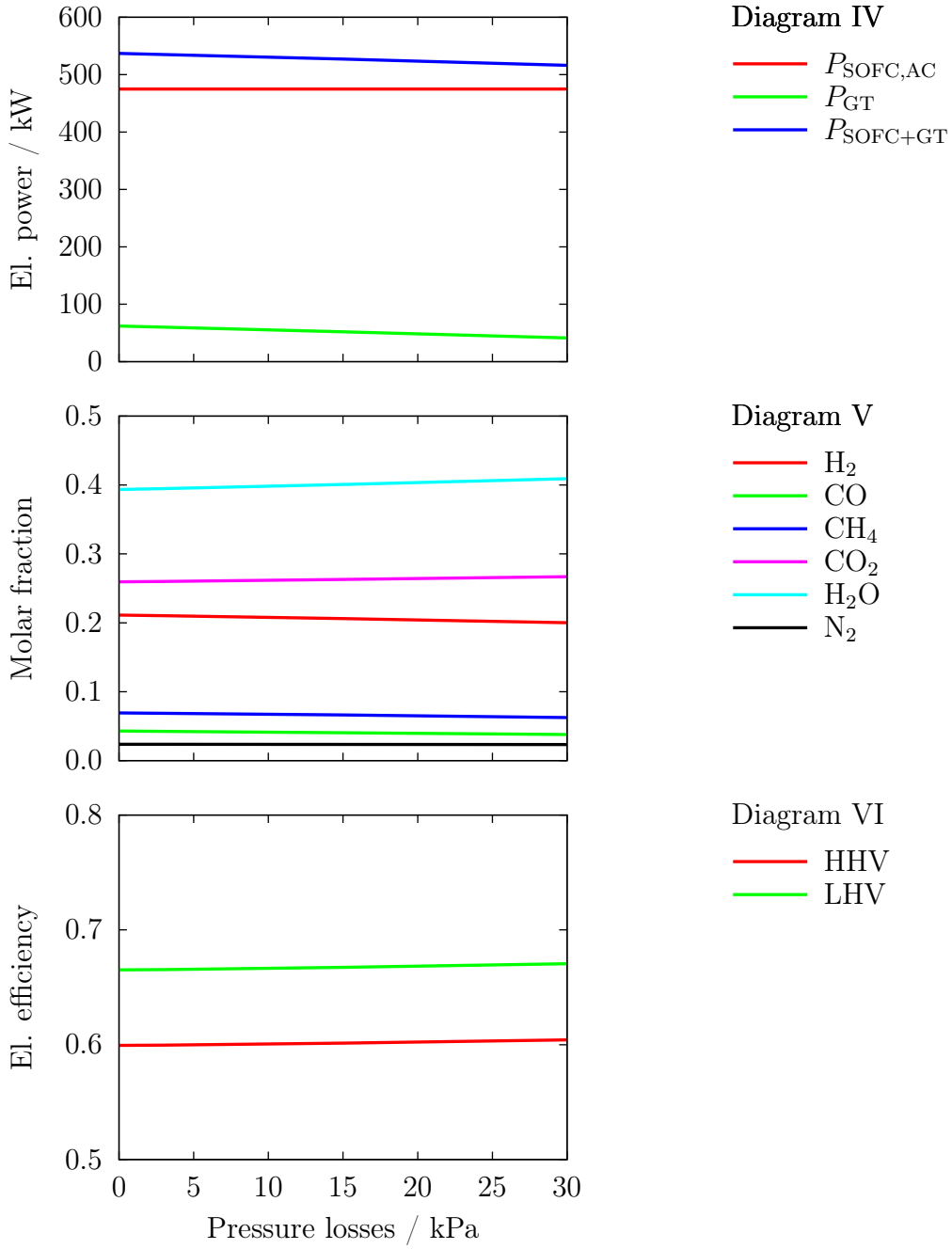

Figure 6.7b: Influence of varying pressure losses on the performance of the hybrid power plant (Diagrams IV–VI).

6.7.1 Results and discussion

Diagram I shows how gas flows are influenced by changes in SOFC system pressure losses. Pressure losses increase the back pressure of the compressor thus reducing the air flow through the SOFC system. A reduced air flow results in less thermal energy that is needed to heat this air flow thus also reducing the fuel mass flow entering the SOFC. The volumetric anode gas flow is dominated by the anode gas recirculation and is therefore only slightly affected.

Diagram II shows that cell voltage and current density are nearly constant. With increasing pressure losses, cell voltage is positively influenced by the increase in cell temperature (Diagram III) and negatively affected by the increase in fuel utilisation. Overall this results in almost constant voltage. Current density is constant accordingly in order to keep electrical power output constant. Fuel utilisation on cell and system level increase as fuel mass flow is reduced. Especially cell fuel utilisation shows a strong increase of 7 percentage points. Air utilisation increases due to the lower air mass flow through the system.

SOFC temperature (Diagram III) increases with increasing pressure losses. This effect is caused by the reduced air flow (Diagram I) which lowers the cooling effect while the thermal power output of the SOFC is nearly constant. SOFC pressure is reduced with increasing pressure losses as these losses are assumed to take place before the air enters the SOFC. The temperature of the air that leaves the SOFC system towards the combustor increases with pressure losses as SOFC temperature increases.

Pressure losses do not have an effect on the power output of the SOFC system as it is kept constant via the system control. Gas turbine electrical power is reduced by additional pressure losses. Less air is compressed, heated and expanded which reduces the power output of the turbine. The electrical power output of the hybrid power plant is therefore reduced by 21 kW.

Gas composition (Diagram V) of the gas entering the SOFC shows a behaviour according to the increase in fuel utilisation. Recirculated anode gas contains a larger amount of product gases and therefore the anode inlet gas contains more water vapour and carbon dioxide. At the same time, the amount of fuel gases is reduced.

Electrical efficiency of the system increases by 0.5 percentage points (based on HHV) with increasing pressure losses from 0 to 30 kPa. This effect is mainly caused by a change in power ratio between SOFC and gas turbine. Less air is provided by the compressor

thus increasing SOFC fuel utilisation and outlet temperature. Less fuel passes through the SOFC unused which increases the efficiency of the overall power plant. This effect is very similar to the results shown in Figure 6.2 where a change in SOFC power changed the power ratio between SOFC and GT.

6.7.2 Conclusions

Changes in pressure losses have a significant effect on the operation of the hybrid power plant. Nearly all parameters that are investigated are influenced by these changes. The main influence is the increase in fuel utilisation and electrical efficiency with increasing pressure losses which are caused by a change in power ratio between SOFC and GT. Note, that the positive effect on system efficiency shown here does not necessarily mean that high pressure losses are desirable. In the above described analysis it is not regarded that power output of the entire power plant is reduced. A reduced air flow limits the operating range of the hybrid power plant. It seems more advisable to change power ratio between SOFC and GT via changing SOFC power or turbine speed while keeping pressure losses low. This sensitivity analysis is however limited to changing single parameters only. In Section 7 it is analysed how different power demands can be met and how a variation in power demand influences system efficiency.

6.8 Gas Turbine Operating Speed

Operating speed of the gas turbine is an important parameter as it strongly influences air mass flow through the system. In the following section it is elucidated how this influences the operating conditions of the SOFC and the performance of the hybrid power plant. Gas turbine speed is varied between 63000 and 67000 rpm. For this analysis the range of variation in turbine speed is limited due to the fixed choice of other parameters. Further variations in turbine speed are shown in Section 7 where it is varied together with the SOFC electrical power output.

6.8.1 Results and discussion

Results of turbine speed variation are shown in Figures 6.8a and 6.8b. Air flow increases strongly with increasing turbine speed (Diagram I). Fuel mass flow increases accordingly

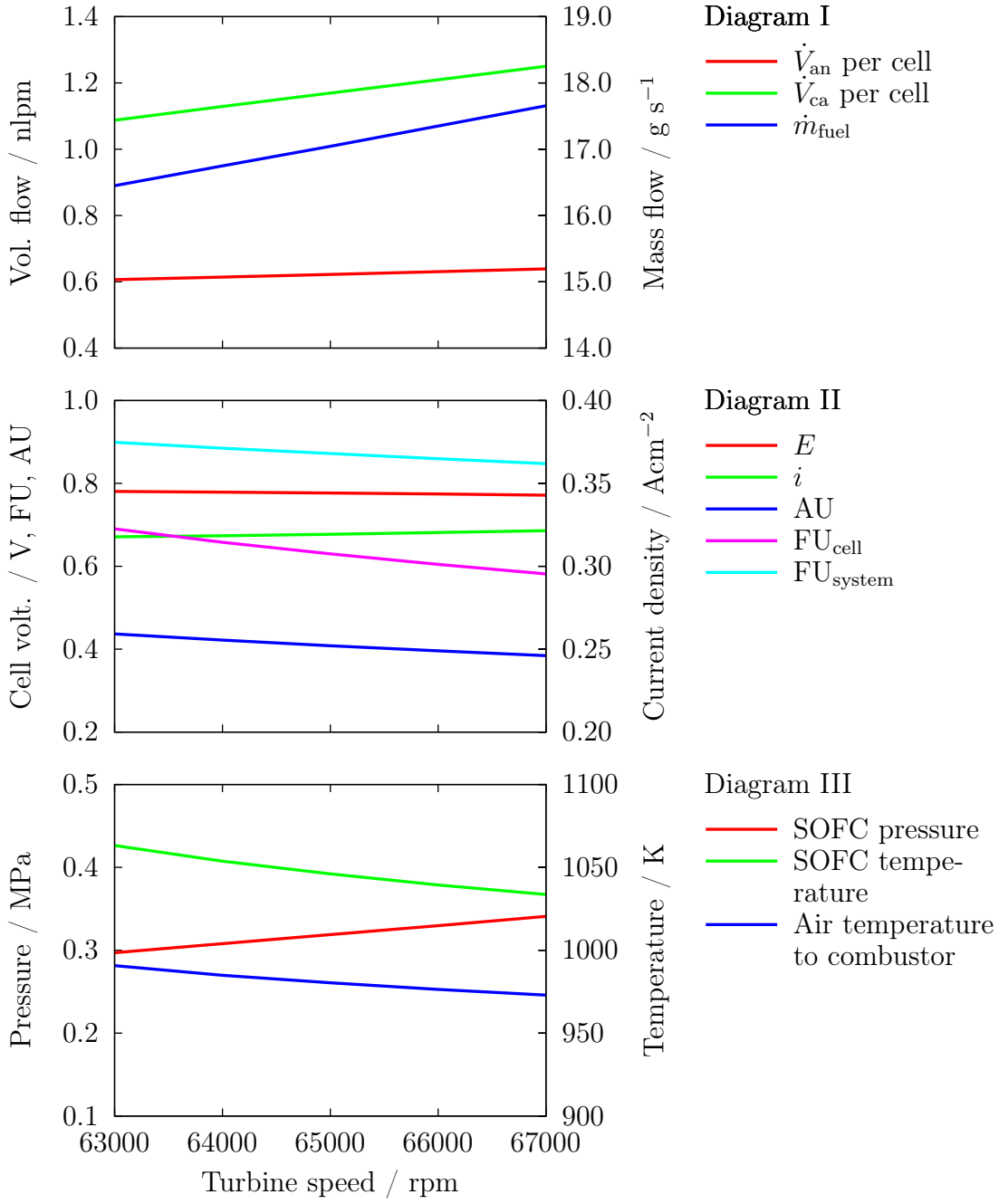

Figure 6.8a: Influence of gas turbine speed on the performance of the hybrid power plant (Diagrams I–III).

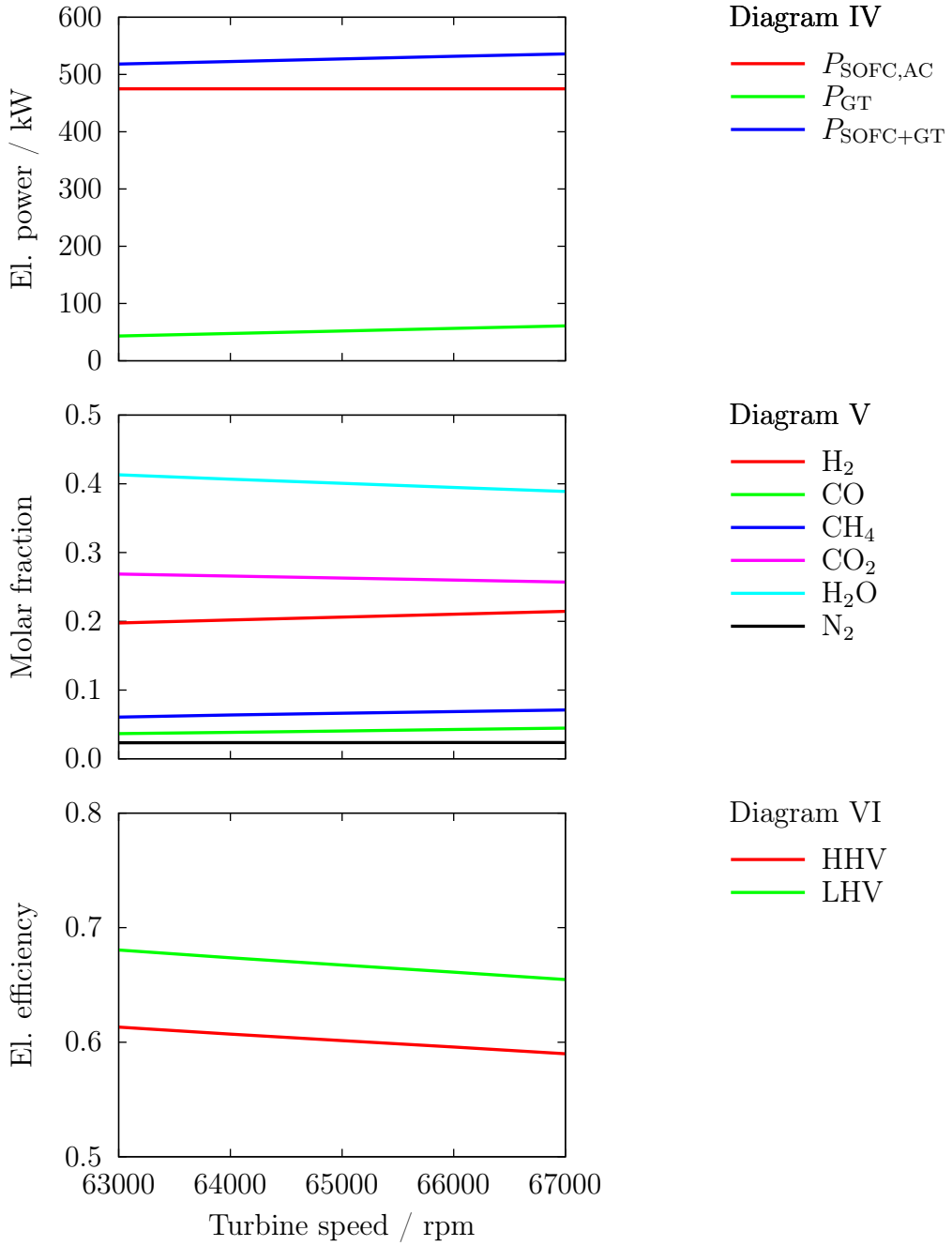

Figure 6.8b: Influence of gas turbine speed on the performance of the hybrid power plant (Diagrams IV–VI).

as more air needs to be heated up. This increase slightly affects the volumetric fuel flow through the cells although it is dominated by the anode gas recirculation.

Current density and voltage of the SOFC are only marginally affected by changes in turbine speed (Diagram II). The increased fuel and air flow with increasing turbine speed reduce the fuel and air utilisation of cell and SOFC system. This causes the fuel cell voltage to rise. Furthermore, gas composition changes towards larger fuel concentrations (Diagram V) and SOFC pressure increases with turbine speed (Diagram III) which both enhances cell voltage. All these effects are overcompensated by the decrease in SOFC temperature with increasing turbine speed. Temperature reduction causes the cell voltage to decrease slightly with increasing turbine speed. Current density increases accordingly to keep electrical power output constant.

SOFC pressure is directly affected by turbine rotational speed as shown in Diagram III. The compression ratio of the compressor increases with rotational speed and thus SOFC operating pressure increases as well. SOFC temperature decreases strongly if turbine speed is increased. The thermal power output of the cell is not affected strongly as electrical power output is kept constant and cell voltage and thus electrochemical efficiency hardly vary. Air mass flow through the SOFC increases. The larger air flow has a stronger cooling effect thus decreasing the SOFC temperature. The temperature of the air leaving the SOFC towards the combustor decreases accordingly.

An increase in turbine speed results in a larger power output of the gas turbine. For the stand-alone operation of the gas turbine this increase is significant, the overall power output of the hybrid power plant however only increases slightly. SOFC power output is kept constant.

Gas composition changes notably with turbine speed. The concentrations of fuel gases (CO, H_2, CH_4) increase with turbine speed. More fuel is supplied (Diagram I) and less fuel is used (Diagram II) thus the overall fuel concentration increases. Concentrations of product gases (H_2O, CO_2) decrease accordingly.

Electrical efficiency of the hybrid power plant decreases as turbine speed is increased as shown in Diagram VI. The temperature of the air going to the combustor (Diagram III) decreases with increasing turbine speed. Therefore more fuel is needed inside the combustor to reach the desired turbine inlet temperature. A larger share of fuel passes through the SOFC unused and therefore the electrical efficiency of the system decreases.

6.8.2 Conclusions

Variation in gas turbine speed can be a useful parameter for the control of the hybrid power plant. Changes in gas turbine speed strongly influence the air mass flow through the system which can be useful for the thermal management of the SOFC. An increase in turbine speed reduces the electrical efficiency of the hybrid power plant. Turbine speed should therefore be chosen with respect to the electrical energy demand. An increasing demand of electrical energy will result in increasing SOFC electrical power and more thermal energy leaving the SOFC. In this case, increasing turbine speed will be appropriate to cool the SOFC.

6.9 Summary and Conclusions

A sensitivity analysis based on a fixed system architecture was carried out in order to evaluate how different components influence the operating characteristics of the hybrid power plant. Most important are the influence of different parameters on SOFC temperature and electrical efficiency. The aim of the hybrid power plant is to achieve unprecedented electrical efficiencies in a large operating range. SOFC temperature constrains the operating range of the power plant as it needs to be kept within certain limits. Therefore, the effect of parameter variation on SOFC temperature and electrical efficiency is summarised in Figures 6.9 and 6.10.

Figure 6.9 shows that SOFC temperature can vary strongly with parameter variation. Temperature changes are caused by three different effects. Paramters that influence the thermal losses of the system like stack count, thermal losses of the pressure vessel and stack insulation thickness also influence SOFC temperature. However, the effect strongly depends on the location of thermal losses. The effect is small if they occur upstream of the recuperator (like thermal losses of the pressure vessel) as they can be compensated inside the recuperator to a large extent. Thermal losses that occur downstream of the recuperator (influenced for example by stack insulation thickness) have a much stronger effect on temperature as no compensation occurs. The second effect is caused by changes in power output. Higher electrical SOFC power leads to higher thermal power as well and thus hotter stacks. Changes in turbine power (via turbine speed and pressure losses) influence the air flow through the stacks and thus the cooling of the cells. The third effect is caused by recirculation of thermal energy either via anode gas recirculation or

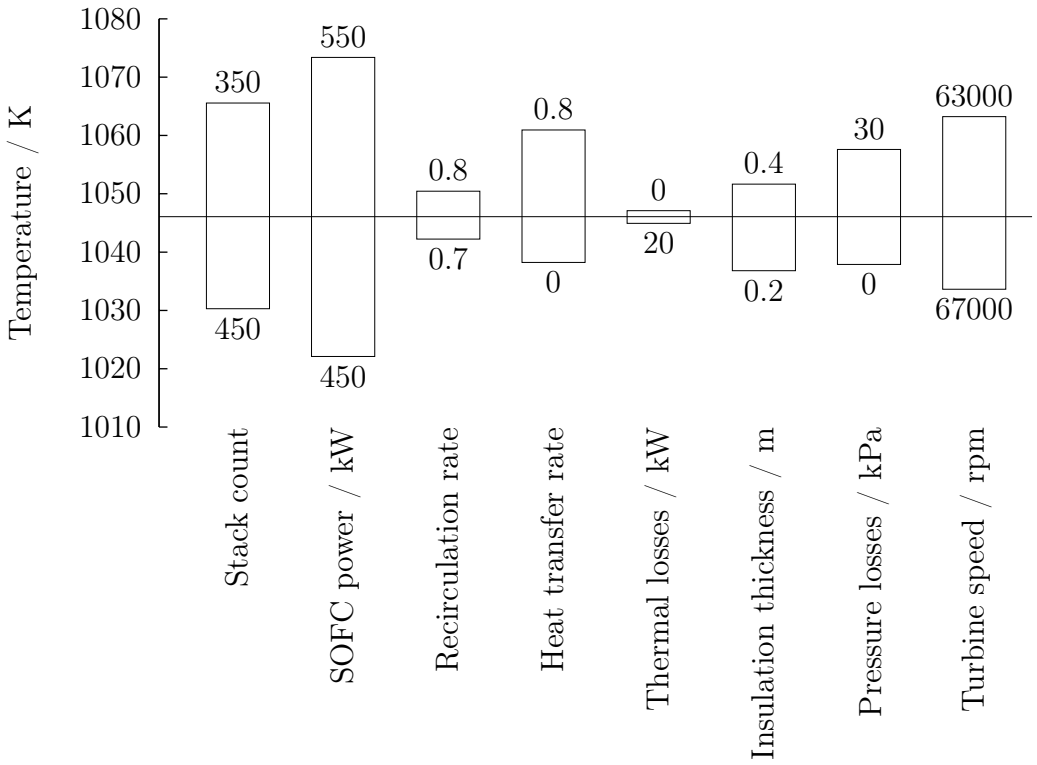

Figure 6.9: Influence of parameter variation on SOFC temperature. Temperature at reference conditions is indicated by the solid line. The numbers indicated the range of parameter variation.

cathode heat recirculation.

Temperature and cell voltage are important operating conditions for SOFC. With the presented system control, temperature and voltage have to some extent a self-regulating effect. If SOFC temperature increases due to changes in operating conditions e.g. a change in cathode heat exchanger transfer rate, the SOFC reacts by increasing cell voltage. This enhances electrochemical efficiency of the cells thus reducing thermal power output of the cell and therefore decreasing cell temperature. As another example, an increase in load demand causes at first a reduction in cell voltage while increasing thermal power output of the cell. This will cause a rise in cell temperature and thus increase cell voltage again. Overall these characteristics of the power plant result in temperature variations over a large range of acceptable SOFC temperatures. At the same time, cell voltage stays very stable within the entire variations of operating conditions.

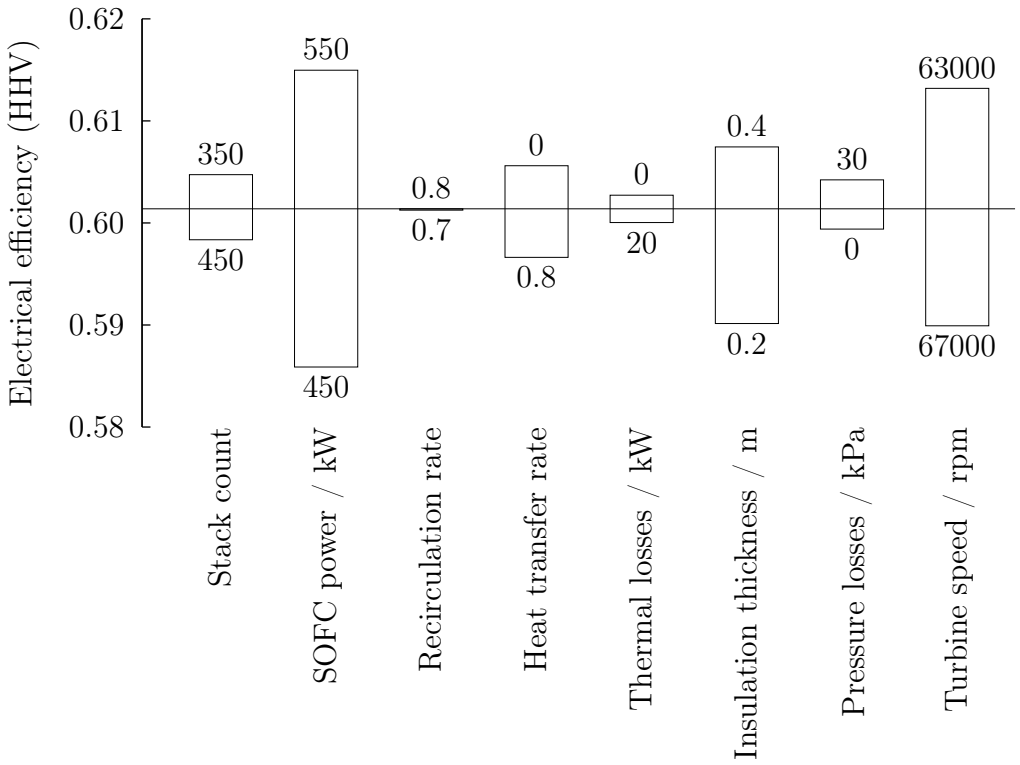

Figure 6.10: Influence of parameter variation on hybrid power plant efficiency. Efficiency at reference conditions is incidated by the solid line. The numbers indicated the range of parameter variation.

Electrical efficiency (Figure 6.10) of the hybrid power plant is also affected via three different phenomena. An increase in thermal losses via a larger stack number (increased surface area) or weaker insulation directly reduces overall electrical efficiency. Furthermore, heat recirculation can have a detrimental effect on efficiency as more fuel needs to be burned inside the combustor in order to achieve the desired turbine inlet temperature. The third and strongest effect is caused by variation in power ratio between SOFC and gas turbine. Varying either gas turbine or SOFC power output strongly influences the electrical efficiency of the power plant. For highest electrical efficiency, SOFC and GT output power have to be matched adequately. This will result in high fuel utilisation of the SOFC at usually high SOFC temperature thus reducing the amount of fuel that is burned inside the combustor und hence solely used by the gas turbine.

Changes in pressure losses also influence the power ratio and therefore the electrical

efficiency of the system. Pressure losses lead to a reduced air flow. This affects thermal management of the cells and reduces the thermal energy required by the gas turbine. Pressure losses therefore influence the power ratio between SOFC and gas turbine.

Anode gas recirculation is essential for an efficient operation of a hybrid power plant. In this study recirculation is only varied within a very limited range in order to prevent carbon deposition inside the reformer. Within the investigated range, the influence on temperature and efficiency is only small.

The number of SOFC stacks does not play an important role regarding the overall electrical efficiency of the power plant. Dimensioning of SOFC stack size should therefore mainly be based on economical aspects and the maximum acceptable current density of the cells. From an economical point of view, few cells are preferable. A smaller number of cells results in higher current densities at constant electrical power thus limiting the maximum electrical power output of the plant.

7 Operating Range of the Hybrid Power Plant

In Section 6, different parameters are varied separately in order to evaluate how the performance of the hybrid power plant is influenced. In this section, most of the parameters are set to a fixed value and simulations are carried out for different power outputs. For this purpose gas turbine speed is set to four different values and simulations are conducted with varying SOFC electrical power. It is shown that the proposed system architecture and control strategy offer a wide range of electrical power output with high electrical efficiency.

In this part of the thesis all results from the previous chapters are taken into consideration. The performance characteristics of the SOFC analysed in Section 4 are reflected via the experimentally validated SOFC model. Durability concerns (Section 5) are regarded in terms of the system operating range. Results of the sensitivity analysis (Section 6) are considered for the choice of parameter settings for the hybrid power plant. Therefore, aspects from electrochemistry on electrode level up to dimensioning of system components are regarded to develop a beneficial system architecture and operating strategy.

7.1 Parameter Settings

Most of the parameters that are varied in the previous section are now set to fixed values in order to simulate a real hybrid power plant. The number of stacks is set to 350 as more stacks have not proven to result in higher system efficiencies. As stacks are one of the most expensive parts of the power plant, less stacks are chosen for the final dimensioning of the system. Anode gas recirculation rate only showed small overall influence on the system and a constant rate of 0.8 is chosen as it helps to lower the fuel utilisation at the cells thus potentially reducing problems concerning cell degradation. Cathode heat exchanger transfer rate only slightly affects electrical efficiency and a value of 0.8 is chosen to keep the fuel utilisation low. For thermal losses of the pressure vessel to the surroundings an average value of 10 kW (at average vessel temperature of 500 K) is selected. A better stack insulation has shown to be effective for increasing overall electrical efficiency and therefore a value of 0.4 m is chosen. Pressure losses of SOFC stacks are usually small but strongly depending on fluid velocity. For these simulations pressure losses are estimated with 15 kPa which includes the entire SOFC system and still leaves room for further system optimisation. The two remaining parameters gas turbine

speed and SOFC electrical power output are both varied throughout this section.

7.2 Results

Figure 7.1 shows the influence of electrical power output of the hybrid power plant on electrical efficiency and SOFC temperature. Results are shown for four different gas turbine rotational speeds from 55000 rpm to 70000 rpm. An acceptable SOFC temperature region is indicated between 950 K and 1125 K. Temperatures outside this region need to be prevented as they can lead to the destruction of sealings (above 1125 K) or very high ohmic resistances (below 950 K).

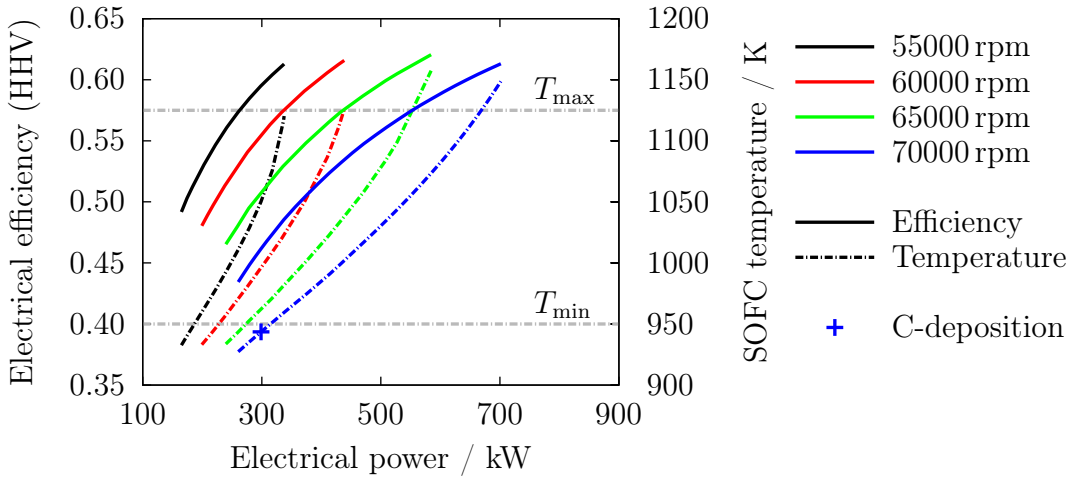

Figure 7.1: Operating range of the hybrid power plant based on the presented system control strategy at different turbine speeds.

All results shown here are based on the before mentioned system operating strategy (Section 3.4.2). The gas turbine can be operated at different speeds and dominates the system control by determining the fuel mass flow through the system. The SOFC operating conditions (like fuel utilisation, cell voltage, and stack temperature) are not actively controlled but are allowed to vary within acceptable limits. At a rotational speed of 70000 rpm the maximum SOFC temperature is reached at the maximum electrical power output of the system of 670 kW. At this point, the electrical efficiency is above 60 %. Cell voltage is at 0.81 V at a current density of 0.44 A cm^{-2}. Cell and system fuel utilisation are 0.5 and 0.83, respectively. Both temperature and efficiency decrease considerably while lowering the electrical power output of the plant and keeping gas

turbine speed constant.

At 370 kW electrical power, electrical efficiency drops below 50 %. While gas turbine electrical power output stays nearly constant, SOFC electrical power output drops significantly. This leads to a significantly lower SOFC operating temperature thus more fuel has to be burned in order to keep the gas turbine at stable operation. Whereas at maximum power the power ratio between SOFC and GT is about 8, it drops to below 5 at 370 kW. Lower gas turbine speeds result in qualitatively similar results however at lower overall eletrical power. Furthermore, the SOFC temperature changes much stronger with power output at lower turbine speeds. As less air is provided by the gas turbine for cooling, changes in power output of the SOFC have a stronger effect at low turbine speeds.

The operating range of the hybrid power plant is further limited by degradation processes. Whereas simulations do not indicate nickel oxidation propensity at any operating point, carbon deposition is likely to take place at low SOFC temperature. A critical operating point is marked in Figure 7.1 for a gas turbine speed of 70000 rpm. At this operating point, thermodynamic equilibrium calculations show the formation of solid carbon. Although the operating point is already outside the possible operating range, it is nevertheless important to consider that carbon deposition could already occur at higher temperatures. For the safe operation of the power plant it is advisable to prevent operation close to this point or increase anode gas recirculation rate to increase O/C ratio. Results did not show carbon deposition at lower turbine speeds. Turbine inlet temperature is lower at low turbine speed thus increasing fuel utilisation resulting in a higher O/C ratio.

In order to reach high electrical efficiency also at part-load, gas turbine speed and SOFC power need to be varied at the same time as shown in Figure 7.2. Turbine speed is reduced from 70000 to 55000 rpm which also reduces electrical power output of the turbine from 74 to 14 kW (at $T_{\mathrm{SOFC}} = T_{\mathrm{max}}$). SOFC temperature stays constant (at its maximum) if turbine rotational speed is gradually decreased while the system power output varies between 670 and 340 kW. Electrical efficiency of the system stays above 60 % within this power range with slightly lower efficiency at high turbine speed. SOFC power output can be further reduced but this will result in a decrease in SOFC temperature and electrical efficiency. Electrical power output of the system can be reduced down to 190 kW where SOFC temperature reaches its minimum and where

electrical efficiency falls below 52 %. Cell voltage is at 0.78 V at a current density of 0.13 A cm^{-2}. Cell and system fuel utilisation are 0.4 and 0.77, respectively. A further reduction of electrical power output is limited by the minimum turbine rotational speed.

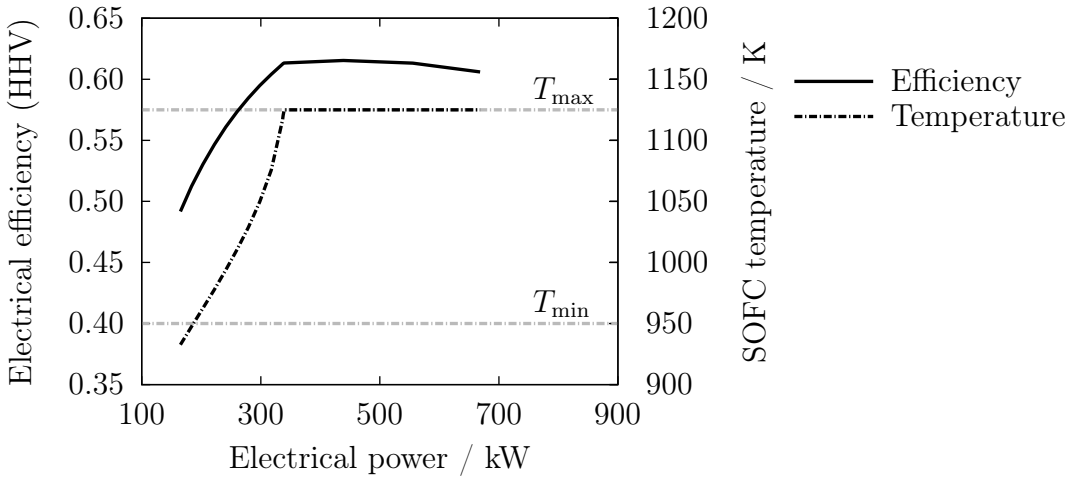

Figure 7.2: Operating range of the hybrid power plant based on the presented system control strategy with variable turbine speed. Variable gas turbine rotational speed allows for a wide power range from 310 to 670 kW with electrical efficiencies above 60 % based on the HHV.

For dynamic operation of the system it is necessary to develop a load following strategy that prevents SOFC temperatures outside the operating range. Fast and large changes in electrical power demand can only be responded to by the SOFC as it provides the largest power share. If the SOFC is operated at low power output but near its maximum temperature a quick load increase can cause overheating of the cell. It is therefore necessary to quickly increase the turbine rotational speed with SOFC power to prevent temperature-induced damages to the SOFC.

7.3 Conclusions

The proposed system architecture and control strategy offers a simple operation of the power plant with high electrical efficiencies and desirable operating conditions for SOFC and GT within a broad power range. Simulation results showed that electrical efficiency can be kept above 60 % (based on HHV) within 310 to 670 kW electrical power output. A further reduction of power output down to 190 kW is possible but at the cost of efficiency.

Within the entire power range, voltage can be kept at 0.74 V or higher without a direct control of the operating conditions of the SOFC. At the same time, cell fuel utilisation is kept below 70 %. Operating conditions are therefore kept perfectly within desired operating conditions of an SOFC. Accelerated degradation of the SOFC should not be a problem under these conditions. At low SOFC temperatures carbon deposition inside the reformer can be a problem.

Power output of the power plant is limited by the SOFC operating temperature. At high power output above 670 kW the SOFC will exceed its maximum operating temperature. At electrical powers below 190 kW SOFC temperature will fall below 950 K and SOFC performance will start to fade strongly. All presented results are based on stationary operation of the power plant.

8 Conclusions

The present thesis elucidates the effect of pressure on solid oxide fuel cells from electrochemistry on electrode surfaces to influences on a hybrid power plant. A detailed electrochemistry model of an SOFC stack is developed and experimentally validated. The stack model is implemented into a hybrid power plant (SOFC and GT) model and a system layout and operating strategy is presented that yields high electrical efficiency over a broad power range.

An increase in pressure generally improves the performance of an SOFC. Theoretical investigations showed that Nernst potential increases with increasing pressure thus causing an increase in OCV. Furthermore, polarisation resistance of an SOFC is reduced by increasing pressure. Whereas ohmic resistances are not affected, gas diffusion through the porous electrodes is facilitated due to a change in diffusion mechanism. Furthermore, activation polarisation is reduced with increasing pressure as adsorption of reactants on the electrode surfaces is enhanced supporting the charge transfer reaction. All results showed a logarithmic behaviour. Effects are strongest at low pressure (up to 0.5–1 MPa) and weaker at higher pressure.

Experimental validation of the model includes polarisation curves as well as electrochemical impedance spectra which allow for separation of different overpotentials. Combined pressure effects result in a significant improvement of SOFC performance. Electrical power output is improved by up to 83 % while keeping electrochemical efficiency constant. With a constant electrical power output, electrochemical efficiency is enhanced by up to 14 %. Experiments were carried out at pressures between 0.135 and 0.8 MPa. All investigations are based on one type of anode-supported SOFC and results will vary quantitatively with other cells.

Nickel oxidation of the anode is more likely to occur at higher pressure as it influences the equilibrium partial pressure of oxygen in the anode gas. Results presented in this work do not cover electrochemical oxidation of nickel thus more detailed studies on pressure effects are necessary. Carbon deposition propensity is highly pressure dependent. Results showed that it should be possible to prevent carbon deposition by keeping the oxygen to carbon ratio above 2 within the entire hybrid power plant.

A hybrid power plant operating strategy is presented which is based on variable SOFC temperature and turbine speed. A sensitivity analysis showed that an adequate power ratio between SOFC and GT is important to achieve high electrical efficiency. Other

parameters like the number of SOFC stacks are of less importance. For the system analysed in this thesis, a wide electrical power range between 310 and 670 kW seems achievable with high electrical efficiency above 60 % based on the HHV. A smaller power output down to 190 kW is possible only with reduced efficiency below 52 %. Power output is limited by minimum and maximum SOFC temperature.

9 Future Perspectives

This work suggests a concept for an operating strategy of a hybrid power plant. All investigations are so far theoretical and based on stationary operation. In future works, the proposed control strategy should be further developed to accommodate dynamic operation. With an increasing share of fluctuating electrical energy suppliers, dynamic operation of power plants may be of increasing importance in the future. Hybrid power plants are generally capable of dynamic operation, however, it may require additional control mechanisms such as a direct fuel feed to the combustion chamber. Transient operation like load changes or start-up and shutdown of the system have to be safe and reliable.

Theoretical work helps to analyse the feasibility of system concepts and to examine the general interrelations between system components. More detailed studies however require experimental validation of the entire system model. Therefore, the most important and ambitious future task will be the actual construction of the hybrid power plant. Many challenges will arise which have not been adressed so far. Proof of concept is necessary to demonstrate that these problems can be solved and that high electrical efficiency within a large power range is achievable. These challenges will be addressed at the DLR during the upcoming years. Construction of a demonstration power plant with an electrical power output between 15 and 30 kW is ongoing. First test of the coupled system is scheduled for 2017.

Provided that tests are successful even more efficient systems could be built. With hybrid power plants consisting of SOFC, gas turbine, and steam turbine electrical efficiencies above 80 % are realistic.

References

[1] T. A. Adams II, J. Nease, D. Tucker, and P. I. Barton (2013). *Energy Conversion with Solid Oxide Fuel Cell Systems: A Review of Concepts and Outlooks for the Short- and Long-Term.* Industrial and Engineering Chemistry Research, 52, pp. 3089–3111. doi:10.1021/ie300996r.

[2] G. D. Agnew, D. Bernardi, R. D. Collins, and R. H. Cunningham (2006). *An internal reformer for a pressurised SOFC system.* Journal of Power Sources, 157, pp. 832–836. doi:10.1016/j.jpowsour.2005.11.101.

[3] G. D. Agnew, R. D. Collins, M. Jorger, S. H. Pyke, and R. P. Travis (2007). *The Components of a Rolls-Royce 1 MW SOFC System.* ECS Transactions, 7, pp. 105–111. doi:10.1149/1.2729079.

[4] P. Atkins (1994). *Physical Chemistry.* Oxford University Press, Oxford, 5th edition.

[5] W. G. Bessler (2006). *Gas Concentration Impedance of Solid Oxide Fuel Cell Anodes I. Stagnation Point Flow Geometry.* Journal of The Electrochemical Society, 153, pp. A1492–A1504.

[6] W. G. Bessler (2007). *Electrochemistry and Transport in Solid Oxide Fuel Cells.* Habilitation thesis, Heidelberg University, Heidelberg.

[7] W. G. Bessler, S. Gewies, and M. Vogler (2007). *A new framework for physically based modeling of solid oxide fuel cells.* Electrochimica Acta, 53, pp. 1782–1800. doi:10.1016/j.electacta.2007.08.030.

[8] W. G. Bessler, S. Gewies, C. Willich, G. Schiller, and K. A. Friedrich (2010). *Spatial Distribution of Electrochemical Performance in a Segmented SOFC: A Combined Modeling and Experimental Study.* Fuel Cells, 10, pp. 411–418. doi:10.1002/fuce.200900083.

[9] W. G. Bessler, M. Vogler, H. Störmer, D. Gerthsen, A. Utz, A. Weber, and E. Ivers-Tiffée (2010). *Model anodes and anode models for understanding the mechanism of hydrogen oxidation in solid oxide fuel cells.* Physical Chemistry Chemical Physics, 12, pp. 13888–13903. doi:10.1039/c0cp00541j.

[10] BMWi, BMU (2010). *Energy Concept for an Environmentally Sound, Reliable and Affordable Energy Supply.*
URL http://www.bmu.de/files/english/pdf/application/pdf/energiekonzept_bundesregierung_en.pdf

[11] BRD (Last changed 2011-07-31). *Gesetz über die friedliche Verwendung der Kernenergie und den Schutz gegen ihre Gefahren (Atomgesetz) / Nuclear Energy Act.*

[12] A. A. Burke, L. G. Carreiro, and J. R. Izzo Jr. (2013). *Pressurized testing of a planar solid oxide fuel cell stack.* International Journal of Hydrogen Energy, 38, pp. 13774–13780. doi:10.1016/j.ijhydene.2013.08.058.

[13] P. Chan (2001). *NASA Glenn Research Center: Thermo Build.*
URL http://www.grc.nasa.gov/WWW/CEAWeb/ceaThermoBuild.htm

[14] L. A. Chick, O. A. Marina, C. A. Coyle, and E. C. Thomson (2013). *Effects of temperature and pressure on the performance of a solid oxide fuel cell running on steam reformate of kerosene.* Journal of Power Sources, 236, pp. 341–349. doi: 10.1016/j.jpowsour.2012.11.136.

[15] P. Costamagna, L. Magistri, and A. F. Massardo (2001). *Design and part-load performance of a hybrid system based on a solid oxide fuel cell reactor and a micro gas turbine.* Journal of Power Sources, 96, pp. 352–368.

[16] N. Epstein (1989). *On tortuosity and the tortuosity factor in flow and diffusion through porous media.* Chemical Engineering Science, 44, pp. 777–779.

[17] M. L. Ferrari (2011). *Solid oxide fuel cell hybrid system: Control strategy for stand-alone configurations.* Journal of Power Sources, 196, pp. 2682–2690. doi: 10.1016/j.jpowsour.2010.11.029.

[18] M. L. Ferrari, D. Bernardi, and A. F. Massardo (2006). *Design and Testing of Ejectors for High Temperature Fuel Cell Hybrid Systems.* ASME Transactions, 3, pp. 284–291. doi:10.1115/1.2211631.

[19] M. L. Ferrari and A. F. Massardo (2013). *Cathode-anode side interaction in SOFC hybrid systems.* Applied Energy, 105, pp. 369–379. doi:10.1016/j.apenergy.2013.01.029.

[20] M. L. Ferrari, M. Pascenti, L. Magistri, and A. F. Massardo (2010). *Micro Gas Turbine Recuperator: Steady-State and Transient Experimental Investigation.* Journal of Engineering for Gas Turbines and Power, 132, p. 022301. doi:10.1115/1.3156822.

[21] M. L. Ferrari, M. Pascenti, L. Magistri, and A. F. Massardo (2011). *MGT/HTFC Hybrid System Emulator Test Rig: Experimental Investigation on the Anodic Recirculation System.* Journal of Fuel Cell Science and Technology, 8, p. 021012. doi:10.1115/1.4002316.

[22] M. L. Ferrari, M. Pascenti, and A. F. Massardo (2008). *Ejector Model for High Temperature Fuel Cell Hybrid System: Experimental Validation at Steady-State and Dynamic Conditions.* Journal of Fuel Cell Science and Technology, 5, p. 041005. doi:10.1115/1.2890102.

[23] M. L. Ferrari, M. Pascenti, and L. M. A. F. Massardo (2010). *Hybrid System Test Rig: Start-up and Shutdown Physical Emulation.* Journal of Fuel Cell Science and Technology, 7, p. 021005. doi:10.1115/1.3176663.

[24] M. L. Ferrari, A. Traverso, L. Magistri, and A. F. Massardo (2005). *Influence of the anodic recirculation transient behaviour on the SOFC hybrid system performance.* Journal of Power Sources, 149, pp. 22–32. doi:10.1016/j.jpowsour.2005.01.059.

[25] A. Ferretti, A. Traverso, G. J. Saunders, M. A. Perna, and A. F. Massardo (2012). *Transient Model Validation of a Desulfurizer and a Syngas Generator for High Temperature Fuel Cells.* Journal of Fuel Cell Science and Technology, 9, p. 011007. doi:10.1115/1.4005122.

[26] E. N. Fuller, K. Ensley, and J. C. Giddings (1969). *Diffusion of Halogenated Hydrocarbons in Helium. The Effect of Structure on Collision Cross Sections.* The Journal of Physical Chemistry, 73, pp. 3679–3685.

[27] E. N. Fuller, P. D. Schettler, and J. C. Giddings (1966). *A New Method for Prediction of Binary Gas-Phase Diffusion Coefficients.* Industrial and Engineering Chemistry, 58, pp. 19–27.

[28] M. Gandiglio, A. Lanzini, P. Leone, M. Santarelli, and R. Borchiellini (2013). *Thermoeconomic analysis of large solid oxide fuel cell plants: Atmospheric vs. pressurized performance.* Energy, 55, pp. 142–155. doi:10.1016/j.energy.2013.03.059.

[29] F. J. Gardner, M. J. Day, N. P. Brandon, M. N. Pashley, and M. Cassidy (2000). *SOFC technology development at Rolls-Royce.* Journal of Power Sources, 86, pp. 122–129.

[30] S. Gewies and W. G. Bessler (2008). *Physically Based Impedance Modeling of Ni/YSZ Cermet Anodes.* Journal of The Electrochemical Society, 155, pp. B937–B952. doi:10.1149/1.2943411.

[31] D. G. Goodwin (2001-2010). *Cantera.*
URL `http://code.google.com/p/cantera/`

[32] D. G. Goodwin (2003). *An open source, extensible software suite for CVD process simulation.* Electrochemical Society Proceedings, 8, pp. 155–162.

[33] S. Hashimoto, Y. Liu, K. Asano, F. Yoshiba, and M. Mori (2011). *Power Generation Properties of Microtubular Solid Oxide Fuel Cell Bundle Under Pressurized Conditions.* Journal of Fuel Cell Science and Technology, 8, p. 021010. doi:10.1115/1.4002314.

[34] S. Hashimoto, H. Nishino, Y. Liu, K. Asano, M. Mori, Y. Funahashi, and Y. Fujishiro (2008). *Effects of Pressurization on Cell Performance of a Microtubular SOFC with Sc-Doped Zirconia Electrolyte.* Journal of the Electrochemical Society, 155, pp. B587–B591. doi:10.1149/1.2903295.

[35] M. Henke, J. Kallo, K. A. Friedrich, and W. G. Bessler (2011). *Influence of Pressurisation on SOFC Performance and Durability: A Theoretical Study.* Fuel Cells, 11, pp. 581–591. doi:10.1002/fuce.201000098.

[36] M. Henke, C. Willich, M. Steilen, J. Kallo, and K. A. Friedrich (2013). *Solid Oxide Fuel Cell - Gas Turbine Hybrid Power Plant.* ECS Transactions, 57, pp. 67–72. doi:10.1149/05701.0067ecst.

[37] M. Henke, C. Willich, C. Westner, F. Leucht, J. Kallo, W. G. Bessler, and K. A. Friedrich (2013). *A validated multi-scale model of a SOFC stack at elevated pressure.* Fuel Cells, 13, pp. 773–780. doi:10.1002/fuce.201300076.

[38] M. Henke, C. Willich, C. Westner, F. Leucht, R. Leibinger, J. Kallo, and K. A. Friedrich (2012). *Effect of pressure variation on power density and efficiency of solid oxide fuel cells.* Electrochimica Acta, 66, pp. 158–163. doi:10.1016/j.electacta.2012.01.075.

[39] M. Hohloch, A. Widenhorn, D. Lebküchner, T. Panne, and M. Aigner (2008). *Micro gas turbine test rig for hybrid power plant application.* ASME Turbo Expo, Berlin, Germany. GT2008-50443.

[40] M. Hohloch, J. Zanger, A. Widenhorn, and M. Aigner (2010). *Experimental characterization of a micro gas turbine test rig.* ASME Turbo Expo, Glasgow, UK. GT2010-22799.

[41] IEA (2010). *World Energy Outlook 2010 Executive Summary.* URL `www.iea.org/weo/docs/weo2010/WEO2010_ES_English.pdf`

[42] M. Iwata, T. Hikosaka, M. Morita, T. Iwanari, K. Ito, K. Onda, Y. Esaki, Y. Sakaki, and S. Nagata (2000). *Performance analysis of planar-type unit SOFC considering current and temperature distributions.* Solid State Ionics, 132, pp. 297–308.

[43] V. M. Janardhanan and O. Deutschmann (2006). *CFD analysis of a solid oxide fuel cell with internal reforming: Coupled interactions of transport, heterogeneous catalysis and electrochemical processes.* Journal of Power Sources, 162, pp. 1192–1202. doi:10.1016/j.jpowsour.2006.08.017.

[44] E. Job (accessed 2009-07-22). *Table of chemical potentials.* Eduard-Job-Foundation for Thermo- and Matterdynamics, www.job-stiftung.de.

[45] T. Kaneko, J. Brouwer, and G. S. Samuelsen (2006). *Power and temperature control of fluctuating biomass gas fueled solid oxide fuel cell and micro gas turbine hybrid system.* Journal of Power Sources, 160, pp. 316–325. doi:10.1016/j.jpowsour.2006.01.044.

[46] R. J. Kee, M. E. Coltrin, and P. Glarborg (2003). *Chemically Reacting Flow. Theory and Practice.* John Wiley & Sons, Hoboken, New Jersey, USA.

[47] R. Kikuchi, T. Yano, T. Takeguchi, and K. Eguchi (2004). *Characteristics of anodic polarization of solid oxide fuel cells under pressurized conditions.* Solid State Ionics, 174, pp. 111–117. doi:10.1016/j.ssi.2004.05.029.

[48] F. Kroll (2012). *Simulation und Regelung eines Brennstoffzelle-Gasturbine-Hybridkraftwerks.* Ph.D. thesis, University of Stuttgart, Stuttgart.

[49] M. Lang, C. Auer, A. Eismann, P. Szabo, and N. Wagner (2008). *Investigation of solid oxide fuel cell short stacks for mobile applications by electrochemical impedance spectroscopy.* Electrochimica Acta, 53, pp. 7509–7513. doi: 10.1016/j.electacta.2008.04.047.

[50] M. Lang, T. Franco, G. Schiller, and N. Wagner (2002). *Electrochemical characterization of vacuum plasma sprayed thin-film solid oxide fuel cells (SOFC) for reduced operating temperatures.* Journal of Applied Electrochemistry, 32, pp. 871–874.

[51] J. Larminie and A. Dicks (2003). *Fuel Cell Systems Explained.* John Wiley, Chichester, 2nd edition.

[52] J. Leeper (2001). *220 kWe Solid Oxide Fuel Cell/Gas Turbine Generator Hybrid Proof of Concept Demonstration Report.* Technical Report P600-01-009 REV. 3, California Energy Commission.

[53] R. Leibinger (2011). *Messfehleranalyse eines Brennstoffzellen-Teststands.* Master's thesis, Beuth Hochschule für Technik Berlin.

[54] F. Leucht (2012). *Der Festoxidbrennstoffzellengenerator im Hybridkraftwerk – Untersuchung von Betriebsweisen und ihrer Wirtschaftlichkeit.* Ph.D. thesis, University of Stuttgart.

[55] F. Leucht, W. G. Bessler, J. Kallo, K. A. Friedrich, and H. Müller-Steinhagen (2011). *Fuel cell system modeling for solid oxide fuel cell/gas turbine hybrid power plants, Part I: Modeling and simulation framework.* Journal of Power Sources, 196, pp. 1205–1215. doi:10.1016/j.jpowsour.2010.08.081.

[56] T.-H. Lim, R.-H. Song, D.-R. Shin, J.-I. Yang, H. Jung, I. C. Vinke, and S.-S. Yang (2008). *Operating characteristics of a 5 kW class anode-supported planar SOFC stack for a fuel cell/gas turbine hybrid system.* International Journal of Hydrogen Energy, 33, pp. 1076–1083.

[57] P. J. Lindstrom and W. G. Mallard (retrieved 2010-03-26). *NIST Chemistry WebBook, NIST Standard Reference Database Number 69.* National Institute of Standards and Technology, Gaithersburg.
URL `http://webbook.nist.gov`

[58] W. L. Lundberg, S. E. Veyo, and M. D. Moeckel (2003). *A High-Efficiency Solid Oxide Fuel Cell Hybrid Power System Using the Mercury 50 Advanced Turbine Systems Gas Turbine.* Journal of Engineering for Gas Turbines and Power, 125, pp. 51–58. doi:10.1115/1.1499727.

[59] J. D. Maclay, J. Brouwer, and G. S. Samuelsen (2011). *Development of a Dynamic Cathode Ejector Model for Solid Oxide Fuel Cell-Gas Turbine Hybrid Systems.* Journal of Fuel Cell Science and Technology, 8, p. 051013. doi:10.1115/1.4003774.

[60] L. Magistri, M. Bozzolo, O. Tarnowski, G. Agnew, and A. F. Massardo (2007). *Design and Off-Design Analysis of a MW Hybrid System Based on Rolls-Royce Integrated Planar Solid Oxide Fuel Cells.* Journal of Engineering for Gas Turbines and Power, 129, pp. 792–797. doi:10.1115/1.1839917.

[61] F. Marsano, L. Magistri, and A. F. Massardo (2004). *Ejector performance influence on a solid oxide fuel cell anodic recirculation system.* Journal of Power Sources, 129, pp. 216–228. doi:10.1016/j.jpowsour.2003.11.034.

[62] A. S. Martinez, J. Brouwer, and G. S. Samuelsen (2012). *Feasibility study for SOFC-GT hybrid locomotive power: Part I. Development of a dynamic 3.5 MW SOFC-GT FORTRAN model.* Journal of Power Sources, 213, pp. 203–217. doi:10.1016/j.jpowsour.2012.04.024.

[63] A. S. Martinez, J. Brouwer, and G. S. Samuelsen (2012). *Feasibility study for SOFC-GT hybrid locomotive power part II. System packaging and operating route simulation.* Journal of Power Sources, 213, pp. 358–374. doi:10.1016/j.jpowsour.2012.04.023.

[64] A. F. Massardo and F. Lubelli (2000). *Internal Reforming Solid Oxide Fuel Cell-Gas Turbine Combined Cycles (IRSOFC-GT): Part A—Cell Model and Cycle Thermodynamic Analysis.* Journal of Engineering for Gas Turbines and Power, 122, pp. 27–35.

[65] T. Matsui, M. Futamura, R. Kikuchi, and K. Eguchi (2007). *Electrode Polarization Characteristics of Solid Oxide Fuel Cells Under Pressurized Conditions.* ECS Transactions, 7, pp. 851–858. doi:10.1149/1.2729175.

[66] B. J. McBride, M. J. Zehe, and S. Gordon (2002). *NASA Glenn Coefficients for Calculating Thermodynamic Properties of Individual Species.* Technical Report NASA/TP—2002-211556, Glenn Research Center, Cleveland, Ohio.

[67] D. McLarty, J. Brouwer, and S. Samuelsen (2013). *Hybrid Fuel Cell Gas Turbine System Design and Optimization.* Journal of Fuel Cell Science and Technology, 10, p. 041005. doi:10.1115/1.4024569.

[68] Mitsubishi Heavy Industries (2013-09-20). *MHI Achieves World's First 4,000-Hour Continuous Operation Of Pressurized SOFC-MGT Hybrid Power Generation System.* Press Information No. 1714.

[69] A. Momma, K. Takano, Y. Tanaka, T. Kato, and A. Yamamoto (2013). *Experimental Investigation of the Effect of Operating Pressure on the Performance of SOFC and SOEC.* ECS Transactions, 57, pp. 699–708. doi:10.1149/05701.0699ecst.

[70] F. Mueller, R. Gaynor, A. E. Auld, J. Brouwer, F. Jabbari, and G. S. Samuelsen (2008). *Synergistic integration of a gas turbine and solid oxide fuel cell for improved transient capability.* Journal of Power Sources, 176, pp. 229–239. doi:10.1016/j.jpowsour.2007.10.081.

[71] F. Mueller, F. Jabbari, J. Brouwer, R. Roberts, T. Junker, and H. Ghezel-Ayagh (2007). *Control Design for a Bottoming Solid Oxide Fuel Cell Gas Turbine Hybrid System.* Journal of Fuel Cell Science and Technology, 4, pp. 221–230. doi:10.1115/1.2713785.

[72] F. Mueller, F. Jabbari, R. Gaynor, and J. Brouwer (2007). *Novel solid oxide fuel cell system controller for rapid load following.* Journal of Power Sources, 172, pp. 308–323. doi:10.1016/j.jpowsour.2007.05.092.

[73] P. Nehter (2007). *A high fuel utilizing solid oxide fuel cell cycle with regard to the formation of nickel oxide and power density.* Journal of Power Sources, 164, pp. 252–259. doi:10.1016/j.jpowsour.2006.08.037.

[74] J. Neidhardt, M. Henke, and W. G. Bessler (2011). *Kinetic Modeling of Nickel Oxidation in SOFC Anodes.* ECS Transactions, 35, pp. 1621–1629. doi:10.1149/1.3570148.

[75] J. P. Neidhardt, D. N. Fronczek, T. Jahnke, T. Danner, B. Horstmann, and W. G. Bessler (2012). *A Flexible Framework for Modeling Multiple Solid, Liquid and Gaseous Phases in Batteries and Fuel Cells.* Journal of The Electrochemical Society, 159, pp. A1–A15. doi:10.1149/2.023209jes.

[76] H. Nishino, S. Hashimoto, Y. Liu, K. Asano, M. Mori, Y. Funahashi, and Y. Fujishiro (2007). *Cell Performance of Microtubular SOFCs with Sc-Doped Zirconia Electrolyte under Pressurized Conditions.* ECS Transactions, 7, pp. 597–601. doi:10.1149/1.2729141.

[77] M. Nishiura, S. Koga, T. Kabata, N. Hisatome, K. Kosaka, Y. Ando, and Y. Kobayashi (2007). *Development of SOFC/Micro Gas Turbine Combined Cycle System.* ECS Transactions, 7, pp. 155–160. doi:10.1149/1.2729085.

[78] T. Panne, A. Widenhorn, and M. Aigner (2008). *Steady State Analysis of a SOFC/GT Hybrid Power Plant Test Rig.* ASME Turbo Expo, Berlin, Germany. GT2008-50288.

[79] T. Panne, A. Widenhorn, J. Boyde, D. Matha, V. Abel, and M. Aigner (2007). *Thermodynamic Process Analyses of SOFC/GT Hybrid Cycles.* 5th IECEC, St. Louis, Missouri, USA. AIAA 2007-4833.

[80] S. K. Park and T. S. Kim (2006). *Comparison between pressurized design and ambient pressure design of hybrid solid oxide fuel cell-gas turbine systems.* Journal of Power Sources, 163, pp. 490–499. doi:10.1016/j.jpowsour.2006.09.036.

[81] L. Petruzzi, S. Cocchi, and F. Fineschi (2003). *A global thermo-electrochemical model for SOFC system design and engineering.* Journal of Power Sources, 118, pp. 96–107. doi:10.1016/S0378-7753(03)00067-3.

[82] S. Primdahl and M. Mogensen (1998). *Gas Conversion Impedance: A Test Geometry Effect in Characterization of Solid Oxide Fuel Cell Anodes.* Journal of the Electrochemical Society, 145, pp. 2431–2438.

[83] E. R. Ray, R. A. Basel, and J. F. Pierre (1995). *Pressurized Solid Oxide Fuel Cell Testing.* Technical Report DOE/MC/28055-96/C0600, Westinghouse.

[84] K. P. Recknagle, E. M. Ryan, B. J. Koeppel, L. A. Mahoney, and M. A. Khaleel (2010). *Modeling of electrochemistry and steam-methane reforming performance for simulating pressurized solid oxide fuel cell stacks.* Journal of Power Sources, 195, pp. 6637–6644. doi:10.1016/j.jpowsour.2010.04.024.

[85] R. C. Reid, J. M. Prausnitz, and B. E. Poling (1988). *The Properties of Gases and Liquids.* McGraw-Hill, int. edition.

[86] R. A. Roberts and J. Brouwer (2006). *Dynamic Simulation of a Pressurized 220 kW Solid Oxide Fuel-Cell-Gas-Turbine Hybrid System: Modeled Performance Compared to Measured Results.* Transactions of the ASME, 3, pp. 18–25. doi:10.1115/1.2133802.

[87] D. Sarantaridis and A. Atkinson (2007). *Redox Cycling of Ni-Based Solid Oxide Fuel Cells Anodes: A Review.* Fuel Cells, 7, pp. 246–258.

[88] H. I. H. Saravanamuttoo, G. F. C. Rogers, H. Cohen, and P. V. Straznicky (2009). *Gas Turbine Theory.* Prentice Hall, Harlow, 6th edition.

[89] V. H. Schmidt and L. M. Lediaev (2009). *Pressure and gas concentration effects on voltage vs. current characteristics of a solid oxide fuel cell and electrolyzer.* In P. Singh and N. P. Bansal, editors, *Advances in Solid Oxide Fuel Cells IV*, pp. 105–115. Wiley, Hoboken, New Jersey.

[90] S. Seidler, M. Henke, J. Kallo, W. G. Bessler, U. Maier, and K. A. Friedrich (2011). *Pressurized solid oxide fuel cells: Experimental studies and modeling.* Journal of Power Sources, 196, pp. 7195–7202. doi:10.1016/j.jpowsour.2010.09.100.

[91] M. Shelton, I. Celik, E. Liese, and D. Tucker (2010). *A Study in the Process Modeling of the Startup of Fuel Cell/Gas Turbine Hybrid Systems.* Journal of Engineering for Gas Turbines and Power, 132, p. 012301. doi:10.1115/1.2830551.

[92] S. C. Singhal (2000). *Advances in solid oxide fuel cell technology.* Solid State Ionics, 135, pp. 305–313. doi:10.1016/S0167-2738(00)00452-5.

[93] S. C. Singhal and K. Kendall, editors (2003). *High Temperature Solid Oxide Fuel Cells: Fundamentals, Design and Application.* Elsevier, Oxford.

[94] B. Tarroja, F. Mueller, J. Maclay, and J. Brouwer (2010). *Parametric Thermodynamic Analysis of a Solid Oxide Fuel Cell Gas Turbine System Design Space.* Journal of Engineering for Gas Turbines and Power, 132, p. 072301. doi: 10.1115/1.4000263.

[95] K. Tomida, M. Nishiura, S. Koga, K. Miyamoto, Y. Teramoto, S. Yoshida, N. Matake, S. Suemori, T. Kabata, Y. Ando, and Y. Kobayashi (2010). *Development of SOFC-GT Combined Cycle System with Tubular Type Cell Stack.* Fuel Cell Seminar, San Antonio, Texas, USA.

[96] A. Traverso, L. Magistri, and A. F. Massardo (2010). *Turbomachinery for the air management and energy recovery in fuel cell gas turbine hybrid systems.* Energy, 35, pp. 764–777. doi:10.1016/j.energy.2009.09.027.

[97] A. Traverso, A. Massardo, R. A. Roberts, J. Brouwer, and S. Samuelsen (2007). *Gas Turbine Assessment for Air Management of Pressurized SOFC/GT Hybrid System.* Journal of Fuel Cell Science and Technology, 4, pp. 373–383. doi:10.1115/1.2714567.

[98] A. Traverso, F. Trasino, L. Magistri, and A. F. Massardo (2008). *Time Characterization of the Anodic Loop of a Pressurized Solid Oxide Fuel Cell System.* Journal of Engineering for Gas Turbines and Power, 130, p. 021702. doi:10.1115/1.2772638.

[99] A. Tsai, L. Banta, D. Tucker, and R. Gemmen (2010). *Multivariable Robust Control of a Simulated Hybrid Solid Oxide Fuel Cell Gas Turbine Plant.* Journal of Fuel Cell Science and Technology, 7, p. 041008. doi:10.1115/1.4000628.

[100] A. Tsai, L. Banta, D. Tucker, and R. Gemmen (2010). *Relative Gain Array Analysis of a Solid Oxide Fuel Cell Gas Turbine Hybrid Plant.* Journal of Fuel Cell Science and Technology, 7, p. 031004. doi:10.1115/1.3206973.

[101] A. Tsai, D. Tucker, and D. Clippinger (2011). *Simultaneous Turbine Speed Regulation and Fuel Cell Airflow Tracking of a SOFC/GT Hybrid Plant With the Use of Airflow Bypass Valves.* Journal of Fuel Cell Science and Technology, 8, p. 061018. doi:10.1115/1.4004643.

[102] A. Tsai, D. Tucker, and C. Groves (2011). *Improved Controller Performance of Selected Hybrid SOFC-GT Plant Signals Based on Practical Control Schemes.* Journal of Engineering for Gas Turbines and Power, 133, p. 071702. doi: 10.1115/1.4002253.

[103] D. Tucker, L. Lawson, and R. Gemmen (2005). *Characterization of Air Flow Management and Control in a Fuel Cell Turbine Hybrid Power System using Hardware Simulation.* ASME Power Conference, Chicago, Illinois, USA.

[104] D. Tucker, J. VanOsdol, E. Liese, L. Lawson, S. Zitney, R. Gemmen, J. C. Ford, and C. Haynes (2012). *Evaluation of Methods for Thermal Management in a Coal-Based SOFC Turbine Hybrid Through Numerical Simulation.* Journal of Fuel Cell Science and Technology, 9, p. 041004. doi:10.1115/1.4006044.

[105] J. VanOsdol, E. Liese, D. Tucker, R. Gemmen, and R. James (2010). *Scaling a Solid Oxide Fuel Cell Gas Turbine Hybrid System to Meet a Range of Power Demand.* Journal of Fuel Cell Science and Technology, 7, p. 015001. doi:10.1115/1.3115623.

[106] S. E. Veyo, L. A. Shockling, J. T. Dederer, J. E. Gillett, and W. L. Lundberg (2002). *Tubular Solid Oxide Fuel Cell/Gas Turbine Hybrid Cycle Power Systems: Status.* Journal of Engineering for Gas Turbines and Power, 124, pp. 845–849.

[107] A. V. Virkar, K.-Z. Fung, and S. C. Singhal (1997). *The Effect of Pressure on Solid Oxide Fuel Cell Performance.* Technical Report DOE/FETC/C–98/7303.

[108] M. Vogler, A. Bieberle-Hütter, L. Gauckler, J. Warnatz, and W. G. Bessler (2009). *Modelling Study of Surface Reactions, Diffusion, and Spillover at a Ni/YSZ Patterned Anode.* Journal of The Electrochemical Society, 156, pp. B663–B672. doi: 10.1149/1.3095477.

[109] C. Willich, A. Tomaszewski, M. Henke, J. Kallo, and K. A. Friedrich (2013). *Temperature Effect due to Internal Reforming in Pressurized SOFC.* ECS Transactions, 57, pp. 401–409. doi:10.1149/05701.0401ecst.

[110] C. Willich, C. Westner, M. Henke, F. Leucht, J. Kallo, and K. A. Friedrich (2012). *Pressurized Solid Oxide Fuel Cells with Reformate as Fuel.* Journal of The Electrochemical Society, 159, pp. F711–F716. doi:10.1149/2.031211jes.

[111] P. C. Wu, H. S. Jheng, and S. S. Shy (2013). *Pressurized Solid Oxide Fuel Cells: Measurements of Impedance Spectra and Anodic Concentration Polarization.* ECS Transactions, 57, pp. 215–225. doi:10.1149/05701.0215ecst.

[112] Y. Yi, A. D. Rao, J. Brouwer, and G. S. Samuelsen (2004). *Analysis and optimization of a solid oxide fuel cell and intercooled gas turbine (SOFC-ICGT) hybrid cycle.* Journal of Power Sources, 132, pp. 77–85. doi:10.1016/j.jpowsour.2003.08.035.

[113] L. Zhou, M. Cheng, B. Yi, Y. Dong, Y. Cong, and W. Yang (2008). *Performance of an anode-supported tubular solid oxide fuel cell (SOFC) under pressurized conditions.* Electrochimica Acta, 53, pp. 5195–5198. doi:10.1016/j.electacta.2008.02.032.